Development of Low Energy Positron Beams and their Application to the Study of the Surface Region in Metals

David T Britton

B.Sc. Lond., MSc. Lond.,A.R.C.S.

Thesis Submitted for the Degree of Ph.D.

September 1987

Royal Holloway & Bedford New College

University of London

Abstract

Two low energy positron beams have been designed, built and their performance characteristics evaluated. Both are magnetically guided systems using a combination of a solenoid and Helmholtz coils. Slow positrons are produced by the moderation of fast positrons, from a ^{22}Na source, in annealed polycrystalline tungsten mesh with efficiencies greater than 2×10^{-4}. The original beam, built to high vacuum specifications, has been incorporated into a fully automated microcomputer controlled Doppler-broadening spectrometer system. The newer beam line is built,to UHV specifications, into a liquid helium cryostat. It also has a vertical geometry making the whole system far more versatile and allowing the study of liquid surfaces.

Doppler-broadening analysis has been applied to measurements taken using both beams applied to pure metals (Mo and Ga). A two-state model incorporating diffusion of thermal positrons back to the surface has been found to be inadequate at low incident positron energies. In this regime epithermal positron and positronium emission is significant. A model of simple back-scattering of epithermal positrons was found to be successful in fitting the experimental lineshape parameters.

Both fast and slow positron techniques have been applied to the study of inert gas precipitates in metals. Using conventional methods a detailed Doppler-broadening study has been carried out on the anealing of bulk Cu samples containing 3 atomic % Kr in the form of a high concentration of solid precipitates at 300K. Melting of the Kr and bubble growth are clearly seen. Deconvolution of the annihilation lineshape indicates that positrons are trapped at the Cu-Kr interface.

Slow positrons have been used to profile the defect distribution of Mo implanted with a high dose of Kr ions. Using the simplest model of a step-function distribution there is reasonable agreement with the expected Kr profile.

Dedication

It is all too easy to say that what I have achieved is purely the result of my hard work. This is not true, I have been offered and have seized upon many opportunities. This thesis is humbly dedicated to my friends in these and other lands who are denied those same opportunities.

Contents

Chapter 1 Positrons in Solids and at Surfaces

1.1 Introduction

The positron and the electron are anti-particles of each other and the final event of their meeting is their mutual annihilation to produce gamma-rays. All too often this is taken as the starting point in a discussion of the behaviour of positrons in solids. As the first half of this thesis concerns the production of slow positron beams by extracting thermalised positrons from solids, annihilation has been deferred until after all other positron interactions.

The positron is a light fermion with the same rest mass as the electron, 511 keV/c^2, and opposite charge +e. It has the same intrinsic spin, 1/2, and the same magnetic moment $ge/2m_ec$ (Brandt 1983). The Pauli exclusion principle does not apply for the two particles in a positron-electron system, ie $< \psi_+(\mathbf{r})|\psi_-(\mathbf{r}) > \neq 0$ in general.

Although annihilation is a quantum phenomenon arising directly from the same formalism by which Dirac (1930) predicted the existence of the positron for most purposes the positron can be treated as a light classical particle. It has a characteristic range in solids, it loses energy by collisions until it is in thermal equilibrium with its surroundings and its motion can be thought of as diffusion. In a low energy positron beam line the positron has a definite trajectory and a kinetic energy $\frac{1}{2}mv^2$.

Many other aspects of positron physics, however, cannot be thought of in classical terms, eg the formation of the positron-electron bound state (positronium), the calculation of annihilation and trapping rates or emission of thermal positrons from surfaces. Some of the classical descriptions of positron behaviour in solids are only possible because of the scarcity of positrons in nature. The picture of a classical particle diffusing in a solid lattice is applicable

partly because there is only one positron in the system and it is therefore most probably in the lowest state of a conduction band. As positrons survive typically 10^{-10} seconds in matter a source of intensity 10 GBq (3Ci) would be needed for more than one positron to be in the sample at any one time. Most sources are more than a factor of 30 000 weaker than this.

1.2 Production of Positrons

Positrons are produced in two ways, either by pair production or from the β^+ decay of radiaoctive nuclei. The former has only limited applications, specifically in linac based facilities where electron bremsstrahlung is used to generate the primary positrons for intense pulsed beams. There are more than 200 positron emitting isotopes but only a handful of these are useful. Mackenzie (1983) has listed 13 but generally only four are in common use. These are ^{22}Na, ^{58}Co, ^{64}Cu and ^{68}Ge. The others being excluded because of high production costs or extremely short half lives.

Of the main four sources copper has the shortest half life (12.8 hours) but this is offset by its ease of production by neutron irradiation of ^{63}Cu. It also is the only one of these not to produce a fiducial gamma ray and so is not generally useful for timing measurements. For most purposes, except where intensity is required, the longer lived ^{22}Na is the most useful. It has a half life of 2.6 years and can be deposited directly onto a sample from solution.

1.3 Positron Interactions with Condensed Matter

Positrons emitted in the beta decay of radiaoctive nuclei have a typical beta spectrum with an endpoint energy of the order of 1MeV, for ^{22}Na E_{max} = 0.54MeV. The attenuation of beta radiation is well described on a macroscopic scale by an exponential law (Nieminen 1983). The stopping profile

for monoenergetic positrons is somewhat different (Chap. 6). Brandt & Paulin (1977) have calculated the profile from the attenuation of positrons from ^{64}Cu (E_{max}=0.65MeV) to be $P(z) = \exp(-\alpha z)$ where

$$\alpha = \frac{C\rho}{{E_{max}}^{1.43}}$$

E_{max} is measured in MeV, ρ is the material density and $C = 16 \pm 1$ cm^2/g.

Fast positrons entering a material rapidly lose energy in electron collisions down to epithermal energies (a few eV). After which any of the scenarios indicated in figure 1.1 can occur (Mills 1983). An epithermal positron can scatter back through the surface to be emitted as a free positron or positronium. A positron can continue to lose energy by phonon scattering until it is in thermal equilibrium with the lattice. Thermal positrons can diffuse deeper into the material where they eventually annihilate with electrons or back to the surface. Slow positrons reaching the surface can either be trapped in a surface state or be reemitted as free positrons or positronium. Some of the incident fast positrons will also be backscattered as indicated by the diffraction channel marked on the figure.

1.3.1 Positrons in Solids

Thermal positrons are essentially free in a perfect lattice. The repulsive ion cores effectively produce a periodic potential centred between the lattice sites (fig. 1.2). The solutions to the Schrödinger equation with the boundary conditions that $\psi = 0$ at the lattic sites and $\nabla\psi = 0$ at the Wigner-Seitz cell boundary are Bloch waves with wave-numbers equal to the reciprocal lattice vectors. To put it simply the positron wave-function is an infinite plane wave with half-wavelength equal to the lattice spacing. Because of this quantum effect the classical positron diffusing in a solid with a kinetic energy of $\frac{3}{2}$kT has a zero-point potential energy E_0 above the vacuum level. This is one of

the contributing factors in the emission of slow positrons from materials with negative positron workfunctions (Chap. 2).

If one of the lattice atoms is missing then there is a much deeper effective potential (fig. 1.2) which acts as a very strong trap for the positron. This is true not only for single vacancies but for all open-volume defects. As will be discussed later (Chap. 5) the characteristics of the positron-electron annihilation radiation differ for a localised positron with respect to a delocalised one. Consequently one of the greatest strengths of the positron annihilation technique is the study of defect behaviour in solids.

A positron localised within a trap will have a significant momentum compared to the thermal energies (40meV at 300K). This is essentially as a result of the Heisenberg uncertainty principle $\Delta p \Delta x \approx \hbar$. For monovacancies this zero-point motion can be significant. Rice-Evans et al (1981) report a zero-point kinetic energy of 0.4eV for positrons trapped at thermally produced vacancies in Cd at 574K, a factor of 5 greater than the thermal energy.

The sensitivity of positron techniques to the growth or introduction of mechanical defects depends quite obviously on how long the positron would exist in the perfect lattice and the probability of capture by a single defect. This probability is expressed as the defect specific trapping rate μ which is essentially governed by the size of the trap and the mobility of the positron (West 1974);

$$\mu = 4\pi D_+ r_0$$

where r_0 is a trap radius. D_+ is the positron diffusion coefficient, a measure of the distance a positron will diffuse before annihilation. For a bulk (perfect lattice) decay rate λ, this distance is given by $L_+ = \sqrt{\lambda D_+}$. Then the total trapping rate for all defect species is $\kappa = \sum_i \mu_i C_i$ where C_i are the concentrations. The probability for the positron to annihilate while trapped at any single type of defect is then $\mu_i C_i/(\lambda + \kappa)$.

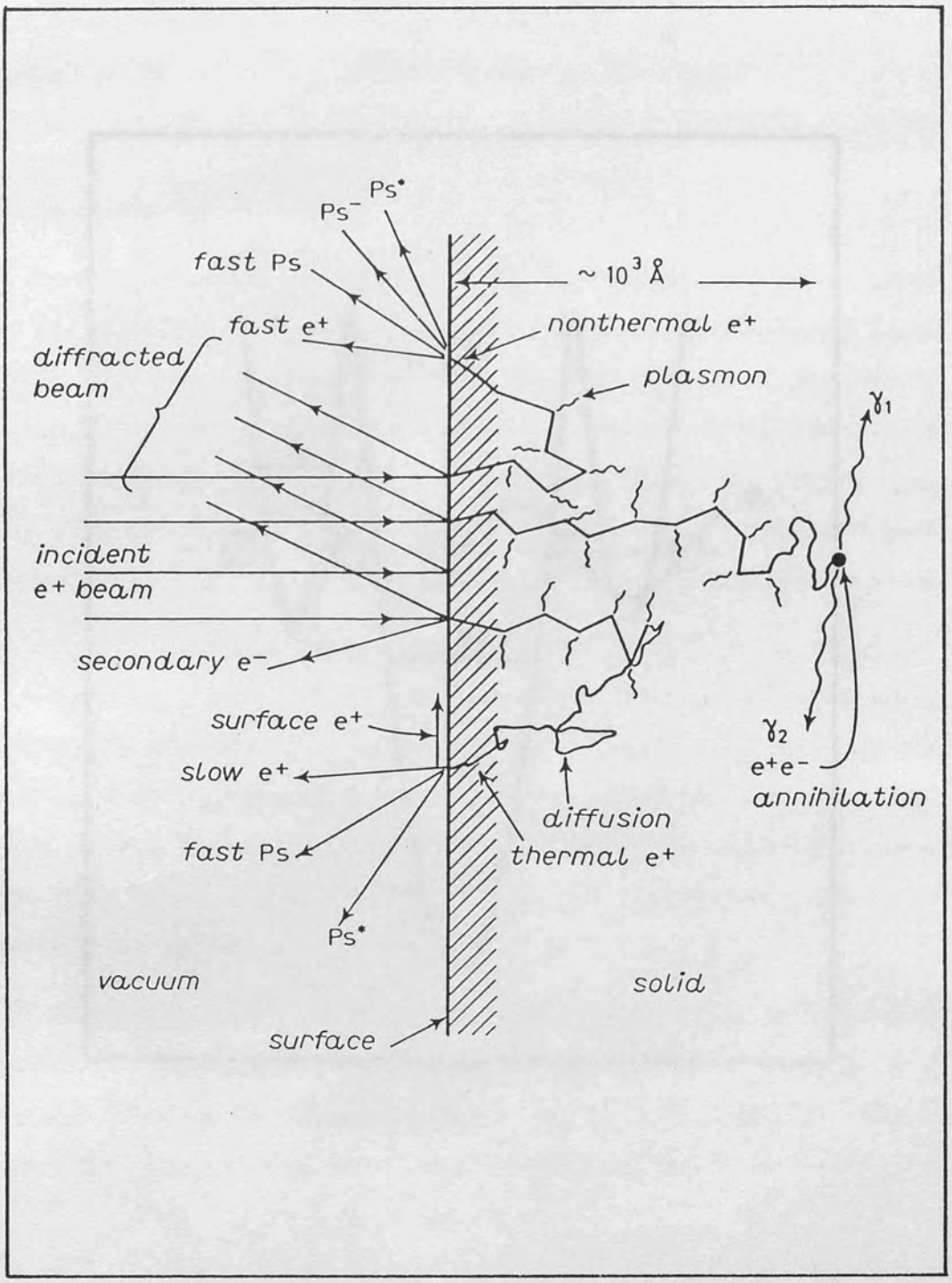

Figure 1.1

Positron interactions at a surface. From Mills (1983).

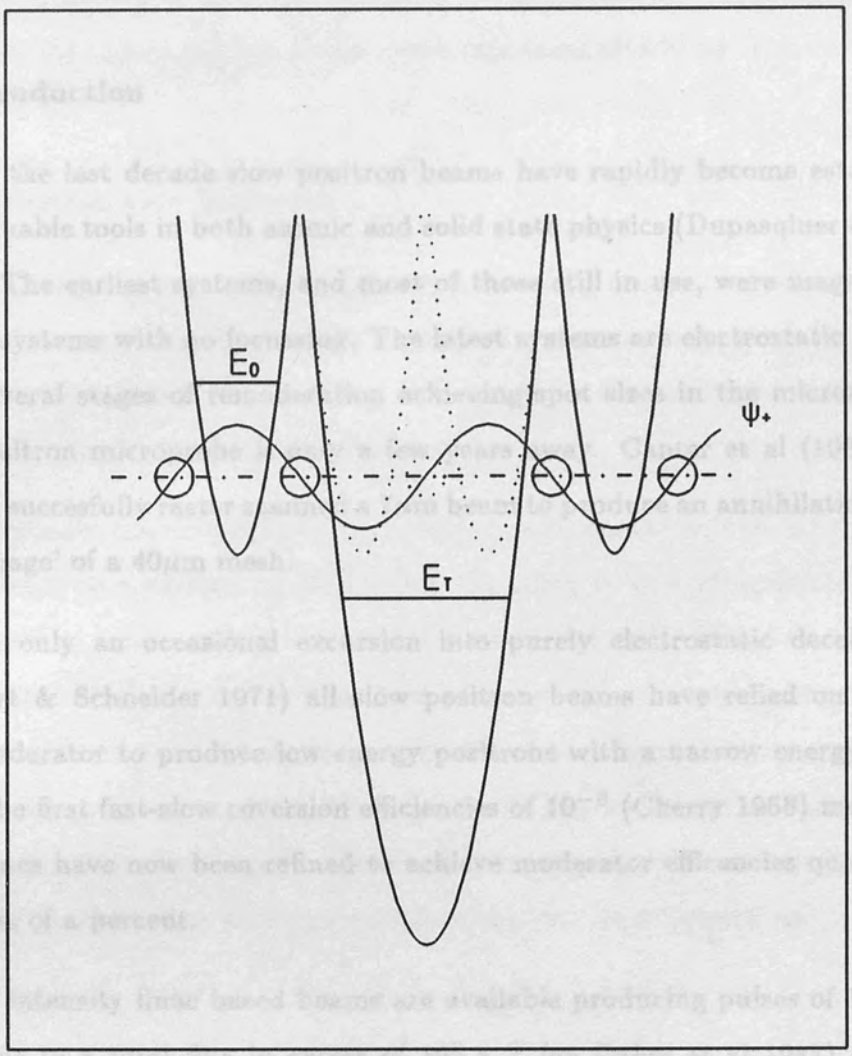

Figure 1.2

Potentials on a positron in a solid showing the effect of a missing ion core. The wavefunction ψ_+ refers to the undefected lattice.

Chapter 2 Slow Positron Beams

2.1 Introduction

Over the last decade slow positron beams have rapidly become established as invaluable tools in both atomic and solid state physics (Dupasqiuer & Zecca 1985). The earliest systems, and most of those still in use, were magnetically guided systems with no focussing. The latest systems are electrostatic systems with several stages of remoderation achieving spot sizes in the micron range. The positron microprobe is only a few years away. Canter et al (1987) have already succesfully raster scanned a 7μm beam to produce an annihilation count rate 'image' of a 40μm mesh.

With only an occasional excursion into purely electrostatic decelleration (Lohnert & Schneider 1971) all slow positron beams have relied on the use of a moderator to produce low energy positrons with a narrow energy width. From the first fast-slow coversion efficiencies of 10^{-8} (Cherry 1958) moderator techniques have now been refined to achieve moderator efficencies quotable in fractions of a percent.

High intensity linac based beams are available producing pulses of 10^7 slow positrons to a total flux in excess of 10^9 s^{-1} (eg Dahm et al 1987) In these systems the source of energetic positrons is pair production from electron Bremsstrahlung in a heavy metal target (usually tungsten).

2.2 Moderation of Positrons

A moderator is any material which reemits positrons with energies of a few eV. There are basically two modes of emission from a surface, either the material has a negative positron workfunction Φ_+ or epithermal positrons with energies

below the electron band gap energy E_g can scatter elastically through the surface. Emission is only the first part of the problem, methods of getting the positrons to exit surface of the moderator need also to be considered

2.2.1 Workfunction Emission

When fast positrons enter a metal they are rapidly thermalised to their lowest energy state, an essentially free Bloch wave with a zero-point energy E_0 relative to the periodic lattice (figure 2.1). This would be the same for an additional electron occupying a conduction band.

Additionally the extension of the electron wave-functions beyond the metal lattice leads to a surface dipole D with the effect of attracting electrons into and repelling positrons from the bulk. Considering only these two terms the positron workfunction Φ_+ is directly analogous to the electron work function. However a third term needs to be introduced to account for the correlation between the positron and the electron cloud. At low electron densities this correlation energy E_{corr} approaches the positronium binding energy (Hodges & Stott 1973). Hence the positron work function can be expressed as

$$\Phi_+ = E_0 + D - E_{corr}$$

As far as the work-function is concerned the image potential need not be considered although this will act as trap for any non-energetic positrons at the surface.

2.2.2 Epithermal Emission

The emission of hot positrons and positronium has been observed from a wide variety of surfaces for low incident energy positrons (Mills & Crane 1984, Howell,Rosenberg & Fluss 1986). This is probably due to elastic scattering

off the ion cores (Chapter 6) . Initially the dominant process in the slowing down of positrons is inelastic electron scattering until the positron no longer has sufficient energy to excite an electron from the valence to the conduction band. In this regime the dominant slowing down process is acoustic phonon scattering and the energy transfer is small.

In addition to phonon scattering the positron will undergo elastic scattering with a characteristic scattering length dependent on the material. If it scatters from a point less than the scattering length from the surface then there is a good chance of reemission. As with work-function emission epithermal positrons are unlikely to be trapped in surface states although any thermal positrons which diffuse back to the surface will be.

2.2.3 Practical Moderators

The majority of practical moderators in use are workfunction moderators operating in the backscatter mode. Such a moderator requires a high density to stop positrons in the surface region and to be as near defect free as possible with a clean surface to have a high probability of reemission. Ideally a single crystal would give the best conversion efficiency. Cu(111) (Mills 1979) and W(110) (Lahtinen et al 1986) are both currently used with efficiencies greater than 0.1%. The latter has a quoted efficiency of 0.28% for a ^{58}Co source which is the highest value reported for a workfunction type moderator.

Any beam utilising a true backscatter moderator geometry requires a very small, and hence intense source, as this will cast a shadow in the reemitted positron beam. Until the recent development of thin film transmission moderators a useful compromise for the larger ^{22}Na sources was the 'Venetian blind' geometry (Dale et al 1980) using polycrystalline tungsten vanes(fig. 2.2) perpendicular to the beam direction. Woven mesh moderators are simply an extension of this original idea. In this geometry the reemitted positrons

are emitted at high angles and collected by an electric field giving a pseudo-transmission moderator geometry. With polycystalline moderators efficiencies are typically a factor of 10 lower than for single crystal tungsten. The large angular spread precludes the use of this geometry in electrostatic systems where a small spot size is required although it is has proved very useful in magnetic systems where intensity, but not brightness, is paramount.

The last year has seen great progress in the introduction of thin single crystal transmission moderators which have efficiencies comparable with mesh moderators ($\sim 2 \times 10^{-4}$) (M Charlton,N Zafar priv. comm.) This is still a long way below the theoretical efficiency of 10^{-3} for 10μm W(110) and Cu(111)(Vehanen & Mäkinen 1985). However transmission moderators have the same inherent advantage as single crystal backscatter moderators; the slow positrons are emitted perpendicular to the plane of the moderator with a small angular divergence. This makes them ideal primary moderators for electrostatic systems using the larger, and longer lived, ^{22}Na sources.

Another useful concept in limited applications is the self-moderating source. An example of this is the ^{64}Cu source used in the reactor based beam used at Brookhaven National Laboratories (Weber et al 1986). Copper is irradiated in the reactor to produce ^{64}Cu, a positron emitting isotope with a half life of 13 hrs, through the reaction ^{63}Cu(n,γ)^{64}Cu. This is then vapourised and deposited epitaxially on a W(110) crystal to produce a Cu(111) crystal. Positrons from the decay of ^{64}Cu in the crystal are moderated *in the crystal* and emitted at workfunction energies from the surface. In principle the same technique could be used with a single crystal of copper sitting permanently in the neutron flux of a reactor.

Moderators relying on epithermal emission require a long scattering length and a high probability of a hot positron being within this distance from the exit surface. In the backscatter mode this implies a dense material with a

high stopping power which is imcompatible with a long scattering length. All practical moderators involving this mechanism have actually been composite materials, the most succesful of which was MgO smoked gold (Canter et al 1974) which was in widespread use before polycrystalline tungsten.

The most efficient moderator to date (Gullikson & Mills 1986) is an epithermal moderator operating in transmission mode. Solid neon deposited directly onto a ^{22}Na source capsule achieved a conversion efficiency of 0.56%. Neon is a perfect insulator but there is no reason to suppose that any other thin insulating film would not function to some degree as a transmission moderator.

2.2.4 Field Assisted Moderators

As yet there is no practical version of the field assisted moderator (FAM) proposed by Beling et al (1987). The concept is remarkably simple, drift positrons across a transmission moderator under the influence of an an applied electric field. Efficiencies of the order of 10% should be possible for primary moderation. The realisation however is proving very difficult with most of the problems arising from the need to apply a high field to the moderator and then to get the positrons through the electrical contacts.

Both semiconductors and insulators are likely candidates for such a device and both workfunction and epithermal emission could be used. So far most development has been on Si with epitaxial $NiSi_2$ contacts with emphasis on drifting thermal positrons and workfunction emission. Insulating materials however should give better results, if a high field can be maintained epithermal positrons can be drifted ballistically with sufficient energy to traverse the defected region at the contact.

2.3 Beam Transport

Positron beams fall into two categories, magnetically guided or electrostatically focussed systems, each of which has its own respective merits and disadvantages. In practice all magnetic systems are actually hybrid systems with electrostatic fields used to collect positrons from the moderator and to accelerate them into the target area. Magnetic systems cannot be focussed but are much simpler to build and could be used as a front-end to a brightness enhanced beam line at an accelerator or reactor where the beam needs to be transported a long distance from the moderator.

2.3.1 Magnetic Guidance

A magnetically guided system has no longtitudinal acceleration of the positrons whatsoever. The positrons are confined by gyratron motion about an axial magnetic field provided by a solenoid or a series of single coils at approximately the Helmholtz spacing. For a transverse velocity component v_T and an axial field B the diameter of the spiral path is given by $d = v_T m\pi/eB$, or in terms of the transverse energy component E_T (in eV)

$$d = \frac{\pi\sqrt{2E_T}}{B\sqrt{e/m}}.$$

For tungsten the maximum value of E_T can be taken as 2eV and then as an order of magnitude for B in mT (1mT=10G) $d \approx 5\pi/B$ mm giving a typical diameter of 0.5mm for 3mT. Clearly sub-millimetre lateral resolution in this type of system is impractical for moderate magnetic field strengths, although for most purposes high spatial resolution is not required.

For every slow positron passing down the beam line 10 000 fast positrons, which are essentially unnaffected by the field, are emitted from the source. Considering only the solid angle of emission for a straight beam line of cross-sectional area 1cm^2 to reduce the fast flux to 1% of the slow would require a

flight tube 10m long.

There are two methods of removing the fast component from the beam. The easiest is to bend the beam line through a shallow angle so that the fast positrons annihilate in the wall of the tube. Although it is possible to bend the positron beam through any angle as a rule large angles with small radii of curvature are undesirable. As positrons move in a curved field they experience a drift velocity (Kaupilla et al 1977)

$$v_D = \frac{m}{eRB}(v_L^2 + \frac{1}{2}v_T^2)\hat{\mathbf{R}} \times \hat{\mathbf{B}}$$

where $\mathbf{R}$ is the radius of curvature and $\mathbf{B}$ the magnetic field, v_L and v_T are the longtitudinal and transverse velocity components. From this expression it can be seen that the total drift can be minimised by keeping the angle small and the drift velocity reduced by having a slow bend. For small drifts this can be compensated by introducing an extra component in the magnetic field so that the field lines, which are the guiding centres of the helical positron paths, move in the opposite direction to the drift. This is usually achieved by an extra correction coil inclined at an angle to the plane of the flight tube.

The other method of excluding fast positrons, and one which can be used to select accurately v_L, is to pass the beam through a region of crossed electric and magnetic fields (Schultz 1984). A suitably selected pair of $\mathbf{E} \times \mathbf{B}$ plates can be used to displace the beam laterally with no increase in transverse momentum. For a pair of plates of length l to move the beam a distance d (fig. 2.3) with no increase in momentum the necessary conditions are

$$l = \frac{2n\pi v_L}{B}$$

and

$$d = \frac{2n\pi E}{B}$$

where E is the applied electric field and n is any integer. Two such pairs of plates in tandem will bring the beam back onto its original axis. A baffle in

between can be used to intecept fast positrons. Hutchins et al (1986) have improved on this idea by using curved plates to remove the distortion due to the finite beam diameter giving different displacements.

The fundamental limitation on any magnetically guided system is its inability to be focussed down to a small spot size. This is a property of the inherent high transverse momentum of the beam. Wherever the positron trajectory is not parallel to the magnetic field lines, either where the field diverges or where there is electrostatic convergence of the beam, momentum will be transferred to the perpendicular component. In geometrical optics Liouville's theorem states that for an initial ray a height r above the axis at and angle θ the product $r\theta\sqrt{E}$ is conserved (Canter 1987). With mesh moderators this problem due to magnetic guidance is irrelevant because of the large initial transverse momentum.

2.3.2 Electrostatic Systems

A highly focussed beam requires an electrostatic system with a moderator with a very low intrinsic transverse energy E_T. For a generalised electrostatic system (fig. 2.4) the initial angular spread θ is $2(E_T/E)^{1/2}$ where E is the longtitudinal beam energy. Focussing onto an image of diameter d_2 at a distance z behind a final aperture of diameter d_1 the final angle ϕ is d_1/z for small ϕ. Then the limiting condition from phase space arguments is (Canter 1987)

$$D\theta \leq d_2\phi$$

where D is the moderator diameter. Substituting for the angles

$$2D\sqrt{E_T} \leq \frac{d_1 d_2}{z}\sqrt{E}$$

This description is valid for all systems, although normally the exit aperture does not exist but limitting the pencil angle and lens filling results in the same constraints.

In any system, but particularly electrostatic beams, grids should be avoided. Not only does a grid absorb a large fraction of the positron flux but aberrations increase the angular spread of the beam. Treating any hole in the mesh as a Calbick lens (fig. 2.5) of aperture radius r at a distance L from the object (moderator). The penetration of field E_1 through the aperture will lead to a radial field component E_r and corresponding force eE_r. Then the final radial velocity component will be

$$v_r = \frac{e}{m}\int_{t_1}^{t_2} E_r dt$$

integrated over the time passing through the aperture. Making the crude approximation $dz = v_z dt$

$$v_r = \frac{e}{mv_z}\int_{z_1}^{z_2} E_r dz$$

Constructing a cylinder through the aperture with the same radius r and using Gauss' law

$$\pi r^2(E_1 - E_2) + 2\pi r \int_{z_1}^{z_2} E_r dz = 0$$

from which

$$\frac{v_r}{v_z} = er\frac{(E_1 - E_2)}{2mv_z^2}$$

Substituting for $\frac{1}{2}mv_z^2 = eV$ and $E_1 - E_2 = V/L$

$$\frac{v_r}{v_z} = \frac{r}{4L}$$

so a mesh of spacing $d = 2r$ will give the beam an extra angular spread $d/8L$.

Removal of the fast positrons is not difficult in electrostatic systems. Ideally the slow beam can be reflected through 90^o with a hemispherical or cylindrical analyser although Canter (1987) has reported equally good results with a plane electrostatic mirror. With brightness enhanced beams using secondary backscatter moderators the reflection can be incorporated into the remoderation stage.

A severe problem in electrostatic beams is annihilation of reemitted positrons in the target area. This does not occur in magnetic systems if the target area is electrostatically field-free as the positrons simply spiral back along the beam line. Consquently a much larger free volume is needed around the target in an electrostatic beam line to eliminate spurious annihilations.

2.3.3 Brightness Enhancement

A charged particle beam can be characterised either by its total flux I or its brightness, flux/unit area/solid angle. For a beam of diameter d and pencil half angle θ and energy E the brightness per volt R_v is given by

$$R_v = \frac{\mathrm{I}}{\pi d^2 \theta^2 E}$$

but from Liouville's theorem $r\theta\sqrt{E}$ is constant and so the brightness cannot be increased by any amount of fancy optics. In practical terms this gives a minimum spot size corresponding to $\theta = \pi/2$. At moderation

$$d\theta = 2D\sqrt{\frac{E_T}{E}}$$

where D is the moderator diameter. From this it follows that

$$d_{min} = \frac{4D}{\pi}\sqrt{\frac{E_T}{E}}$$

and

$$R_v = \frac{\mathrm{I}}{4\pi D^2 E_T}$$

In 1980 Mills proposed a novel solution to this problem, in remoderation the phase space $r\theta\sqrt{E}$ is not conserved. If a beam is focussed down to a small area with a high angular convergence onto a moderator crystal the reemitted positrons will always have the angular spread detemined by the intrinsic transverse energy due to the moderator. If the remoderated intensity is $\mathrm{I}' = \varepsilon\mathrm{I}$

and the beam is focussed down to a diameter D' then the brightness per volt is enhanced by

$$\frac{B'}{B} = \frac{\varepsilon D^2}{D'^2}$$

In one stage of remoderation, for a typical efficiency of 10% for keV positrons on W(110) with a reduction in diameter of 20 the brightness per volt would be increased by a factor of 40.

The two beams using brightness enhancement currently in operation (Canter et al 1987) or development (Brusa et al 1986) both use a backscatter geometry for remoderation. The Brandeis system (Canter et al 1987) uses two stages of remoderation each reducing the beam diameter by a factor of 10 from 10mm to 0.1 mm with a gain in brightness of 500. Using higher focussing this system has achieved spot sizes less than 10 microns. A transmission geometry would be much simpler in terms of the electron optics but suffers from an inherent loss of intensity of a factor of four (Canter 1986). In a film rather than a semi-infinite solid half the positrons will be reemitted in the reverse direction and the aberrations involved in focussing result in twice the spread in an axially symmetric (transmission) system.

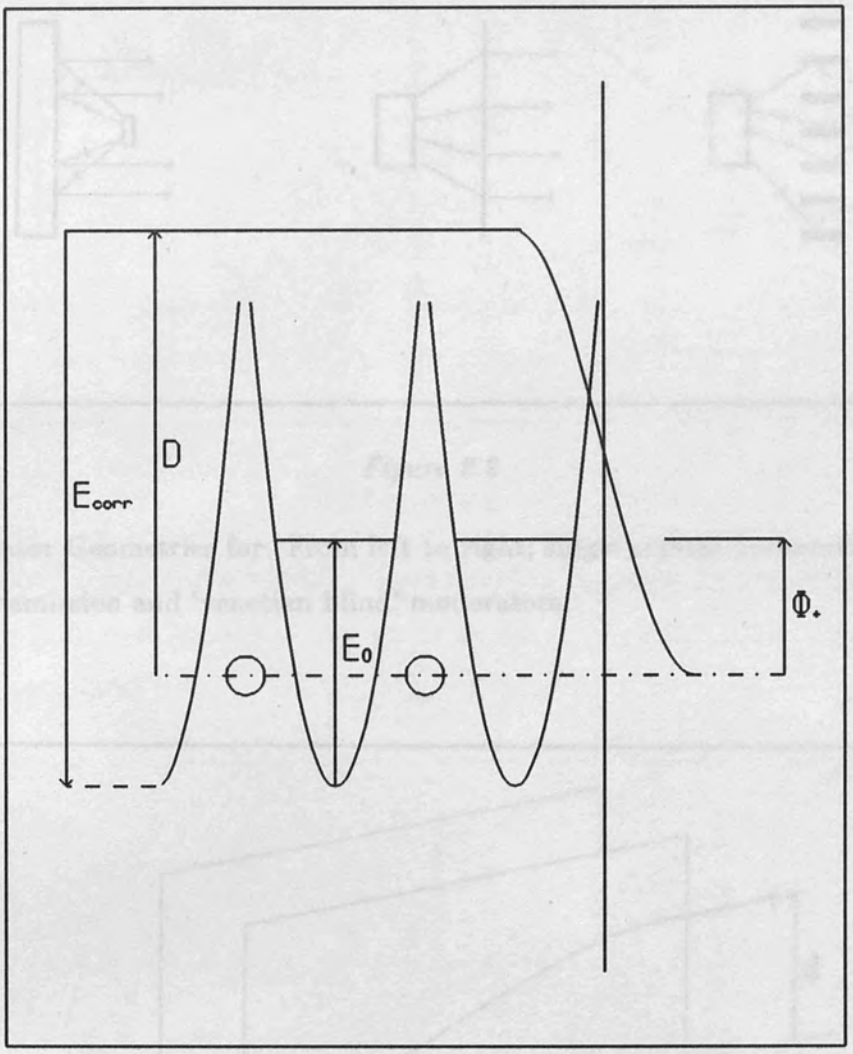

Figure 2.1

The potentials at a surface contributing to the positron workfunction. The image potential has been omitted as it does not influence the value of Φ_+.

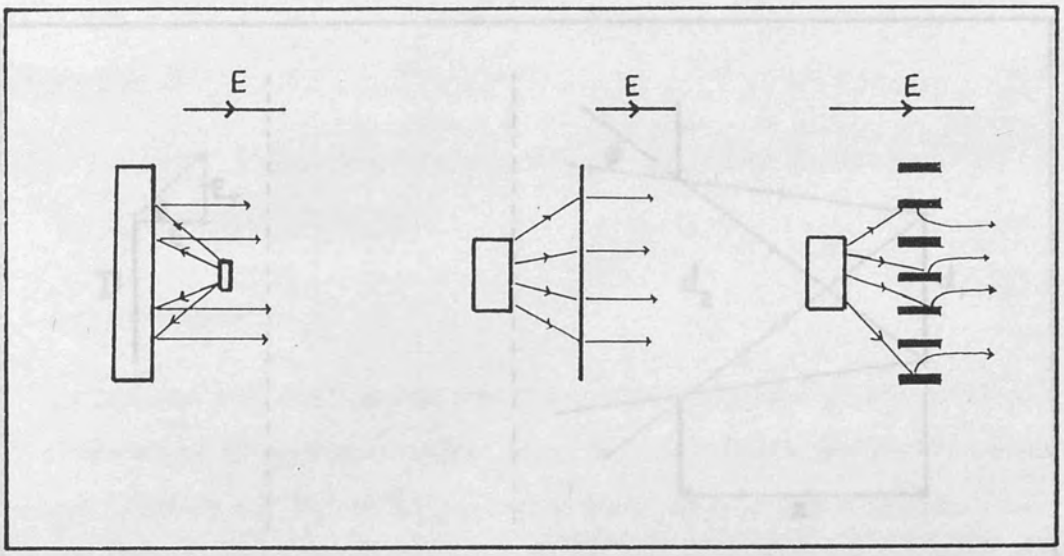

Figure 2.2

Moderator Geometries for. From left to right; single crystal backscatter, thin foil transmission and 'venetian blind' moderators.

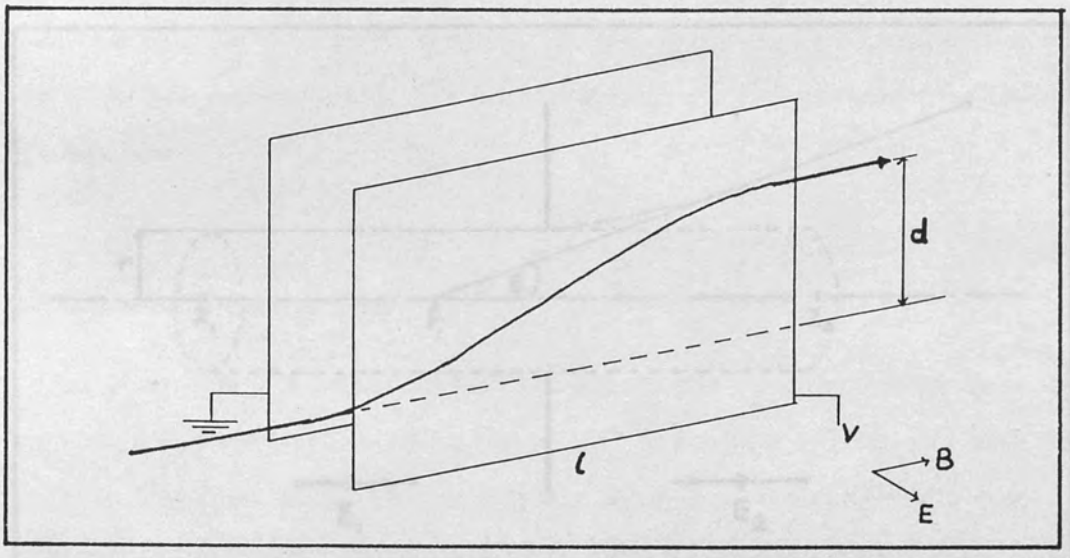

Figure 2.3

$\mathbf{E} \times \mathbf{B}$ plates used to deflect a positron beam vertically through a distance d with no increase in transverse momentum.

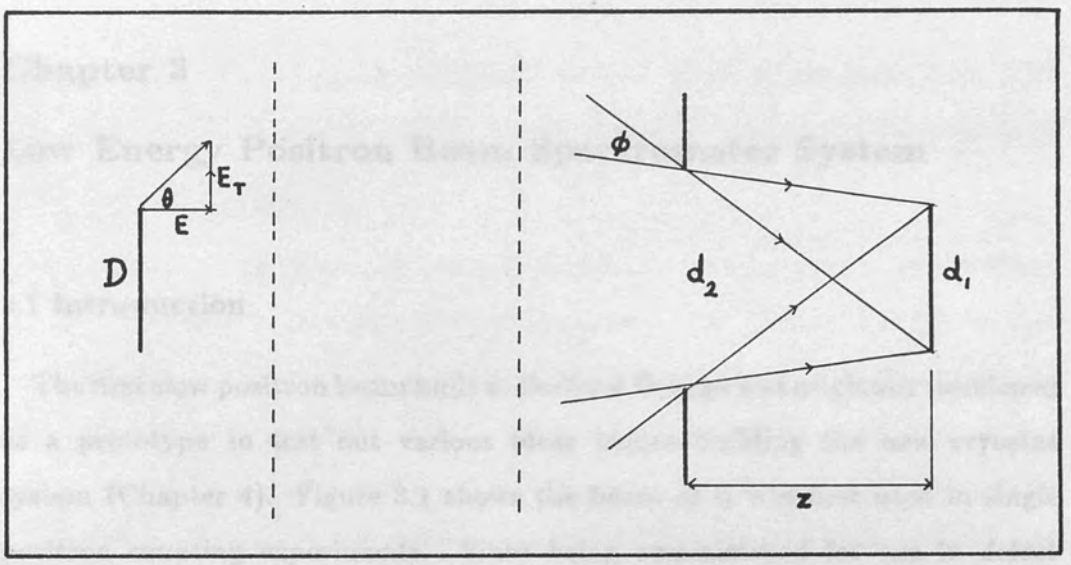

Figure 2.4

Generalised electrostatic positron beam showing emission from a moderator of diameter D & final focussing onto an image d_1.

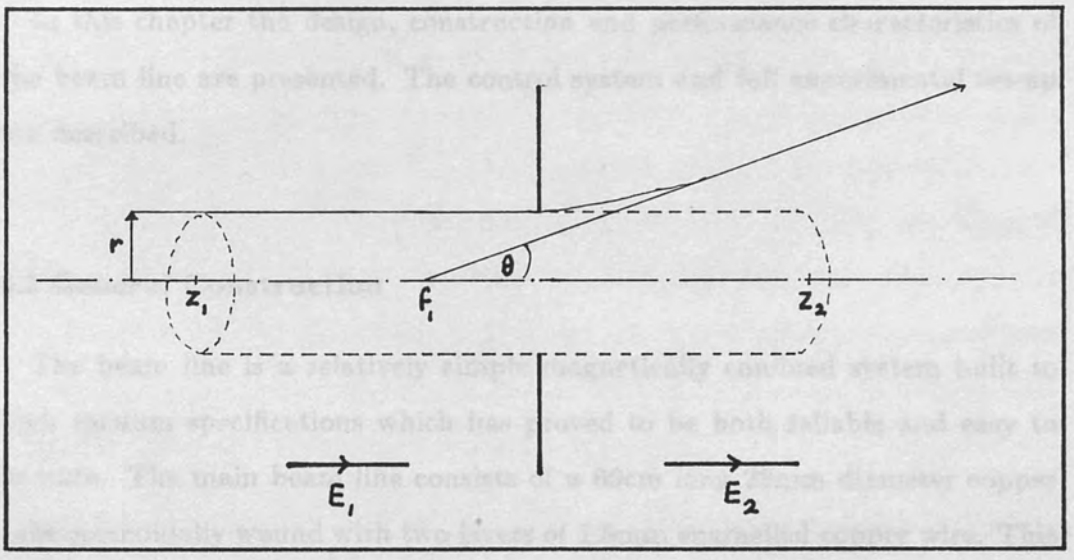

Figure 2.5

Calbick lens showing the cylinder construction used in evaluating the radial component of field by Gauss' law.

Chapter 3

Low Energy Positron Beam Spectrometer System

3.1 Introduction

The first slow positron beam built at Bedford College was originally developed as a prototype to test out various ideas before building the new cryostat system (Chapter 4). Figure 3.1 shows the beam as it was first used in single positron counting experiments. Since being commisioned for use in defect profiling measurements the system has been extended to include a furnace target chamber and a Doppler-broadening spectrometer system controlled by an Acorn BBC-B microcomputer (fig. 3.2). Temperature and voltage controllers designed and built by Mr. Leon Ellison of the departmental electronics workshop have been incorporated into the system allowing automatic operation.

In this chapter the design, construction and performance characteristics of the beam line are presented. The control system and full experimental set-up are described.

3.2 General Construction

The beam line is a relatively simple magnetically confined system built to high vacuum specifications which has proved to be both reliable and easy to operate. The main beam line consists of a 60cm long 28mm diameter copper tube solenoidally wound with two layers of 1.5mm enamelled copper wire. This is bent through an angle of 30^{o} to eliminate fast positrons from the target area. The solenoid produces a nominal field of 1.5 mT/A.

Correction for $\mathbf{R} \times \mathbf{B}$ drift is acheived by the use of a correction coil inclined at an angle of 60^{o} to the plane of the beam line. The horizontal axis of

the correction coil is approximately 15^o to both arms of the beam line. The calculated field at the centre of the coil is similar to that of the solenoid for a given current.

Connection to the source and target chambers is made using 1 inch screwed demountable unions with neoprene 'O' ring seals. The different chambers used are made from brass. Electrical connections are for the most part via vacuum BNC and HV-BNC sockets. The magnetic field is extended into the source and target regions by Helmholtz coils with the same nominal field strength as the solenoid. Because of the large difference in coil diameters there is a large calculated mismatch in axial field strengths (fig. 3.3) between the solenoid and Helmholtz coils but this does not appear to have any detrimental effect on beam transmission.

3.2.1 Moderator Assembly

The moderator assembly is shown in the inset in figure 3.1. the moderated positrons are collected by an electrostatic field defined by the source, moderator and the beam entrance grid. The source, on the end of a perspex rod, is held in contact with its mounting ring held at a potential V_s. The rod forms a vacuum seal to the outside world through a double 'O' ring seal. The source is a standard sealed ^{22}NaCl capsule with a thin tungsten window from Amersham. Its mounting ring has a 45^o chamfer to match that of the capsule window and is isolated form the moderator by a perspex ring.

The moderator is 100×105 lines per inch tunsten mesh supplied by Unique Wire Weaving of New Jersey annealed at $2\ 000^o$C at 10^{-4} torr for 90s. In the initial experiments reported below a single piece was used although currently two pieces overlaid at 45^o to each other are used. The moderator and its mounting ring are held at a potential V_m and isolated in turn from the entrance grid by a perspex ring. The mounting ring has a 45^o inward chamfer to increase

electrostatic field convergence to collect positrons emitted at wide angles. The spacing is such that a field line starting at the edge of the moderator window will finish at the centre of the entrance grid. The only drawback with this system is that a higher moderator voltage is required to achieve the necessary field penetration into the shadowed region of the moderator; 6V compared with 1.5V for the cryostat system which has a more open moderator geometry.

The entrance grid, 200 centres per inch copper micromesh from Thorn EMI, is held in contact with the beam line at earth. Hence the moderator region is defined by three equipotential planes: the source at V_s, the moderator at V_m and the entrance grid. Moderated positrons in the beam line will have a minimum longtitudinal momentum component corresponding to a kinetic energy V_m. Transverse components will depend on the energy and angle of emission. Any slow positrons emitted in the reverse direction are repelled back towards the beam line by the potential barrier $V_s - V_m$. The source potential makes no contribution to the kinetic energy of the beam line, only to the collection efficiency. The moderator voltage, however, does affect both efficency and energy.

3.3 Beam Characteristics

The performance characteristics of the beam have been evaluated using a single channel electron multiplier (CEM) in the target chamber of the beam line. In addition to slow positron measurements the fast positron and secondary electron intensities were measured. By reversing all the potentials between the source and the CEM cathode, but keeping the voltage drop across the detector constant the beam line can be made to transmit the secondary electrons emitted by the moderator. The fast positron transmission can be observed by simply applying a large negative bias to the moderator. When optimised the respective count rates for a 700 μCi source with a single moderator mesh are 1 200, 6 and

130 000 cps for slow, fast positrons and electrons. This corresponds to a total conversion efficiency of 4.7×10^{-5} or taking the source geometry into account an efficiency of 3.8×10^{-4}.

The slow positron yield is constant for a potential difference $V_s - V_m$ greater than 2V (fig. 3.4) irrespective of the absolute moderator potential. This correlates with the calculated value of the positron work function for tungsten (Nieminen & Hodges 1976) of 2.1eV. A similar esimate of the positron emission energy is given by a direct measurement of count rate versus moderator potential. For a negative potential greater than the work function no moderated positrons can escape from the moderator and a sharp cut-off was observed at $V_m = -2$V (fig. 3.5). In addition there is a levelling off of the count rate for moderator potentials above 5V. This threshold value is probably dependent on the moderator geometry as well as the slow positron emission energy.

The optimum values of solenoid and correction coil currents are interdependent and both need to be optimised concurrently. As the solenoidal field is increased so a larger correction field needs to be applied. Conversely too strong a correction will force the positrons off axis and ultimately into the wall of the tube. Optimum settings for these are 2.5A in the solenoid (fig. 3.6) and 1.5A correction (fig. 3.7).

3.4 Spectrometer System

3.4.1 Target Chamber

For use with a Doppler-broadening spectrometer system the beam line is equipped with a target chamber incorporating a tungsten wire heater, shown in figure 3.8. This is the latest, and most successful, in a series of trial designs although problems still occur when trying to operate at high temperatures *and* at high target biases. When cold the target chamber can be operated in the

range 0-15kV and the furnace can easily heat samples to in excess of 1000K.

The furnace is wound non-inductively from 36 swg pure tungsten wire on a pyrophylite former and encased in fire-cement. The temperature is measured with a T1-T2 thermocouple in a cavity by the sample holder. Ordinarily this should not be in electrical contact with the sample but as a precaution it is optically isolated from its controller. Heat is conducted to the sample by the hollow copper lens element which also serves to keep the sample in a field free region. The outer chamber is water cooled allowing the backplate to be as near as possible to the sample holder, resulting in the detector being less than a centimetre from the sample.

Earlier designs of sample holder had a complete Faraday cage but by removing all grids from the region and incorporating a diaphragm to prevent defocussing the total photon count rate has been improved by a factor of three. Currently at 1kV the total count rate is 1 000 cps above a background of 300 cps for a 123MBq source. Typically the background contributes 3% to the 511keV peak intensity, with 1.5 million counts recorded in the peak over two hours at high biases. Reemitted positrons are most likely to annihilate at the entrance to the target chamber and so will contribute less than 10% of the measured count rate.

3.3.2 Control and Detection System

The complete spectrometer system (fig. 3.9) is controlled from an application running on an Acorn BBC model B microcomputer written in JWB Forth (an extension to the FIG-79 standard). A complete listing is given in appendix 1. The application is menu driven allowing cycling of both temperature and target bias.

The spectrometer consists of an intrinsic Ge coaxial detector and a stabilised Silena Cicero 8K multichannel analyser (MCA). The MCA is fitted

with a bidirectional serial (RS232C) interface allowing easy control from a microcomputer. This is connected to the RS432 serial interface on the BBC-B. Start, stop and reset commands are simple ASCII strings sent from the computer. Data transfer is through the same interface using ACK/NACK protocol. After the contents of each channel are transferred as 6 ASCII characters the MCA waits until the computer sends an acknowledge code. Such rigorous handshaking prevents loss or corruption of data which can occur due to buffer overflow.

The heater is powered from the mains electricity supply through a variac, the output of which is switched by a solid state relay connected to the furnace controller. This takes for its command an 8-bit word, from the BBC user interface, corresponding to a value 0-1000 °C. Once the required temperature has been set all control is autonomous although the temperature is monitored on one of the BBC analogue inputs. The controller employs a standard thermocouple amplifier with its own internal reference giving a linear output with temperature for a type K (T1-T2) thermocouple.

The voltage controller is controlled from the BBC printer port and has 14-bit accuracy in the range -10 to +10kV giving a resolution of 1.22V per bit. As the BBC microcomputer has only an 8-bit data bus the controller has to be latched and 6 words need to be used to set the value. The output voltage can be monitored by connecting the output from a voltage divider to one of the computer analogue inputs.

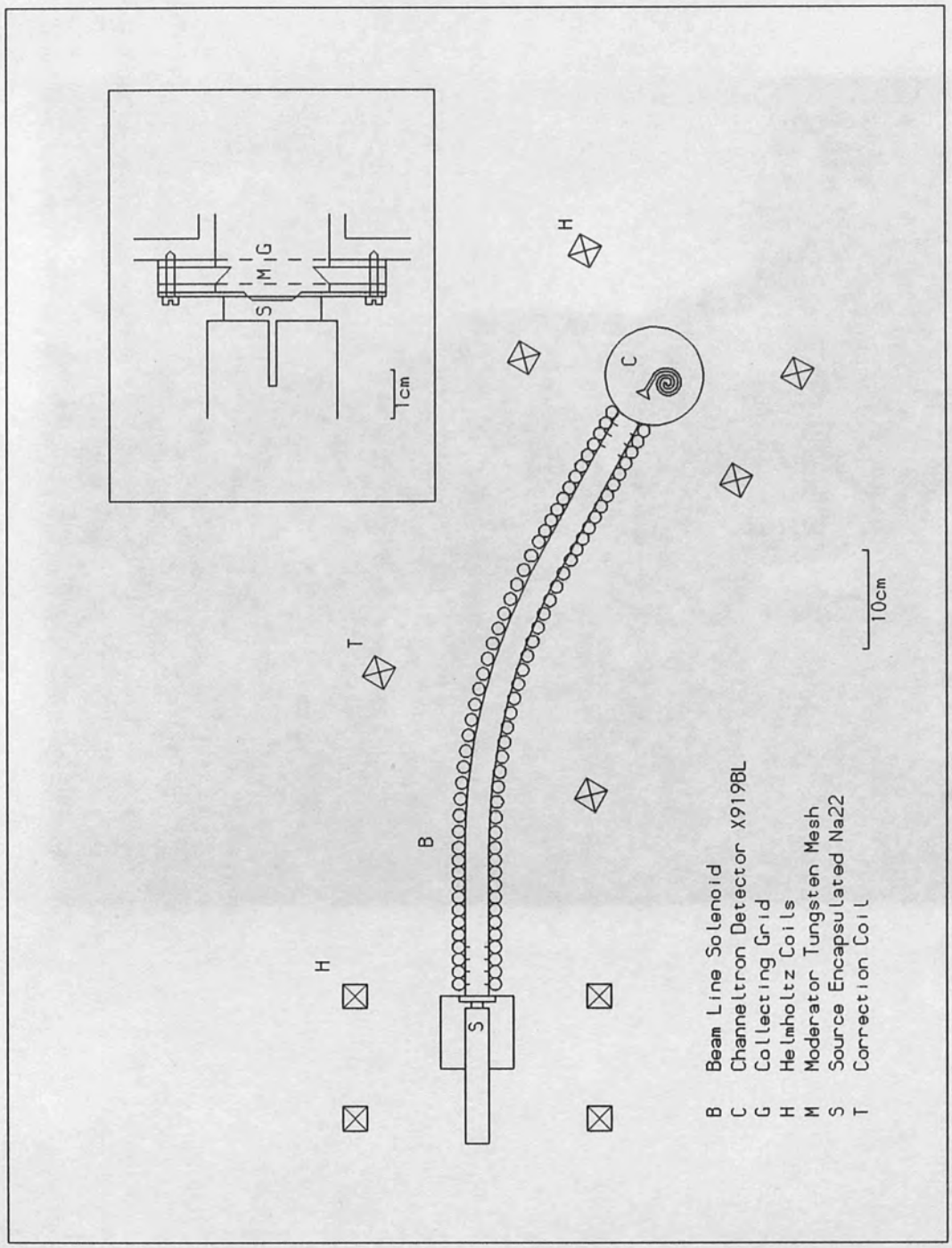

Figure 3.1

The development low energy positron beam as was originally used for single positron counting. The source-moderator assembly is shown in the inset.

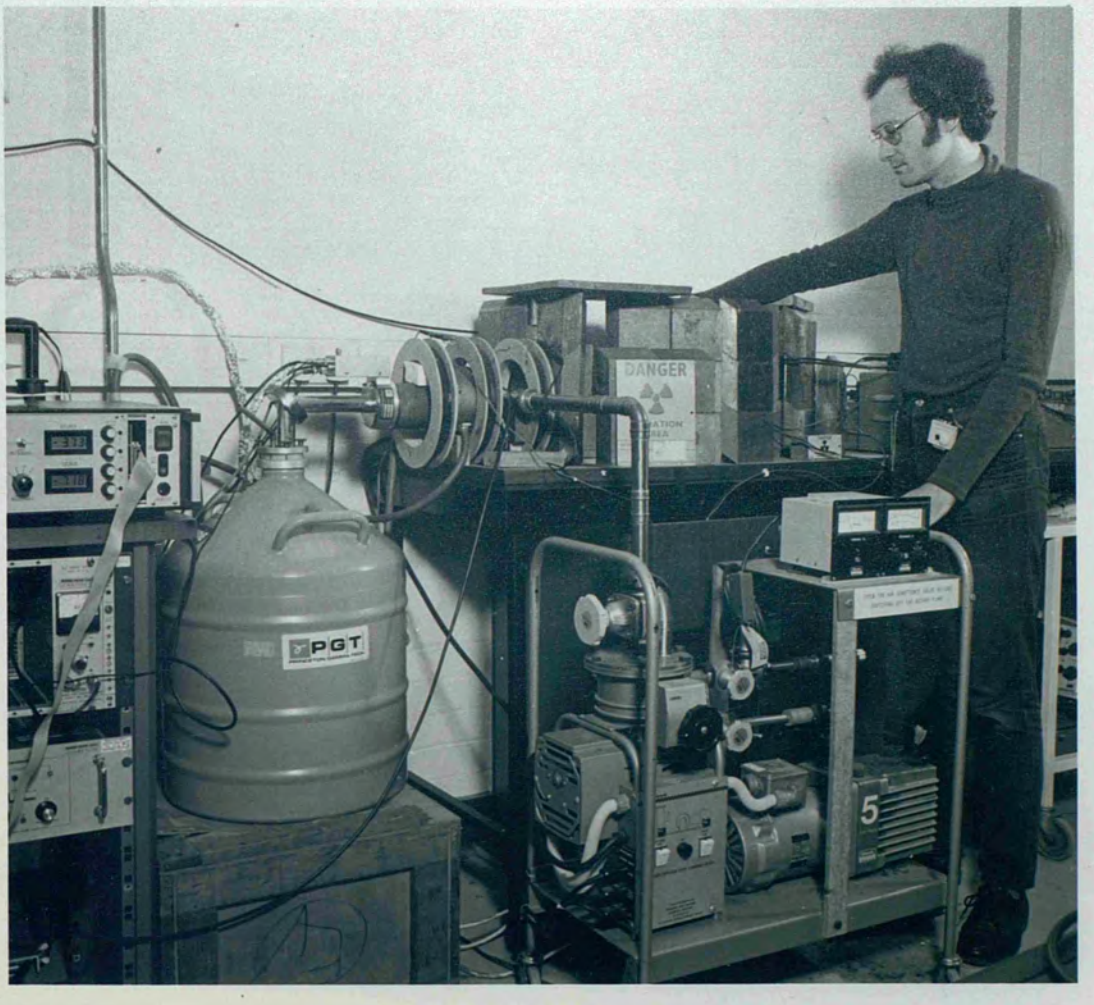

Figure 3.2

Low energy positron beam spectrometer system showing target chamber (centre), Ge detector and automated voltage controller (left).

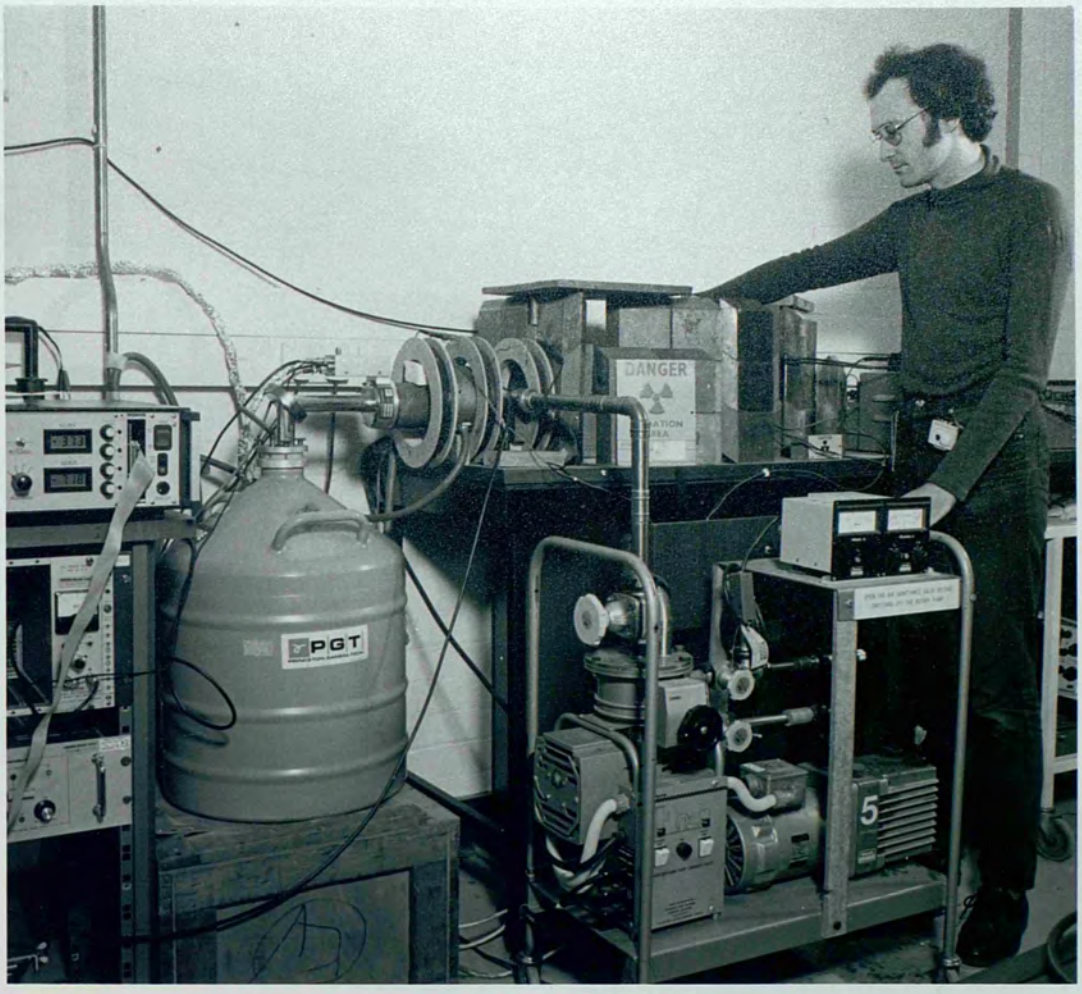
DANGER
PGT
5

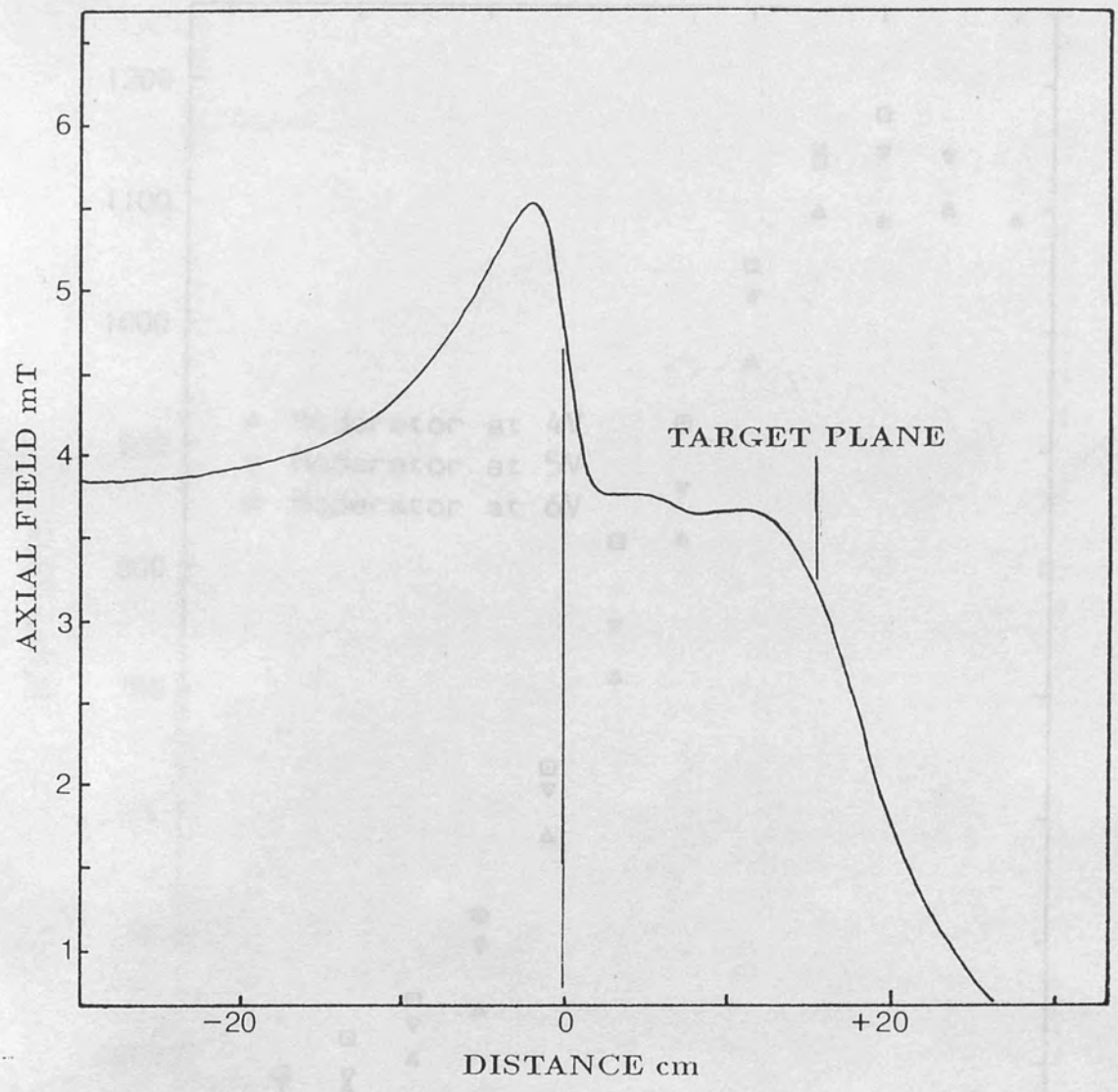

Figure 3.3

Calculated axial magnetic field excluding correction field. Distance is measured from the exit of the solenoid.

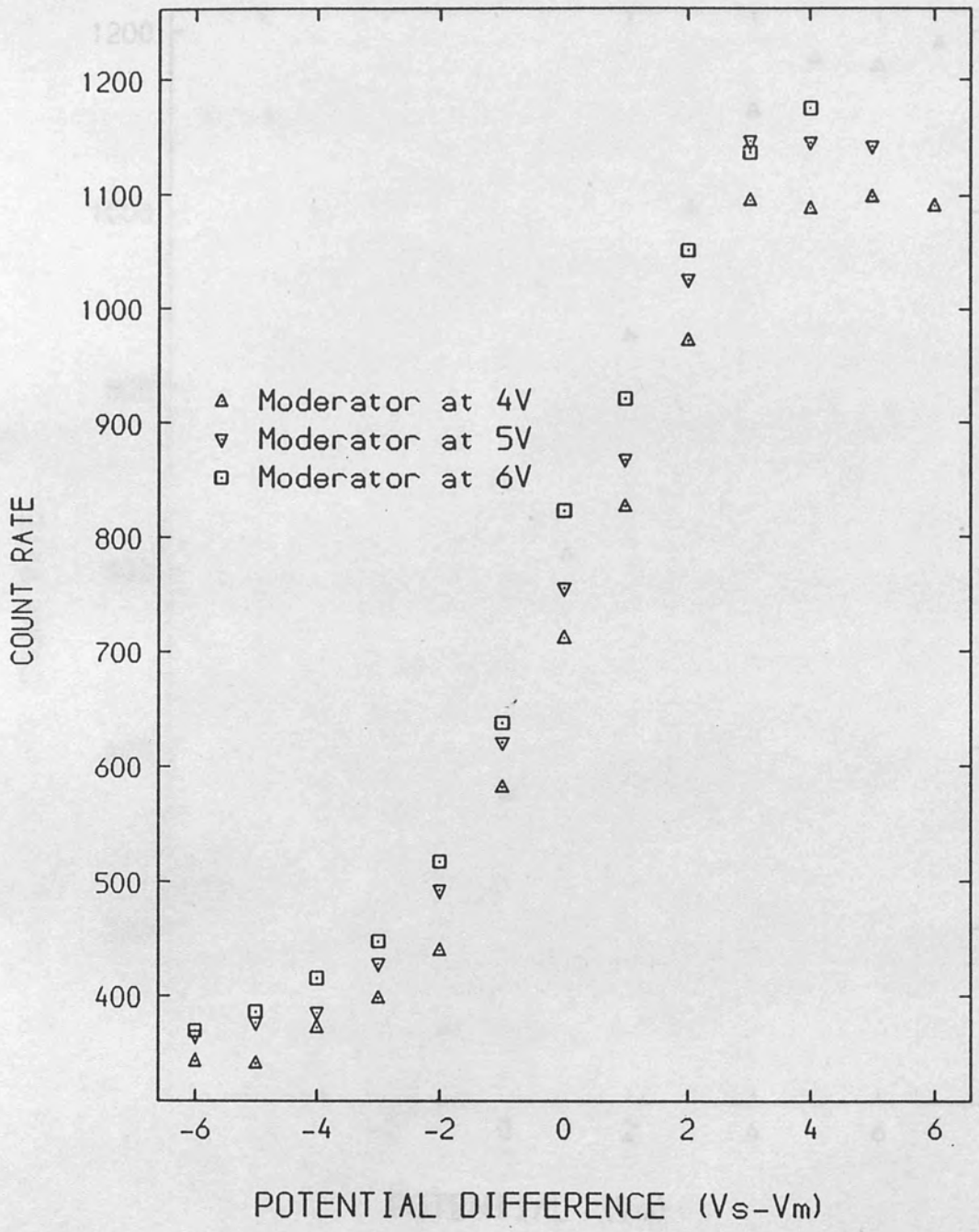

Figure 3.4

The effect of a potential applied to the source on the total count rate for different moderator potentials.

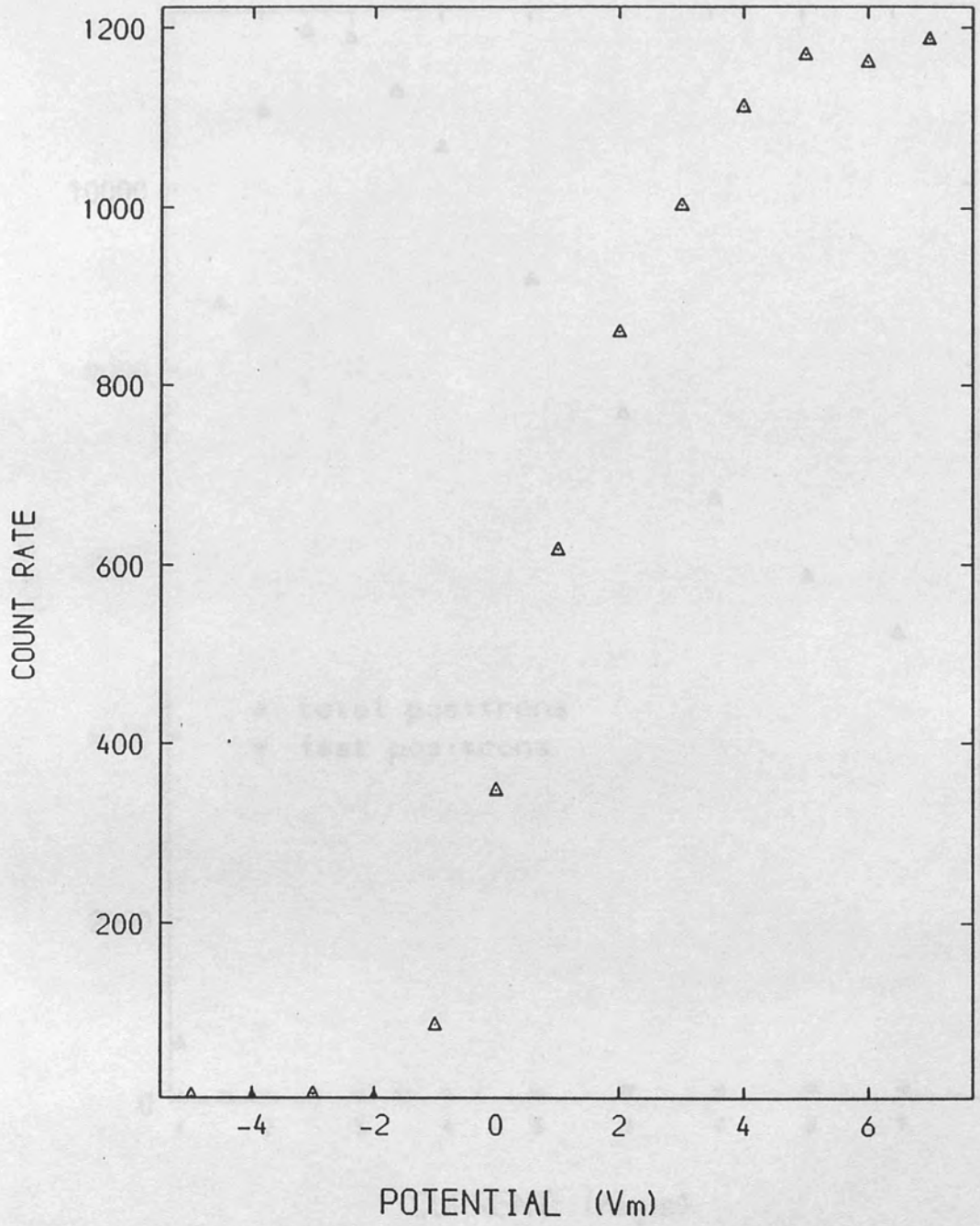

Figure 3.5

The effect of the moderator potential on the total count rate.

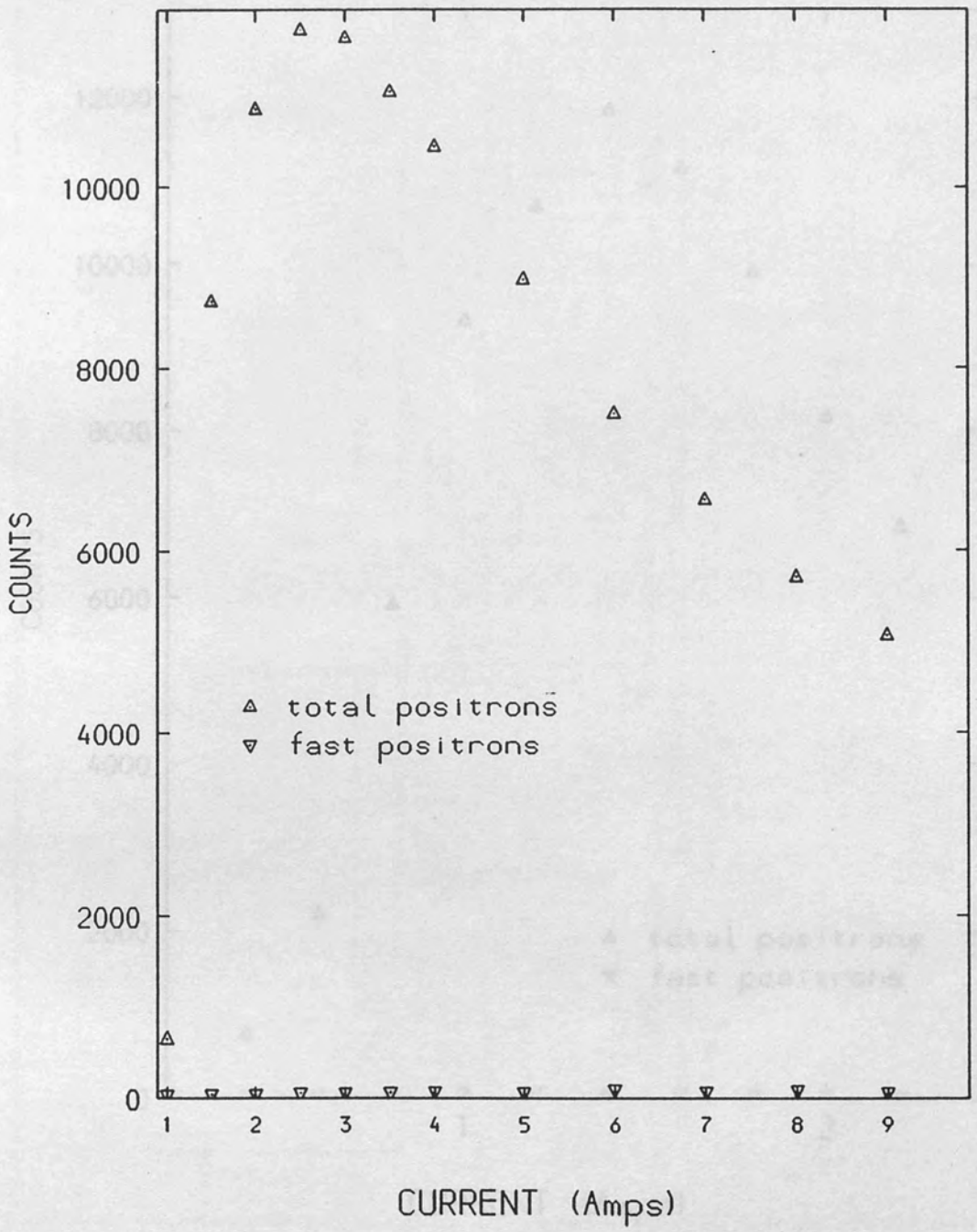

Figure 3.6

The variation of total and fast positron count rates with the solenoid current.

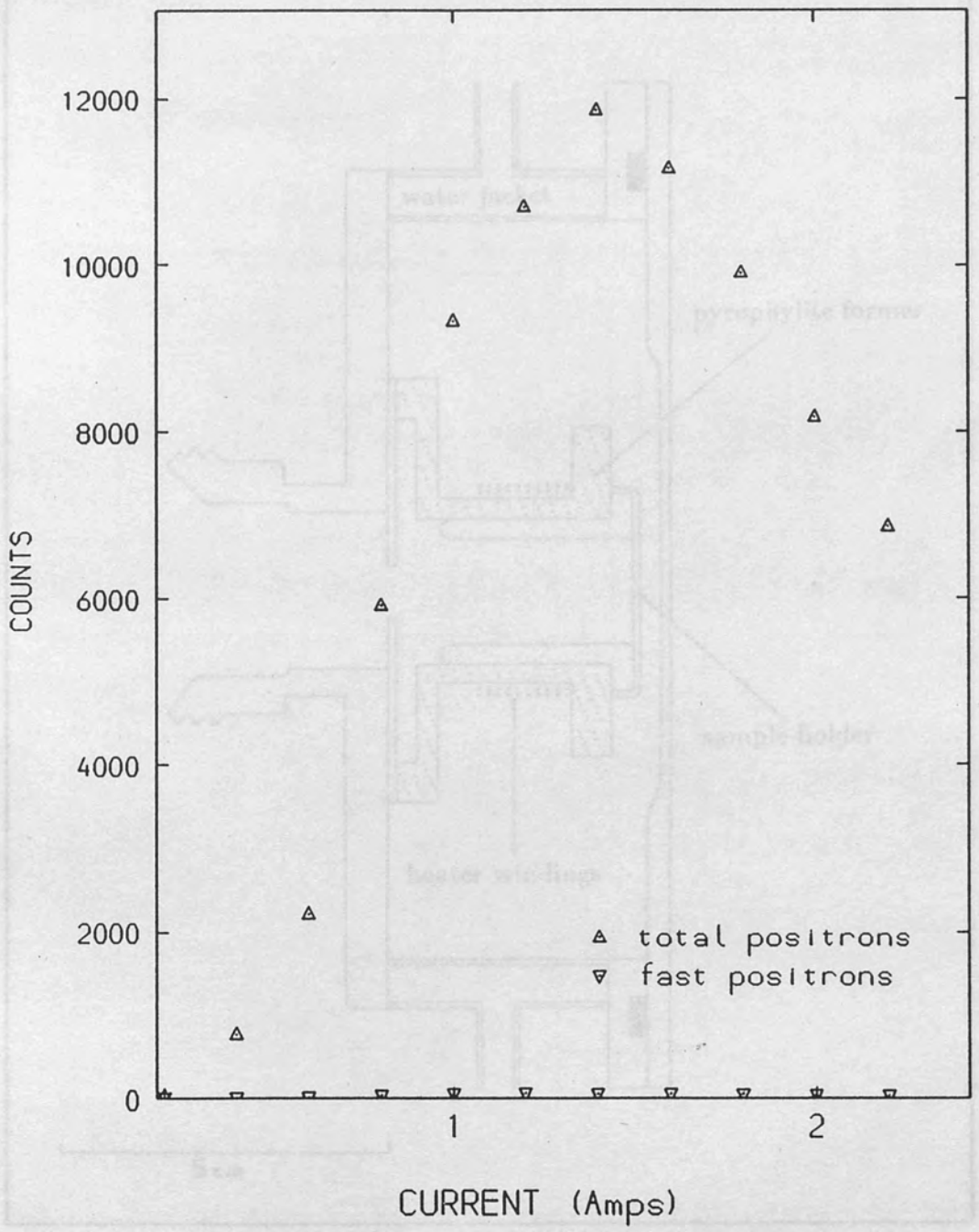

Figure 3.7

The effect of the correction coil current on total and fast positron count rates.

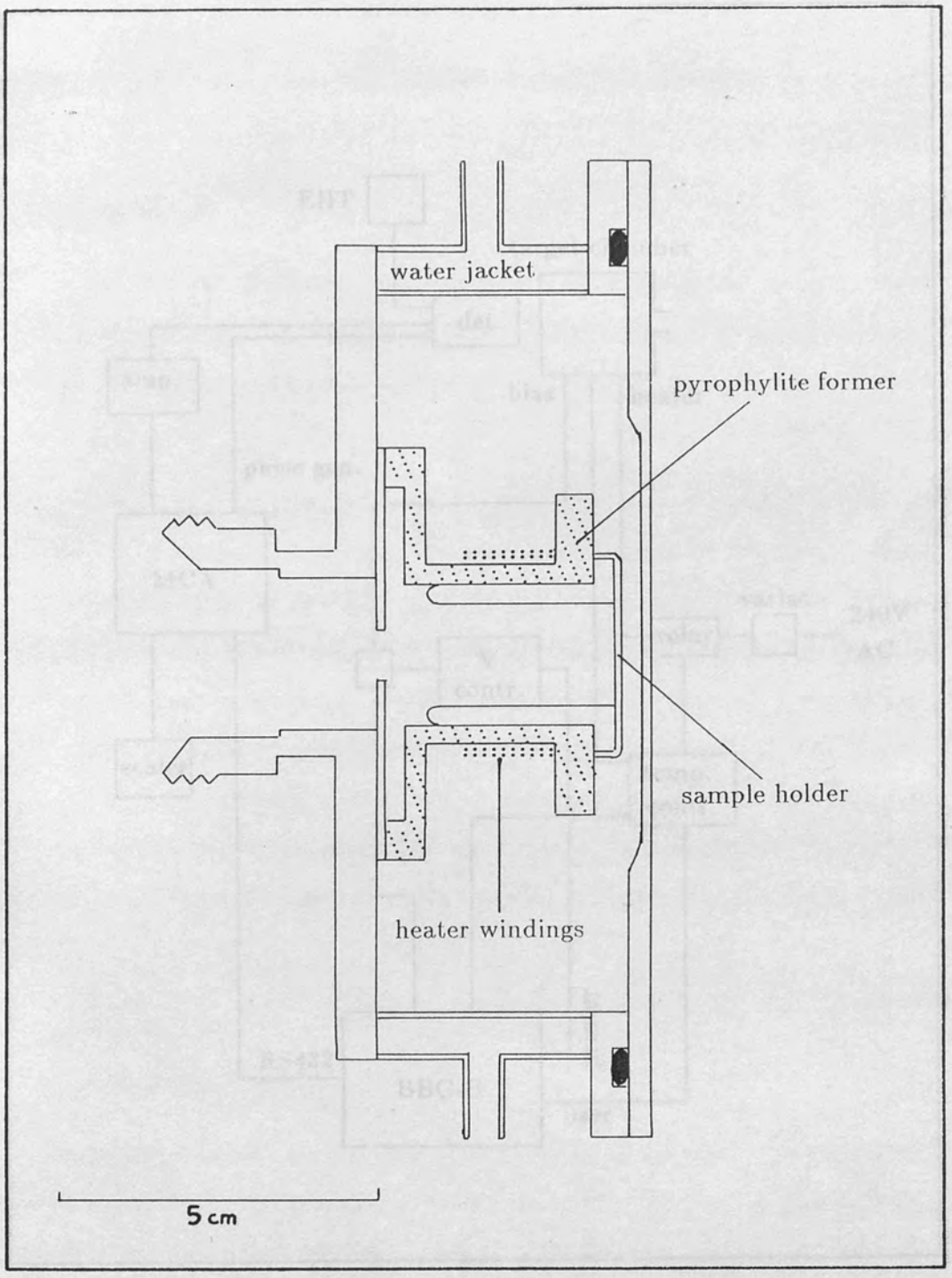

Figure 3.8

Furnace target chamber for low energy positron beam.

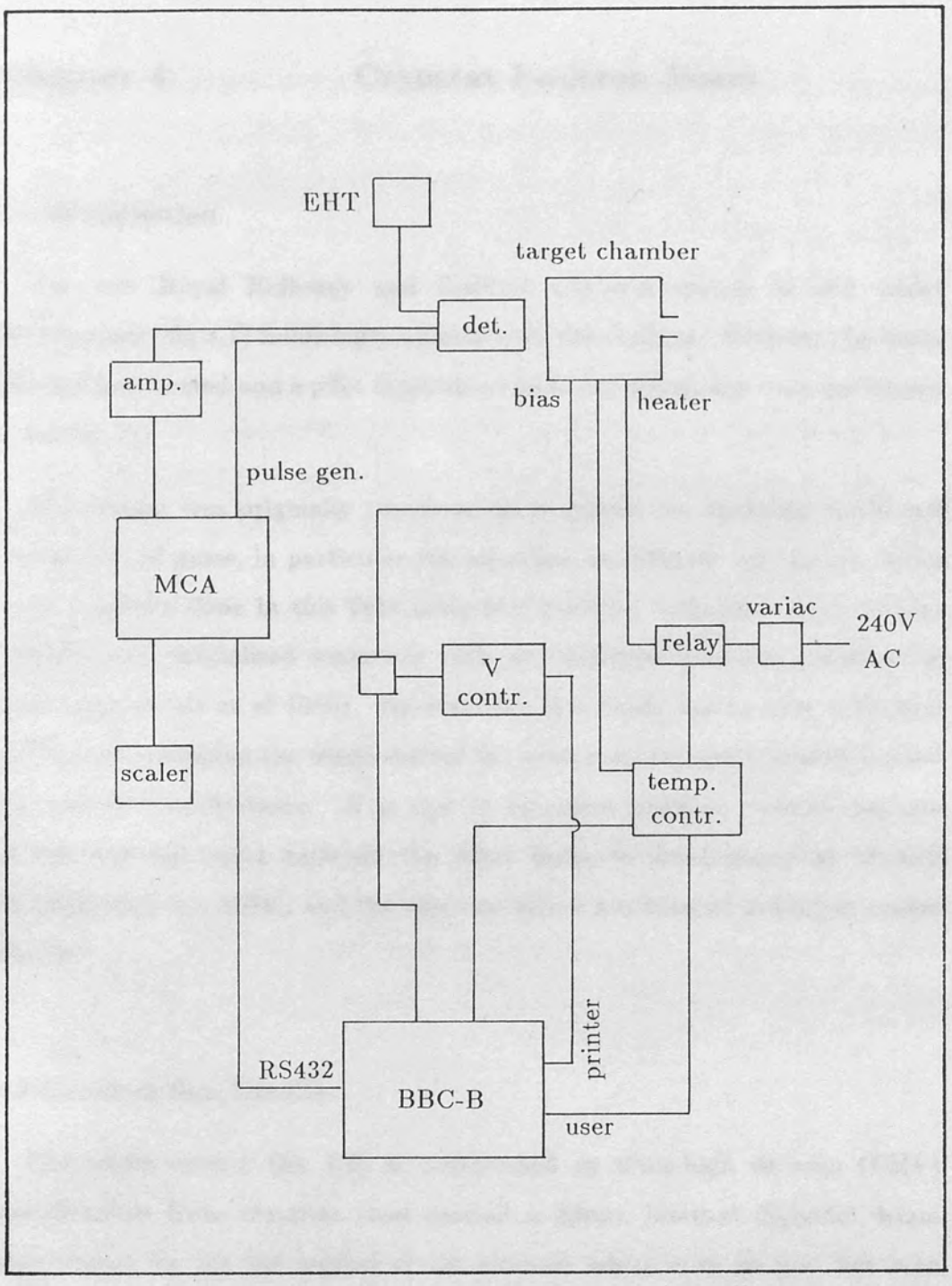

Figure 3.9

Low energy positron beam spectrometer and control system.

Chapter 4 Cryostat Positron Beam

4.1 Introduction

The new Royal Holloway and Bedford Cryostat system is still under development (fig.4.1) following problems with the cryostat. However the beam line has been tested and a pilot experiment on liquid metals has been performed (Chapter 7).

The system was originally conceived as a system for studying condensed monolayers of gases, in particular He, adsorbed on different substrates. Some work has been done in this field using fast positron techniques with powder samples and specialised materials such as exfoliated graphite (Jean et al 1985, Rice-Evans et al 1986). By necessity this beam has to have a vertical configuration making the whole system far more compact and versatile beyond its original specifications. It is one of two slow positron systems capable of investigating liquid surfaces, the other being in development at Munich (Schödlbauer et al 1986), and the only one with a potential of looking at cooled liquids.

4.2 Construction Details

The whole system (fig 4.2) is constructed to ultra-high vacuum (UHV) specifications from stainless steel around a 23mm internal diameter beam pipe except for the tail section of the cryostat which is of oxygen free high conductivity copper. Pumping is acheived with a trapped Edwards E02 50mm diffusion pump with a calculated resultant pumping speed for the system of $1l/s$. Once vacuum conditions have been obatined the system can be isolated and controlled quantities of gas can be administered.

The present cryostat is a modified Oxford Instruments MD4 which has an all stainless steel construction. The bottom section of the beam line is fixed in good thermal contact with the inner (helium) reservoir. Pumping on the helium will allow the sample to be cooled to below 2K. In addition a small heater stage, on which the sample is mounted, enables heating up to 450K. The sample holder is electrically isolated from the rest of the system allowing potentials up to several keV to be applied. The restricted space in the cryostat makes very high voltages impractical, particularly when liquids with a high vapour pressure are studied. As with the prototype system (Chapter 3) the thermocouple will be optically isolated from its monitor to a minimum of 10kV.

The magnetic fields are generated by a hybrid system of Helholtz type coils and a solenoid with an additional correction coil on a double axis to compensate for $\mathbf{R} \times \mathbf{B}$ drift (Kaupilla et al 1977) and slight misalignments. The field along the axis of the cryostat has been calculated to be constant to within 3% (fig. 4.3) for a coil separation of 95% of the Helmholtz spacing. There is however a large mismatch with the solenoid field because of the greatly differing radii but this does not appear to have an adverse effect on beam transmission. The solenoid is doubly wound with 1mm copper wire producing a nominal field of 2.5mT/A. The other coils, wound from the same wire, produce similar field strengths.

4.2.1 Moderator Assembly

Moderation of positrons is acheived using woven 100 $\times$ 105 lines per inch tungsten mesh annealed at 10^{-4} torr for 90s. In the single positron counting experiments reported below a single mesh was used, although in the pilot profiling experiments this was changed for a double mesh. The source is held on the end of a PTFE rod pushed into contact with its mounting plate and electrically isolated from both the beam line and the moderator. Electrical

connections to the outside world are still via vacuum BNC sockets but the neoprene 'O' ring seals have been replaced by viton.

All sources used are standard sealed ^{22}Na units supplied by Amersham International allowing easy interchange between the two beam lines. The source capsule subtends a solid angle of $\pi/2$ steradians with the moderator over a circular area of 8mm diameter.

The moderator assembly (fig. 4.4) has been designed to give limited focussing and maximum electric field penetration. Although the separation between the moderator and the collection grid is twice that of the beam described in the previous chapter, considerably lower moderator voltages are required. The moderator electrode and source mounting ring are manufactured from stainless steel and all insulating components are PTFE. The collecting grid is 200cpi copper micromesh from Thorn EMI.

4.3 Evaluation of Beam Characteristics

For single positron counting the outer tails of the cryostat were removed and the sample holder was replaced with a chamber housing a channel electron multiplier array (CEMA) detector. This detector, shown schematically in figure 4.5, consists of a matched pair of CEMA plates and a phosphor (P20) screen oversilvered with aluminium. An independent bias was applied to the cathode, anode and the screen with a pulse being taken of the anode.

The beam, as observed with the phosphor (fig. 4.6) is roughly circular with a diameter of 7mm. An 18.5 Mbq (500 μCi) sources produces a count rate of 410cps in the detector with a dark count of 10cps. Assuming 100% detection efficiency and taking into account the source geometry this corresponds to an effeciency of 2×10^{-4}. The beam transmission characteristics are remarkably flat with respect to the solenoid current (fig. 4.7) showing a broad peak around

2A. A considerably lower current is needed in the Helmholtz coils around the cryostat, maximum transmission is acheived below 1A.

In this system collection and transmission of slow positrons depends greatly on the electrostatic fields at the moderator. The maximum number of positrons are observed at the detector when the moderator potential is around 1.5V for a single mesh (4.8). When the system was used with a double mesh in the pilot experiments the maximum annihilation rate measured with the Ge detector was for a moderator potential of 3V. This is probably due to the reduced field penetration as the two moderators effectively screen each other from the fields each side of them. The source potential however has no additional effect above 2.5V greater than the moderator potential.

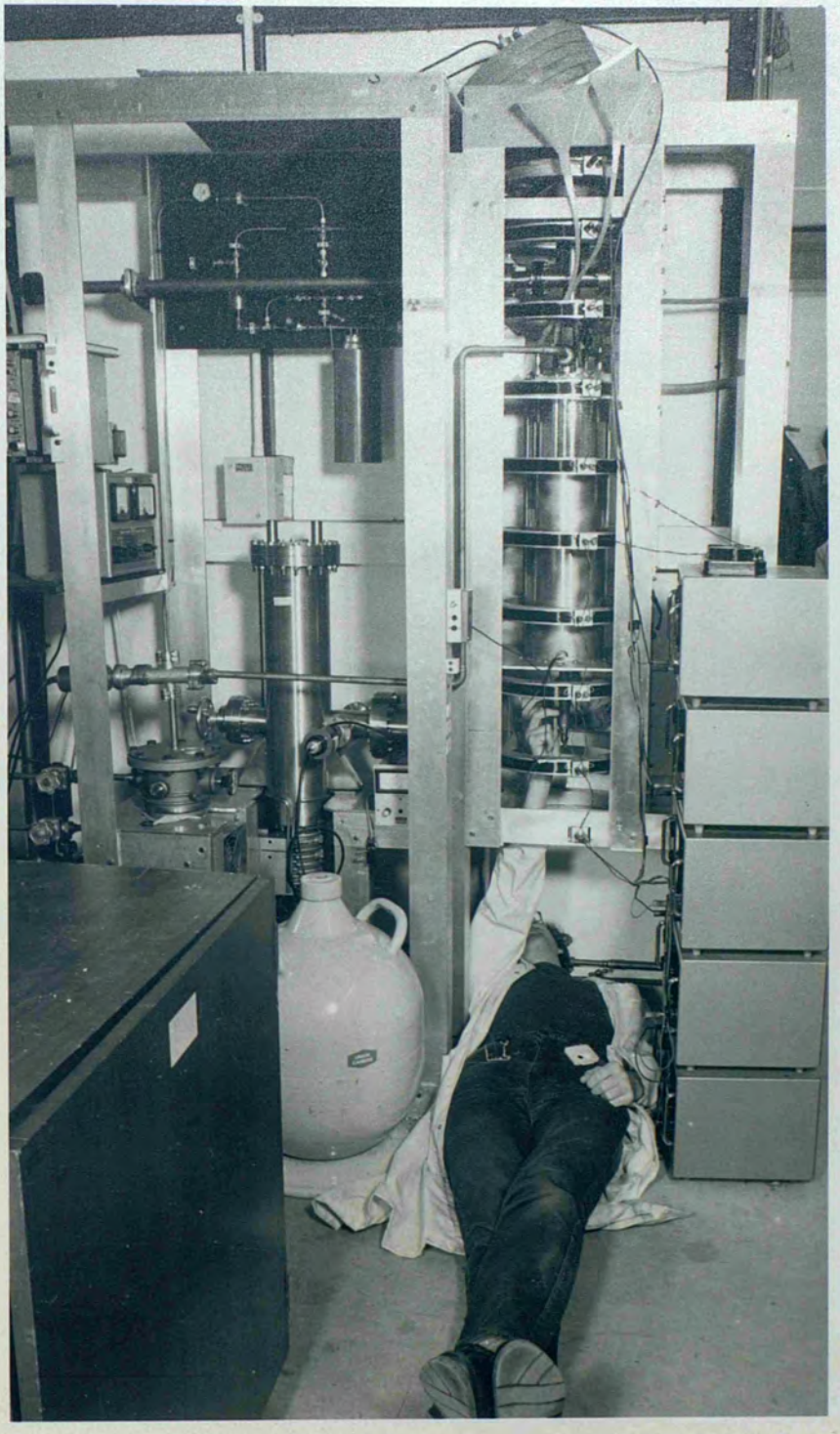

Figure 4.1

The cryostat positron beam under development at Royal Holloway & Bedford New College.

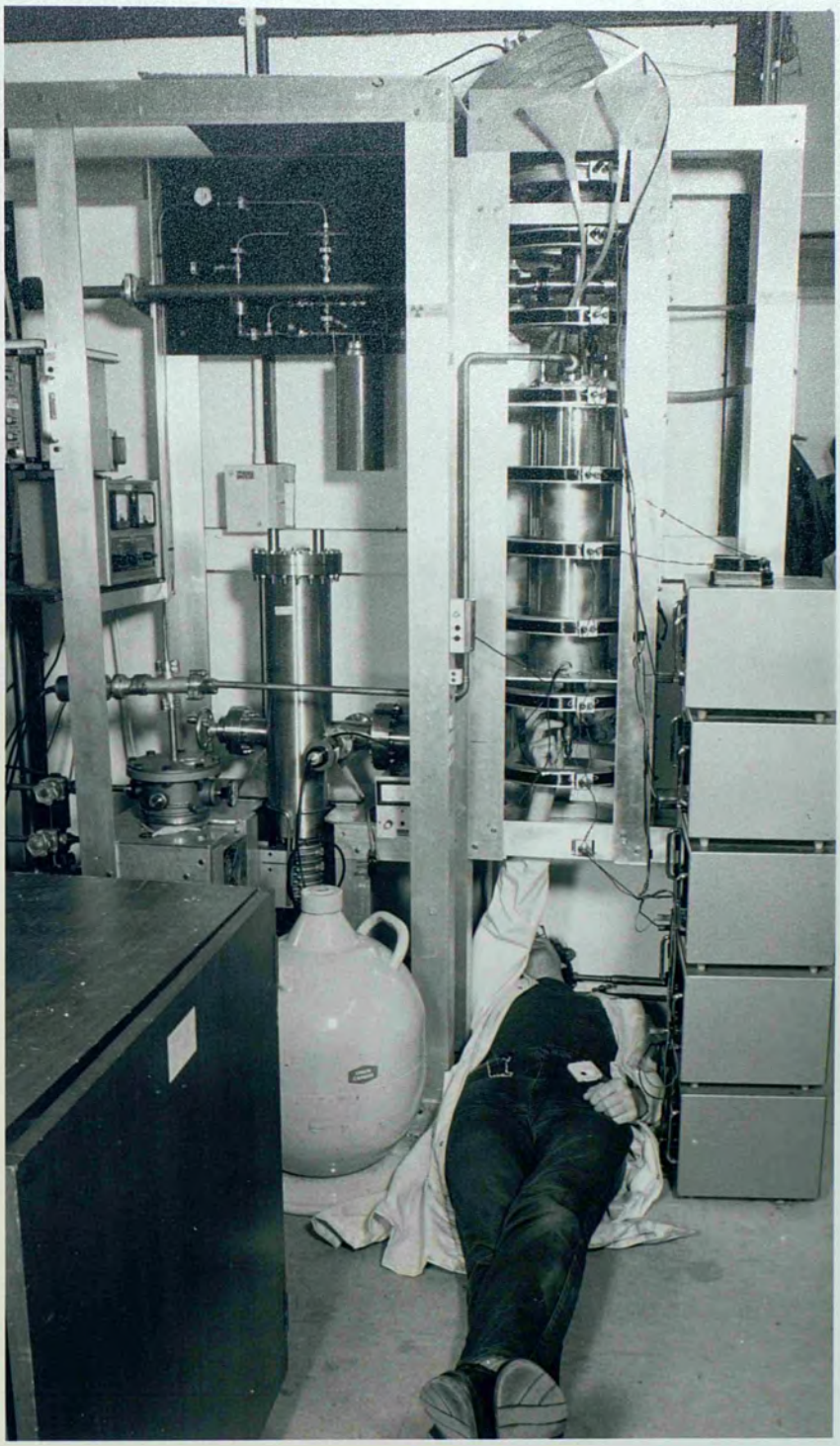

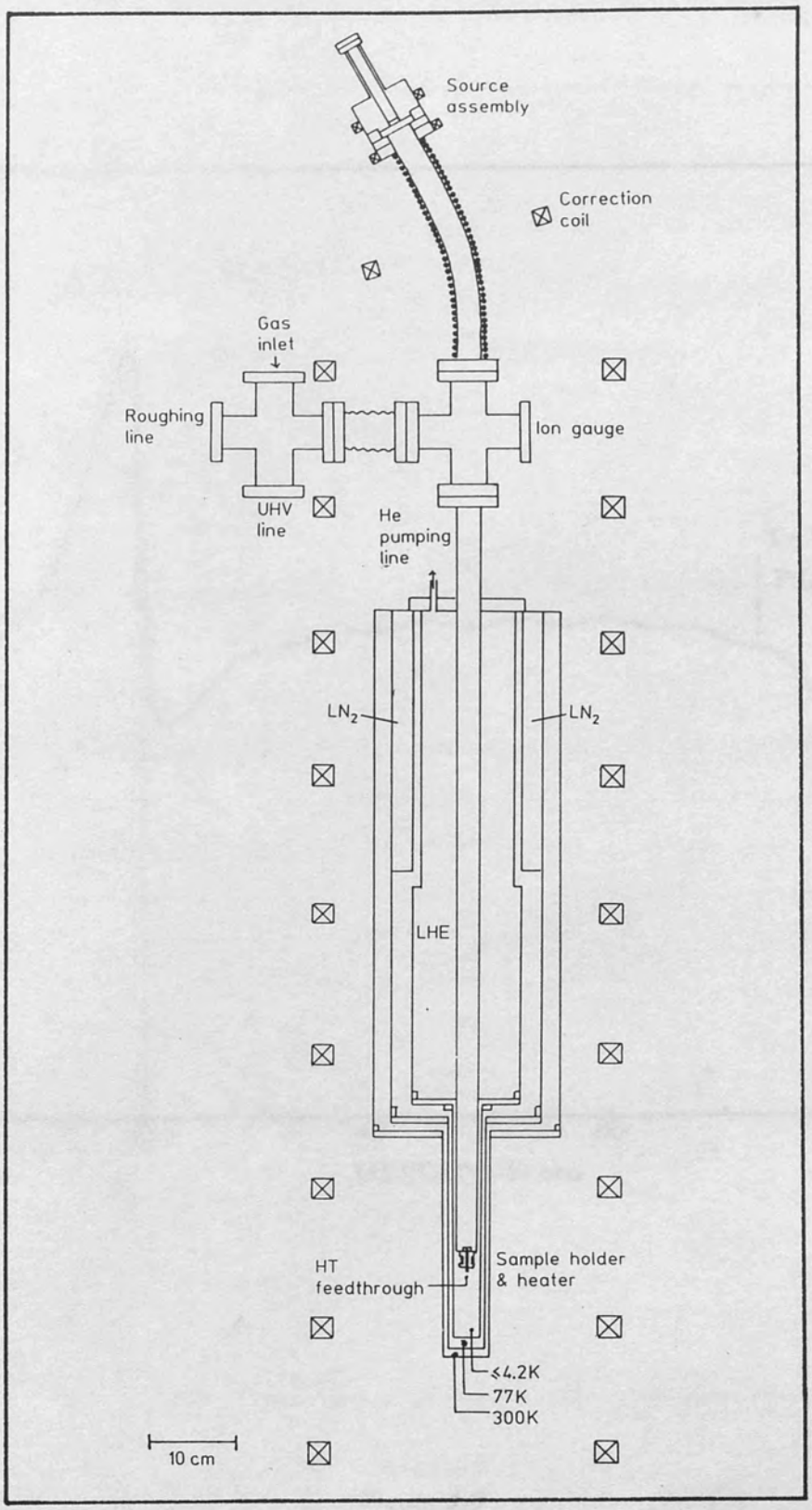

Figure 4.2

Schematic diagram of the cryostat positron beam.

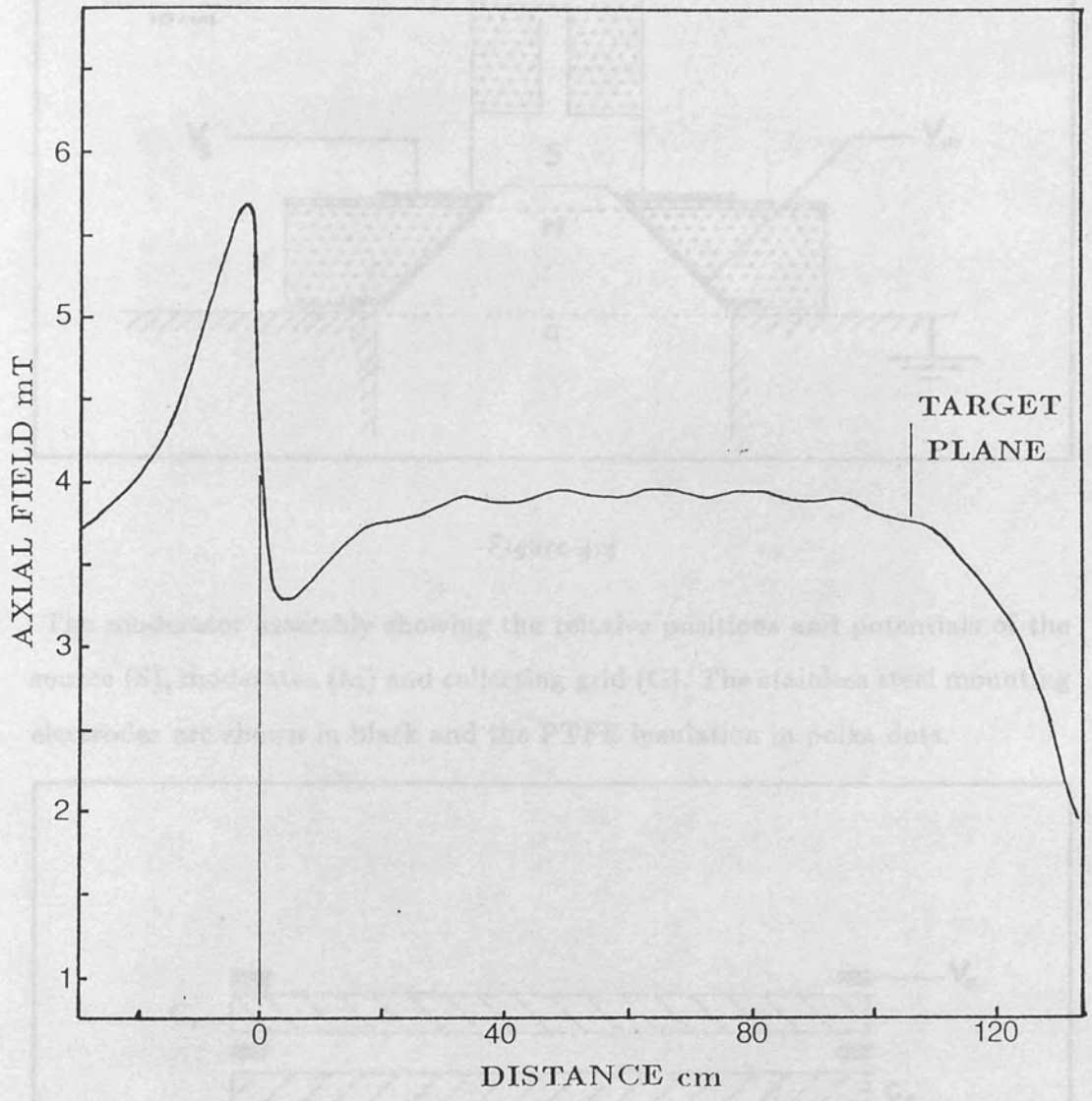

Figure 4.3

Calculated axial field strengths excluding correction field for cryostat. Distance is measured from the exit of the solenoid.

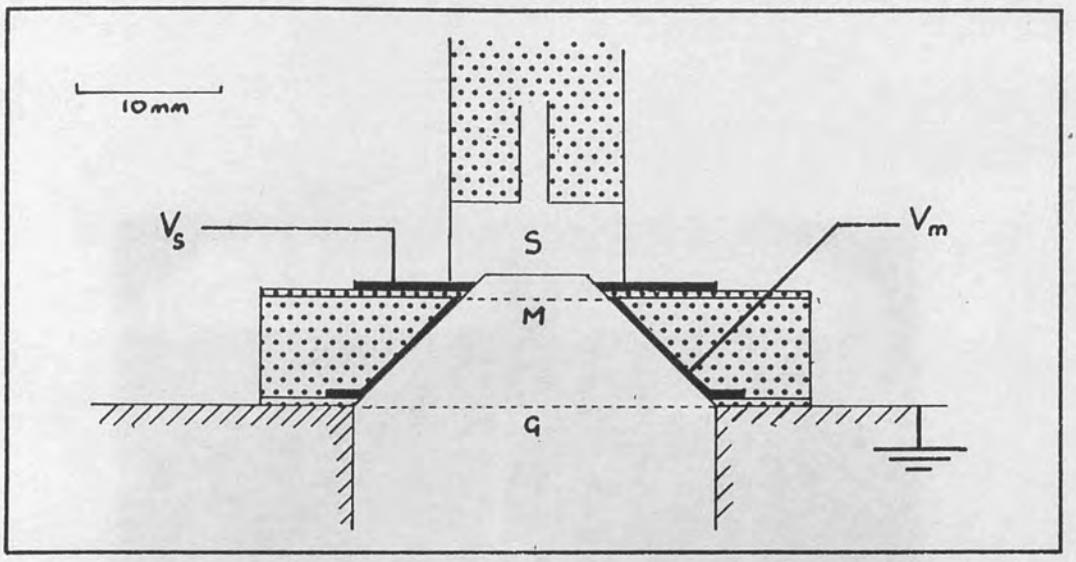

Figure 4.4

The moderator assembly showing the relative positions and potentials of the source (S), moderator (M) and collecting grid (G). The stainless steel mounting electrodes are shown in black and the PTFE insulation in polka dots.

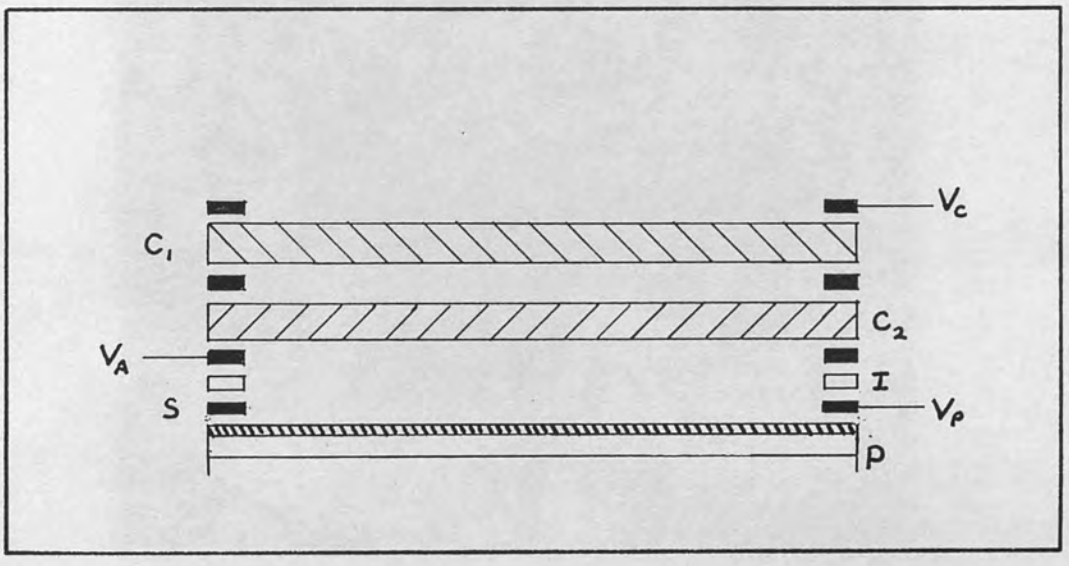

Figure 4.5

Schematic diagram of the detector with a matched pair of CEMA plates (C_1 & c_2) and Al coated phosphor screen (P). These are mounted with stainless steel (S) and PTFE shims (I).

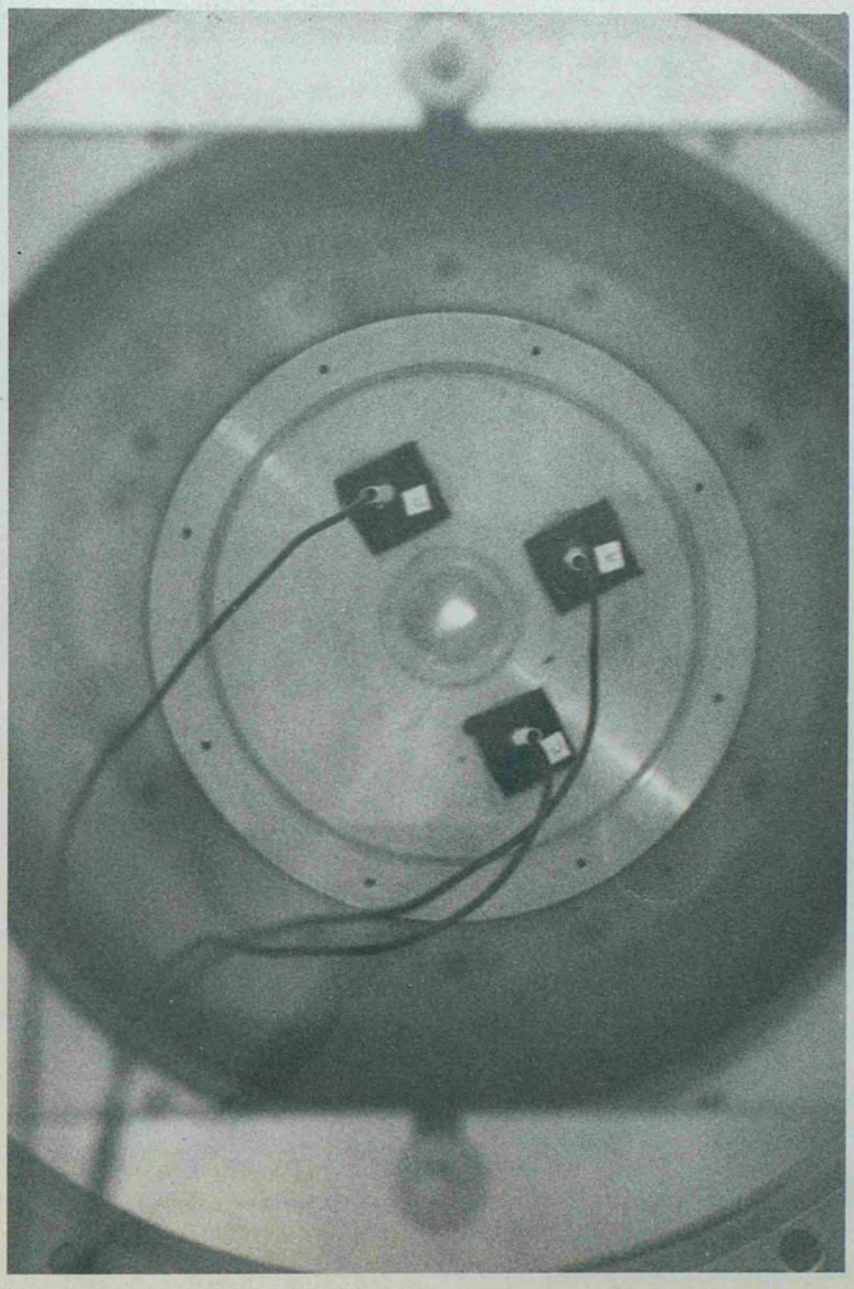

Figure 4.6

The image of the positron beam as seen with the CEMA plate detector.

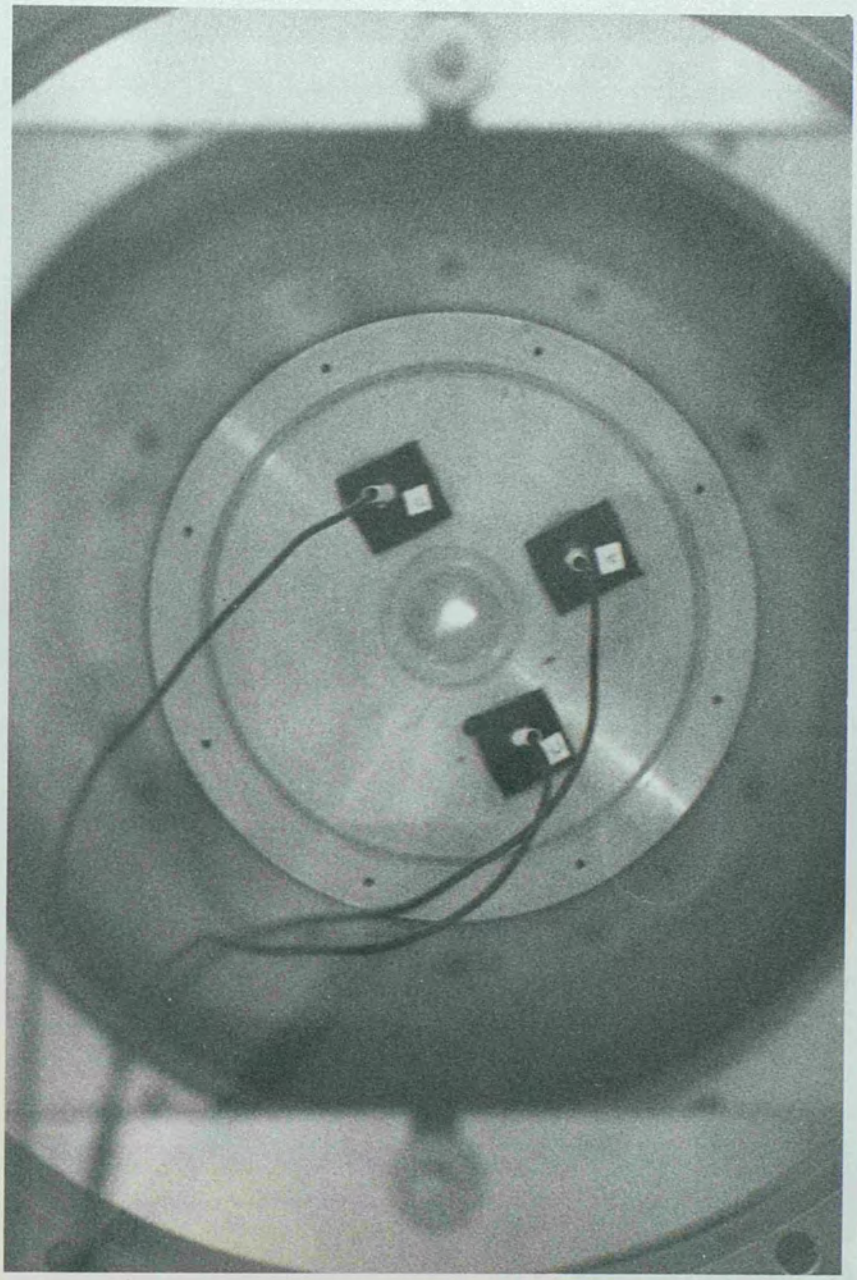

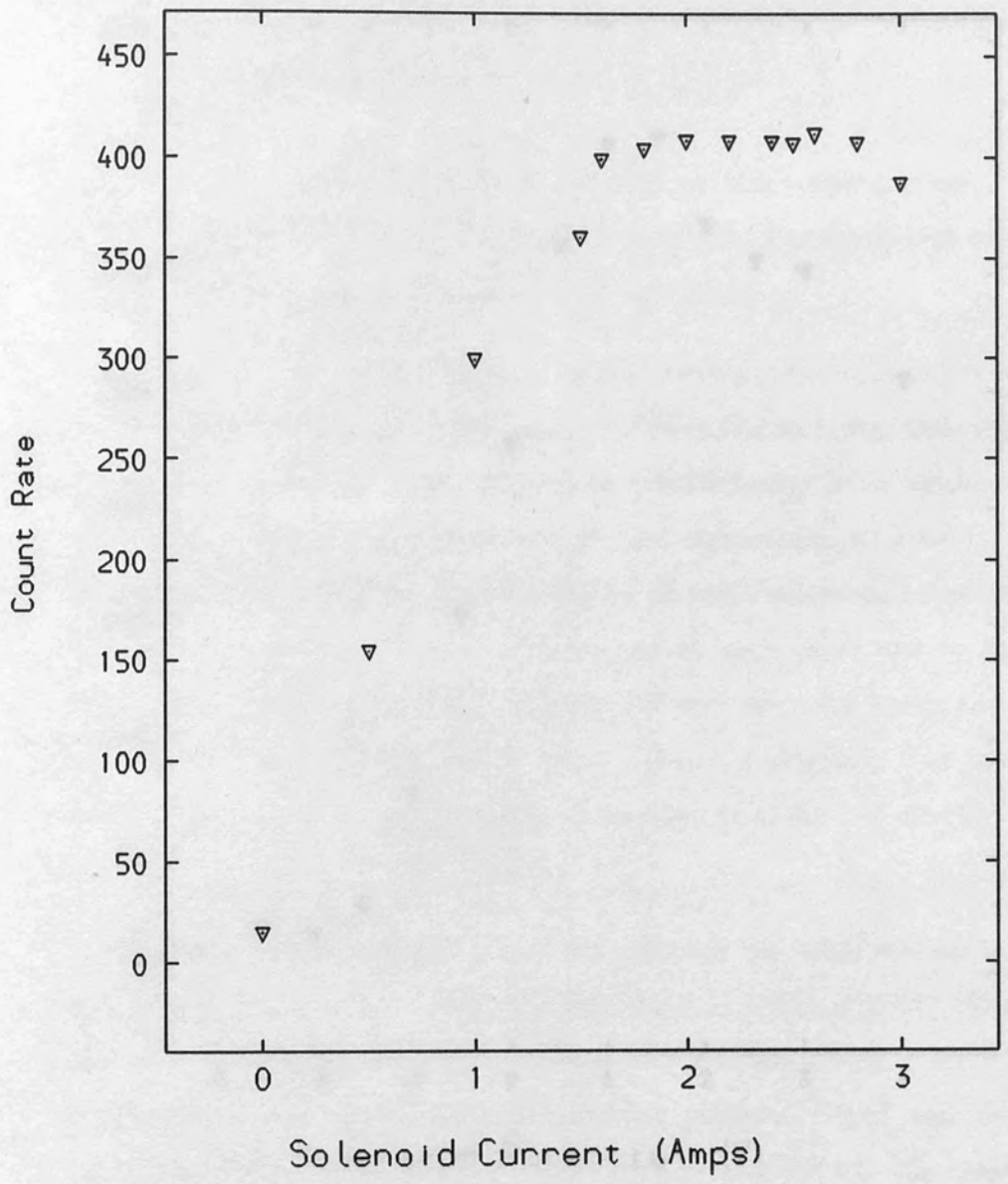

Figure 4.7

The variation of count rate with solenoid current for the cryostat positron beam as measured with a matched pair of channel electron multiplier plates.

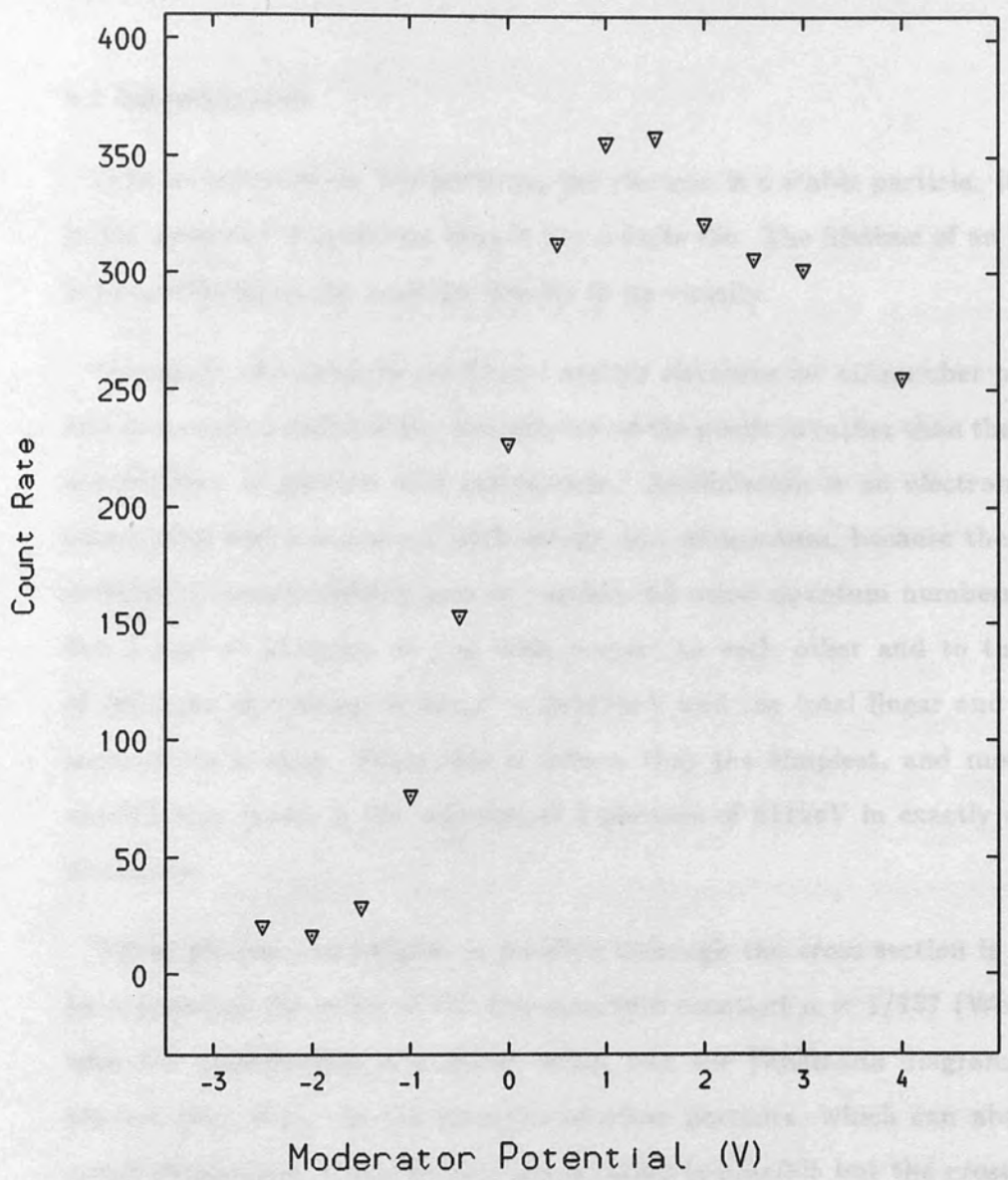

Figure 4.8

The variation of count rate with moderator potential for the cryostat positron beam using a single 100 × 105 lpi tungsten mesh moderator.

Chapter 5 Positron Annihilation

5.1 Introduction

Like its antiparticle, the positron, the electron is a stable particle. It is only in the presence of positrons that it has a finite life. The lifetime of an electron is proportional to the positron density in its vicinity.

Normally, of course, in condensed matter electrons far outnumber positrons and it is usual to think of the annihilation of the positron rather than the mutual annihilation of particle and antiparticle. Annihilation is an electromagnetic interaction which conserves both energy and momentum, because the process involves a complementary pair of particles all other quantum numbers cancel. For a pair of particles at rest with respect to each other and to the frame of reference the energy is $2m_ec^2 = 2x511keV$ and the total linear and angular momentum is zero. From this it follows that the simplest, and most likely annihilation mode, is the emission of 2 photons of 511keV in exactly opposite directions.

Three photon annihilation is possible although the cross section is reduced by a factor of the order of the fine structure constant $\alpha = 1/137$ (West 1974) with the introduction of another vertex into the Feynmann diagram for the process (fig. 5.1). In the presence of other particles, which can absorb the recoil momentum, single photon annihilation is possible but the cross section is even further reduced by a factor $\lambda_c\rho \approx \alpha^3$ as well as the addition of a third vertex. λ_c is the electron Compton wavelength and ρ the density of additional particles.

At low positron energies the cross section for two photon annihilation is inversely proportional to the positron velocity v (West 1979)

$$\sigma = \pi r_0^2 c/v$$

where $r_0 = e^2/m_e c^2$ is the classical electron radius. From this it follows that the annihilation probability

$$\Gamma = \sigma v n_e = \pi r_0^2 c n_e$$

is simply proportional to the electron density n_e.

If the annihilating pair are not at rest then the momentum must be taken up by the annihilating photons, leading to both a spread of energies and a deviation from 180° in the angle of emission. To first order the change in angle is $\delta\theta = p_T/m_e c$ where p_T is the transverse momentum of the annihilating pair. Similarly the measured energy of the annihilation photon is Doppler-shifted by $\delta E/E = v_L/c = p_L/m_e c$. The subscript L denotes the longtitudinal velocity and momentum components of the annihilating pair.

Positron annihilation therefore gives an indication of two aspects of a given physical situation. The positron lifetime samples the local electron density and the energy or momentum spread of the 511keV annihilation line samples the momentum distribution of the electrons involved in the annihilation. Three experimental techniques have evolved, lifetime spectroscopy, angular correlation (ACAR) and Doppler-broadening. The usual approach to lifetime spectroscopy is to use a radiaoctive source which emits a fiducial gamma ray such as ^{22}Na, which is used as start signal in a timing spectrometer (see for example MacKenzie 1983). The annihilation photon is used as the stop signal. In beam experiments this start signal is inapplicable and other methods need to be employed. The most promising approach is to use a pulsed beam which will also guarantee a 100% coincidence rate (Schödlbauer et al 1986).

5.2 Doppler-Broadening

Of the three techniques Doppler-broadening is not only the simplest experimentally but the best suited to most laboratory positron beams.

Although ACAR gives a much higher resolution it is limited in application to intense, reactor or accelerator based, beams. To acheive a high angular resolution two position sensitive, or mobile, detectors need to be tens of metres away from the target. The resulting loss of count rate due to both distance and the need for coincidence counting is dramatic. Doppler-broadening requires a single high-resolution detector close to the sample and is equally as applicable to both traditional, fast positron, experiments as beam studies. A typical Doppler-broadening spectrometer consists only of a high resolution Ge detector with preamplifier, an amplifier and a multi-channel analyser (MCA).

5.2.1 Positron Annihilation in Condensed Matter

Annihilating positrons in condensed matter are normally assumed to be at thermal energies so that to first order the only contribution to the photon momentum distribution is from the electrons. The electron momentum distribution in simple metals can be divided into two distinct components corresponding to the tightly bound core and the nearly free conduction electrons. Calculations for the atomic wavefunctions are complicated and in Doppler-broadening experiments, which have a relatively low resolution, are usually taken to have Gaussian distribution. Annihilation with the conduction electrons, particularly in the alkali metals, gives a parabolic component to the annihilation lineshape. This is easily seen by considering the Fermi surface to be a perfect sphere (Carbotte 1983). The annihilation rate for a given momentum component, p_z, is proportional to the density of states. This is equal to the area of the circle (fig. 5.2) where the Fermi sphere intersects the constant p_z plane. From simple trigonmetry this is $\pi(p_f^2 - p_z^2)$ with a cut-off at $p_z = p_f$.

The core electrons have a higher momentum than the conduction electrons and so in general the parabola is the narrowest component. Consequently a localised (trapped) positron which is more likely to annihilate with the

non-localised conduction electrons will yield a narrower lineshape than a free positron. As the trapping rate at defects is proportional to the defect concentration the Doppler-broadened annihilation line shape is a good measure of the state of the material.

5.2.2 Positronium Formation and Annihilation

The formation of the positron-electron bound state, positronium (Ps), is essentially a surface phenomenon although a quasi-positronium state exists in many insulating solids (Dupasquier 1983). Two ground states, with zero orbital angular momentum, of the Ps atom exist; parapositronium, a singlet $^1S_0$ state, and orthopositronium, a triplet $^3S_1$ state. The energy difference between the two is only 0.84meV, compared with the binding energy of 6.8eV, with the singlet being the lowest (Hautojärvi & Vehanen 1979).

Three quarters of all Ps therefore exists in the S=1 state which cannot decay into two photons, both conservation angular momentum and parity would be violated (West 1979). In the absence of any spin exchange interactions or pick-off, in which the positron in the Ps atom annihilates with an external electron, three quarters of all Ps decays are to 3 photons. This shows up very clearly in the photon energy spectrum as an increase in intensity in the same region as the Compton scattered photons, around 2/3 of the annihilation photon energy.

The momentum of the annihilating pair in parapositronium is the momentum of the atom which is very low. Consequently its Doppler-broadened lineshape component is very narrow compared to that for the annihilation of a free positron.

5.3 Analysis Techniques

A positron annihilation line contains a large amount of information concerning the positron and electron momenta. The changes in the lineshape as the physical conditions yield further information on the physical conditions in the sample. The ratio of conduction to core electrons need not change as the number of defects increases in the sample but the relative probabilities of annihilation with the positron will. Unfortunately the resolution of a Ge detector is limited, typically around 1.4keV at 511keV corresponding to an energy of 1.9eV for the positron-electron pair. Depending on the information required a wide range of analysis methods are available ranging from changes in simple model-independent parameters to a full model-dependent multi-component analysis.

5.3.1 Lineshape Parameter

Many different parameters can be used to describe the shape of the positron annihilation line, the simplest of which is the lineheight parameter of Mackenzie et al (1970). This is simply the normalised count in an arbitary central region of the peak and is usually denoted by S or F (this thesis), although many other letters are used. The value of F is then an indication of the narrowness of the peak. As, in metals, a trapped positron yields a narrower lineshape and the trapping rate varies as the defect concentration F gives an indication of the number of defects in the sample.

Although the absolute value is meaningless changes in this parameter can yield useful information about the system, particulary in vacancy formation studies (Rice-Evans et al 1976) or profiling experiments (Chap. 6). For any experimental line the measured parameter F can be expressed as a superposition of different values f_i corresponding to annihilation at different sites each with

a probability P_i.

$$\mathrm{F} = \sum_i P_i f_i$$

This interpretation makes no a priori assumption about the momentum components in the lineshape. Another, hidden, assumption also exists in this analysis however. Namely that the lineshape at any point, whether in the bulk, at the surface or at a defect, is made up of a linear superposition of the same components. In the same specimen this is not unrealistic.

Other factors are more significant when comparing different samples. F is sensitive to the underlying background which in turn depends on both count rate and geometry. In Doppler-broadening experiments where either the equipment or sample is changed it is customary to overlap the measurements and normalise the parameter values to each other. This can be avoided to some extent by subtracting a suitable background before calculating the lineshape parameter (Chaglar et al 1981).

5.3.2 Running Integrated Difference Curves

The most sensitive way of recording changes in a lineshape is to calculate a difference spectrum by subtracting a reference lineshape. However difference spectra are very poorly defined for low statistics and high dispersion. This problem can be overcome by using the running integral of the difference curve (Coleman 1976) spanning the peak region where the difference is significantly different from zero. The definition of this new curve, The Running Integrated Difference (RID) curve is shown in figure 5.3. The dashed curve in figure 5.1.a is subtracted form the solid curve to produce the difference curve (dashed line) in 5.1.b. Both initial curves have been normalised to unit area. The solid line is the RID curve generated from this curve, the normalisations between the two are arbitary so as to display both on the same graph.

The simplest parameter to define from an RID curve is the peak to peak height S_r which can be seen to be the maximum change in F as defined above. The turning points of the RID curve are those points where the difference curve passes through zero. These are obviously equivalent to the intersections of the two lineshapes, A & B. Defining the values of the RID curve to be S_A and S_B at these points. Also for two curves X_i and Y_i the lineshape parameters F_x and F_y are

$$F_x = \sum_{i=A}^{B} X_i$$

and

$$F_y = \sum_{i=A}^{B} Y_i$$

From the definitions of S_A and S_B

$$S_A = \sum_{i=1}^{A} X_i - Y_i$$

and

$$S_B = \sum_{i=1}^{B} X_i - Y_i$$

Then

$$S_r = S_A - S_B = \sum_{i=A}^{B} X_i - Y_i = F_x - F_y$$

The RID height is only good as a measure of the change in lineshape parameter F if the width $B_r = B - A$ remains constant, ie the definition of F remains unchanged. This is always true if each lineshape can be described as a superposition of the same components and is easily demonstrated for a two component lineshape. Consider two curves X and Y such that

$$X(E) = J_x f(E) + (1 - J_x) g(E)$$

and

$$Y(E) = J_y f(E) + (1 - J_y) g(E)$$

so that only the intensities of the components varies not their form. The turning points A & B are when

$$X(E) - Y(E) = 0$$

so

$$(J_x - J_y)f(E) - (J_x - J_y)g(E) = 0$$

Discounting the trivial solution of two identical lines ($J_x = J_y$) the turning points A & B are given by the solution of

$$f(E) - g(E) = 0$$

which is independent of the component intensities and hence constant unless the component shapes change.

5.4 Component Analysis

Given a useful model for the annihilation lineshape the amount of information available can be greatly increased. Unfortunately to decompose a lineshape into its constituent parts requires the deconvolution of the lineshape and the instrumental resolution function from the experimental data. Early attempts at model independent deconvolution (Jackman et al 1974, Dannefaer & Kerr 1975) employed iterative techniques and were very successful except in terms of computing time.

The development of fast Fourier transform (FFT) routines now allows rapid convolution and deconvolution of any number of discrete arrays such as measured spectra from an MCA. However spurious high frequency components can be introduced during the deconvolution process and filtering of the Fourier specrum is essential. Schaffer et al (1984) have reported the use of an FFT routine with a variable low-pass filter such that all Fourier coefficients beyond the first minimum being set to zero. In a subsequent paper (Schaffer & Jones 1986) they have applied their method to a Doppler-broadening study

of aluminium and have reported an improvement in the conventional lineshape parameters by using the deconvoluted spectra rather than the raw data. In this way accidental changes in the resolution function can be accounted for. They have made no attempt to fit the deconvoluted lineshape with a modelled function.

A measured lineshape $f(E)$ can be described as the convolution of a superposition of different components $g_i(E)$ with the resolution function $r(E)$.

$$f(E) = \sum_i \int_{-\infty}^{+\infty} g_i(x) r(x - E) dx$$

or in a more convenient notation

$$f(E) = \sum_i g_i(E) * r(E)$$

By virtue of the convolution theorem, the same expression after Fourier transformation is much simpler

$$F(e) = \sum_i G_i(e) R(e) = R(e) \sum_i G_i(e)$$

and deconvolution is achieved by point by point division of the transformed lineshape by the transformed resolution function.

Both the measured lineshape and the resolution function contain random statistical errors which result in significant high frequency components in their respective Fourier spectra. These are amplified by the division of one small number by another at high Fourier coeffiecients. Consequently some sort of filtering is essential if the technique is to be used effectively.

5.4.1 FFT Deconvolution Program

A program has been developed to utilise the speed of FFT routines to deconvolute and fit a modelled three component curve to a positron annihilation lineshape. The main program logic is as follows

1 Enter resolution function.

2 Subtract underlying background from resolution function.

3 Normalise resolution function to unit area.

4 Enter initial guesses for fitted parameters.

5 Enter data funtion.

6 Subtract underlying background from data function.

7 *Deconvolution.*

8 Fit modelled function using least squares minimisation.

9 Repeat from step 5 for all data.

Steps 2 and 8 as well as the FFTs used in the deconvolution use NAg FORTRAN library routines. For the underlying background a complementary error function was selected. The whole peak was fitted with a superposition of two normalised Gaussian functions and an inverted parabola. The ^{85}Sr gamma-ray at 514keV was used as the instrumental resolution function. The deconvolution step is further broken down as follows

1 Move the resolution function to a larger array of dimension 2^n (n integer).

2 Fourier transform the resolution function.

3 Take the modulus of the transformed resolution function.

4 Move the data function to a larger array of dimension 2^n.

5 Fourier transform the data function.

6 Take the modulus of the transformed data function.

7 Filter the transformed data function.

8 Divide each data element by the corresponding resolution element.

9 Fourier transform the deconvoluted function.

10 Take the modulus of the deconvoluted function.

11 Compress the deconvoluted array to the original size of the data array.

12 Normalise the deconvoluted function to unit area.

Expanding the data sets into larger arrays allows a wider transformed function. As a rule of thumb for an array of dimension N and a function of full width σ elements the full width of the Fourier transformed function is N/σ. A narrow region ecompassing only the peak region is extended in preference to taking a wider window which introduces additional noise into the Fourier spectrum due to the assymetry of the surrounding spectrum. Selecting an array dimension of $N = 2^n$ is not essential but the majority of FFT routines are most efficient at handling arrays of these dimensions.

Both sides of the peak are used throughout and when the modulus of the transformed function is taken this is centred about the first and last elements of the array. Filtering in this case therefore necessitates suppression of the central section of the spectrum. On compression the data is wrapped around to be centred in the final array.

Filtering is the most important part of the deconvolution process as it can dramatically alter both the width and shape of the peak. Without filtering the white noise generated in the deconvolution process can totally obliterate any recognisable peak. If too many high frequency components are rejected then any narrow components, eg parapositronium, and any discontinuous changes in the line slope will be lost. This latter case becomes important in analysing lineshapes for positron annihilation in metals where the conduction band electrons contribute a parabolic component of finite width. Cutting out the higher frequency components would then result in large oscillatory tails

after inverse transformation. In a multicomponent fit this could quite easily be interpreted as another Gaussian component.

Three types of filter (fig. 5.4) have been tested on the same data using the same fitting routine and initial parameter values. These are

(i) A low-pass filter in which all Fourier coefficients beyond a fixed cut-off value are rejected.

(ii) A dynamic low-pass filter in which the cut-off is set at the first minimum in the Fourier spectrum (Schaffer et al 1984).

(iii) A dynamic filter in which all Fourier coefficients with an intensity less than a predefined fraction (filtering factor) of the peak intensity are set to zero.

Filter (ii) relies on the observation that the signal to noise ratio is of order one at the first minimum. It does however, like filter (i), preclude any components with a finite width, which will have a periodic Fourier spectrum. It is also unlikely to find a low intensity narrow component superimposed on a wider lineshape. Filter (iii) attempts to solve these problems, relying on the assumption that the white noise in the Fourier spectrum is small compared to the Fourier spectrum due to the components in the spectral line. The noise however will be exaggerated after the point by point division by the noise in the resolution function.

5.4.2 Test of the FFT Method

The program described above was tested for all three filtering techniques on two sets of experimental data taken with a high purity Ge detector at a dispersion of 94eV per channel. For filters (i) and (iii) different values for the cut-off and filtering factor were tried. Otherwise apart from the initial guesses of the fitted parameters the program was configured identically for

each data set. The annihilation lineshapes were collected over 350 channels with the FFT performed over 1024 coefficients. The central 150 channels of the deconvoluted peak were fitted with a superposition of two Gaussians and a parabola using an unweighted least squares fit. Each component is characterised by a width parameter (in channels) and a percentage intensity. In addition the peak position and a constant background were fitted as free parameters as a test of deconvolution. In a noisy spectrum the fitting algorithm attempts to find both a peak position well removed from the centre channel and a non-zero background.

No account was taken of the positron momentum. This would appear as a second resolution function blurring any kinks in the deconvoluted lineshape, introducing small tails onto the parabola and slightly widening all the components. However as the positron has very little momentum this effect should be small compared to any filtering errors.

The technique was first tested on data from positron annihilation in copper containing a high density of krypton precipitates (chap. 7). The lineshape can be decomposed into 3 components corresponding to annihilation with Kr and Cu atomic electrons and with conduction band electrons. Both lineshape parameter (chap. 8) and lifetime measurements (Jensen et al 1986) have shown the positron annihilation characteristics to be constant over the temperature range (300-600K) used here. These lineshapes will therefore provide a test of the consistancy of each filtering technique.

The intensities and widths of the parabolic component in each line are shown in figures 5.5 and 5.6 respectively. The fixed low-pass filter (i) gave consistent values for a very narrow range of cut-offs around 50 Fourier coefficients (figs 5.5.b & 5.6.b). This gives 2 Gaussian components of similar intensities ($\sim$ 40%) with widths of 11 & 24 channels and a parabola with a width parameter of 17 channels. For lower cut-offs the intensity of the wider Gaussian fell to zero with

the width of the parabola increasing to that of the lost Gaussian (fig. 5.6.a). Most of the lost intensity was taken up into the parabolic component(fig. 5.5.a). Keeping more of the Fourier spectrum causes the intensities and widths to vary considerably between equivalent spectra. Figures 5.5.c & 5.6.c show results for a cut-off at 75 Fourier coefficients.

The dynamic low-pass filter (ii) of Schaffer (1984) fared little better giving a much wider variation in parabola widths (fig. 5.6.d) as well as a much lower intensity (1-5%) to be compared with the wider Gaussian, associated with the copper, of 40%. In annealed copper the ratio of Gaussian to parabolic intensities is 4:1 at these temperatures (Rice-Evans et al 1976). In a heavily defected sample such as this the parabola should be more intense.

Filter (iii) gave constant results over the different lines for a range of filtering factors between 1 & 2% of the maximum Fourier intensity. However the absolute values depended on the filtering factor. The intensity of the wider Gaussian fell with increasing filtering factor, the parabola intensity and both widths increased. Rejecting all coefficients with a lower intensity than 1% of the maximum gave a wider Gaussian intentesity of 45%; for 2% the returned Gaussian intensity was 40% with the difference being taken up by the parabola. Both widths increased by 2 channels over this range. There was, however, no significant effect on the narrow Gaussian component. For a filtering factor of 0.5% the results were essentially the same as for filter (ii).

For the second test the technique was tried on data from positron annihilation at condensed monolayers of oxygen on graphite which has already been successfully fitted to a 3 component model using repeated numerical convolution at each stage in the least squares fit (Rice-Evans & Moussavi-Madani 1987). As a monolayer of oxygen condenses a third narrow component, corresponding to the annihilation of para-positronium, enters the lineshape. In the 3 component model this third component is taken to be a Gaussian. The development of the

narrow component is seen as a dramatic increase in the lineshape parameter F. When analysed using a two component model (Gaussian + parabola) there is an apparent sharp decrease in parabola width with an accompanying drop in intensity (Rice- Evans et al 1986). With the addition of a third component the widths and relative intensities of the two major components remain constant.

The fixed low-pass filter with a cut-off at 75 Fourier coefficents gave similar results (fig. 5.5.b) to those of Rice-Evans & Moussavi-Madani. Keeping as few as 50 coefficients produced the narrow component for data at 90K although the width was twice as wide (fig. 5.8.a) and its intensity diminished (fig. 5.7.a). With a cut-off at 100 coefficients the intensities and widths of all 3 components fluctuated wildly.

The dynamic low-pass filter (ii) failed to find the narrow component at all but gave similar values for the widths and relative intensities of the other two components.

Filter (iii) did not perform very well at all under these circumstances. With a filtering factor in the range 0.5-1% the narrow component was visible at its most intense with the width independent of the factor (figs. 5.8.c & 5.8.d), but it was not found at lower intensities (figs. 5.7.c & 5.7.d)

5.4.3 Concluding Remarks on Filters

Deconvolution of gamma-ray lineshapes using FFT algorithms allows rapid component analysis, typically 20 seconds on a VAX 11/780 cluster per spectrum. With care, and a suitable model, valuable information can be obtained at much lower computing cost than by iterative methods. None of the three filters tested have proved to be adequate for routine analysis of lineshapes comparable to the use of parameters. Great care needs to be taken in their use particularly when looking for narrow components at low intensity.

Low-pass filters seem to the most successful although the method of Schaffer et al (1984) which would allow the program to select the cut-off does not necessarily give the best results. There appears to be no a priori method of selecting the cut-off level. This has to be done by inspection of the output for equivalent spectra so that consistent results are achieved and a limit on the accuracy can be determined.

Other filters, such as a sink function or a Gaussian weighting of the Fourier spectrum may yield better results although they have not yet been tested. In these cases though there will then be an additional lower limit on the widths of any components as they have the effect of inserting a narrower artificial resolution function.

Once a filter has been found that is applicable over a wide range of spectral conditions, eg poor statistics, narrow components, etc, then the method should find use as a rapid and accurate means of analysis.

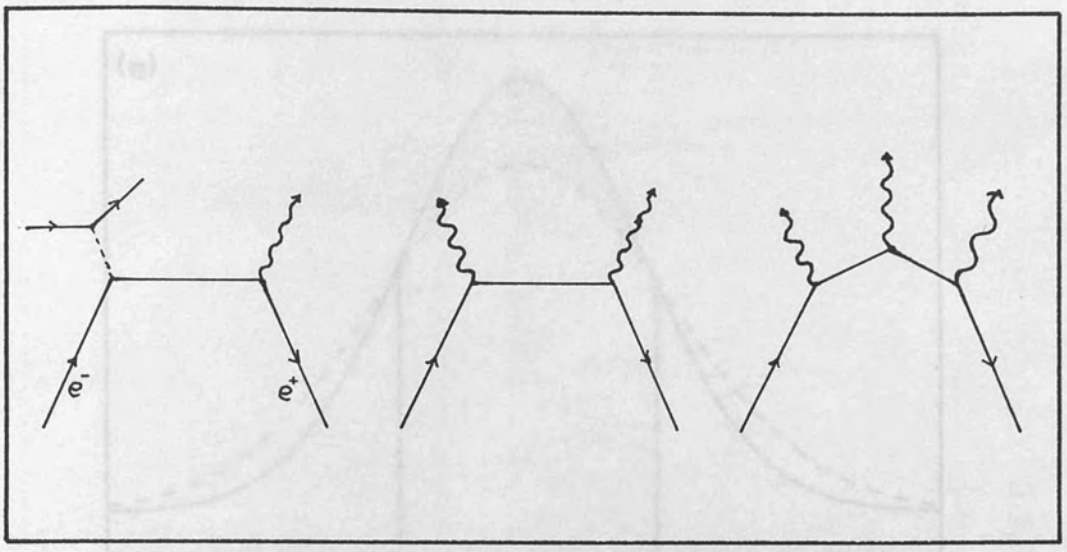

Figure 5.1

Feynmann diagrams for one, two and three photon annihilation of a positron and an electron.

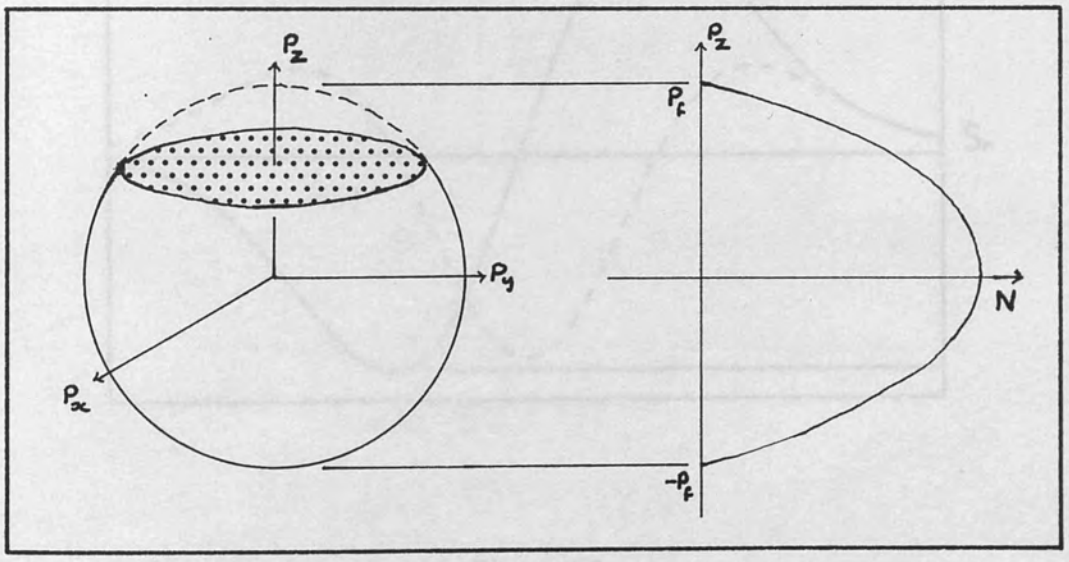

Figure 5.2

Definition of the free electron parabola. The density of states $N(P_z)$ is equal to the shaded area where P_z cuts the Fermi sphere.

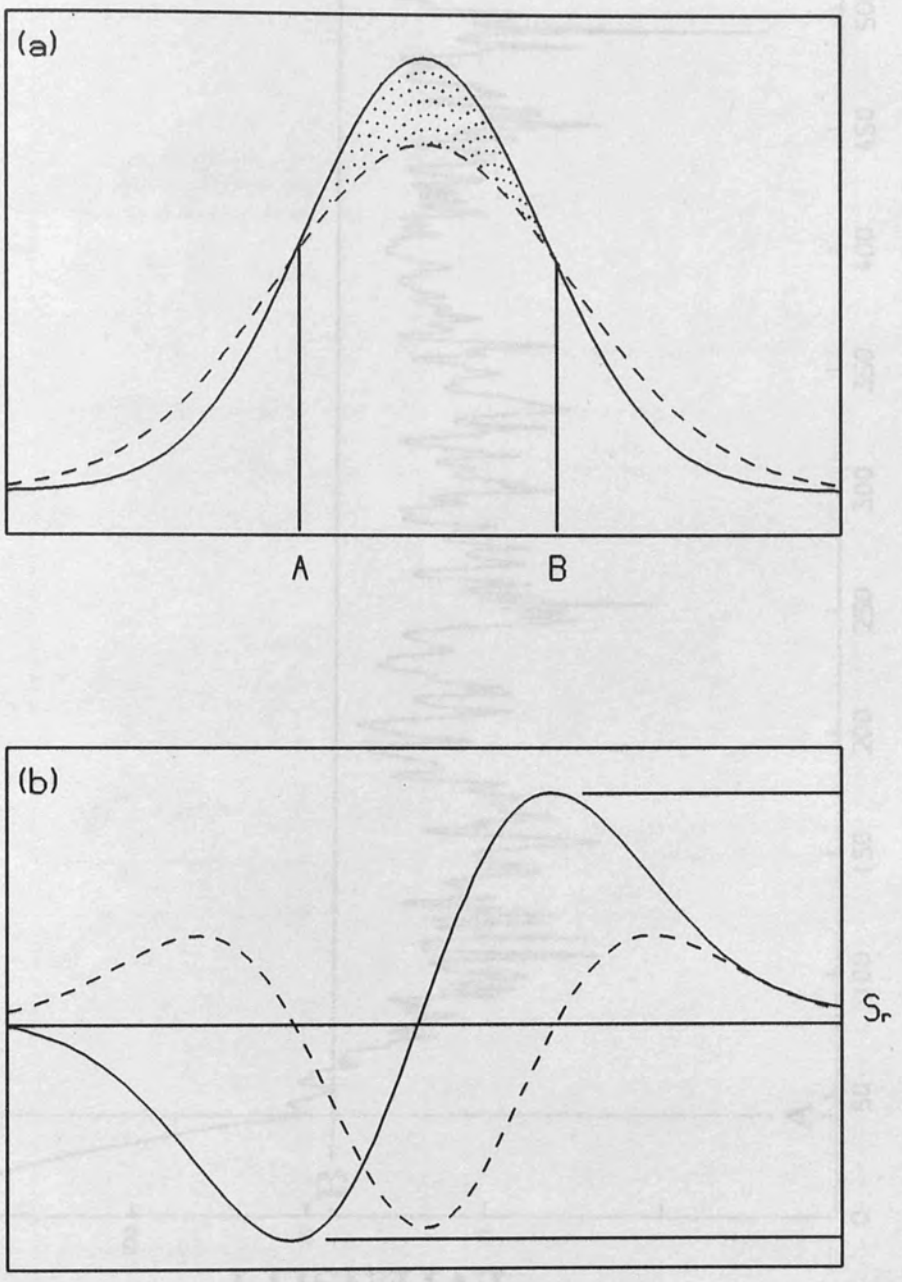

Figure 5.3

The definition of a running integrated difference (RID) curve. The broken line line in (b) is the difference of the dashed curve from the solid in (a). The solid curve in (b) is the RID curve. Its height S_r is equal to the shaded area in (a).

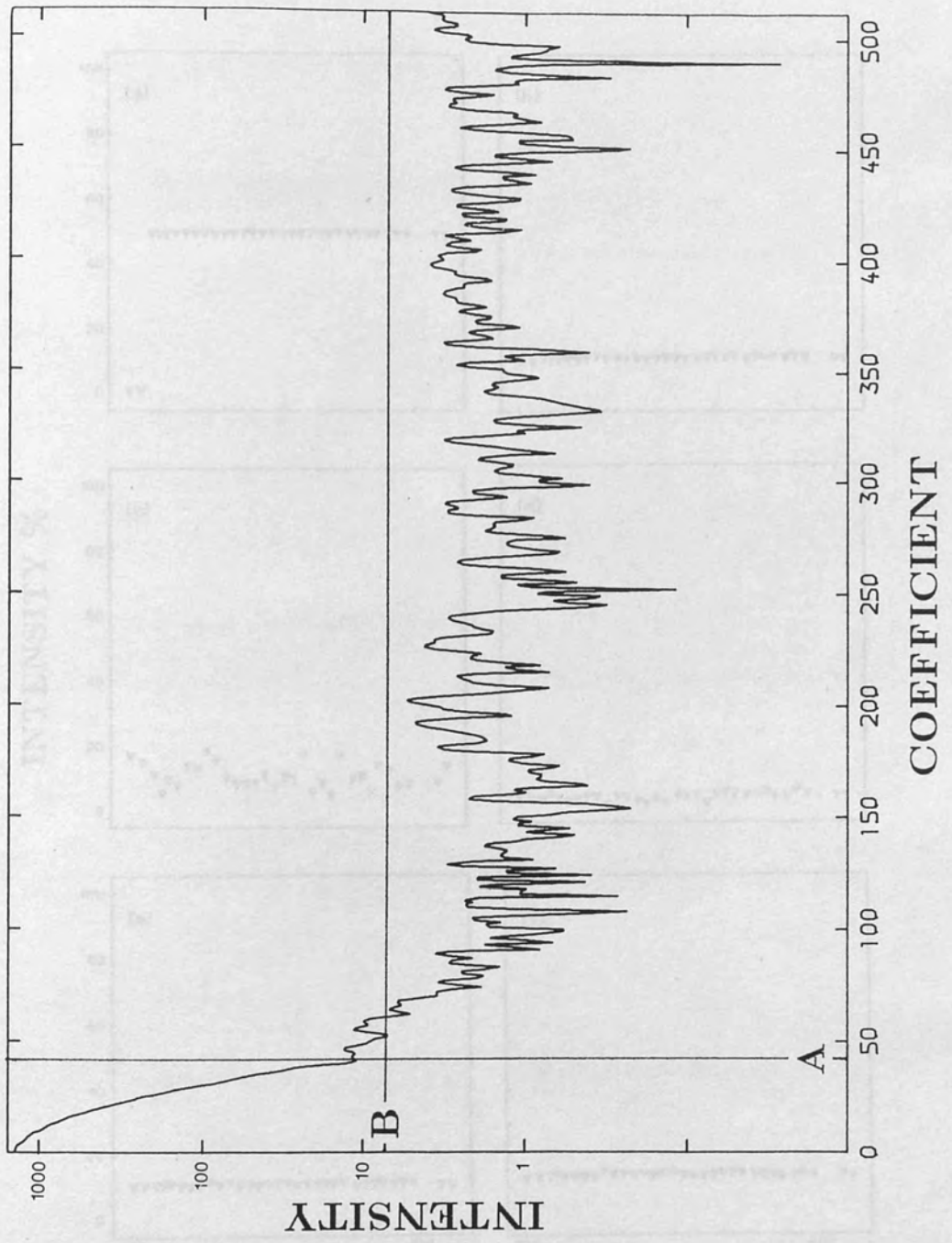

Figure 5.4

The left half of a Fourier spectrum showing the different filters used. With a low-pass filter (i) at the first minimum (ii) the area to the left of A is used. With filter (ii) the coefficients above B are used.

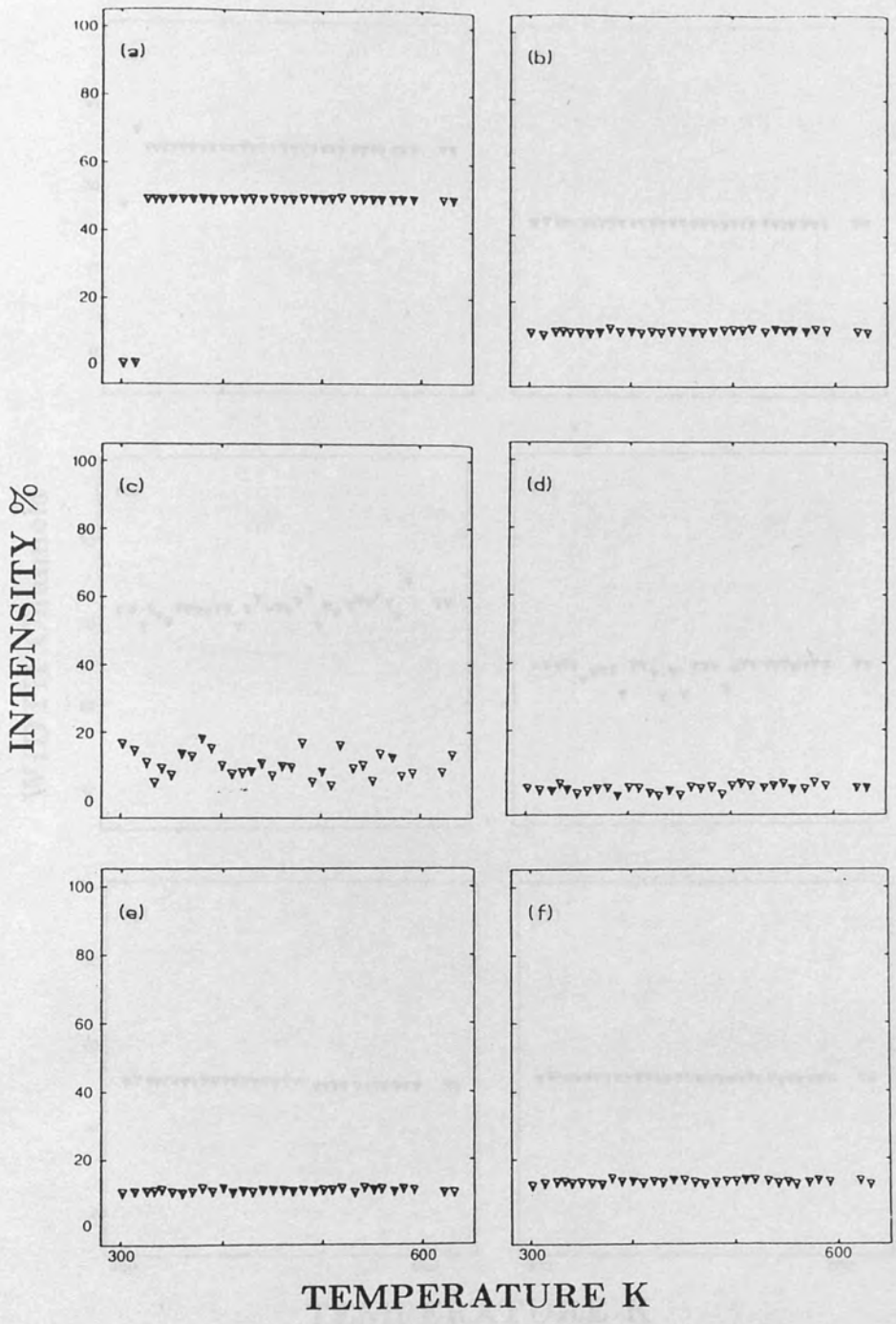

Figure 5.5

The intensity of the parabola in Cu(Kr) for different filters. Low-pass filters with cut-offs at 25 (a), 50 (b), 75 coefficients (c) and at first-minimum (d) and a dynamic filter with filtering factors of 1% (e) and 1.5% (f).

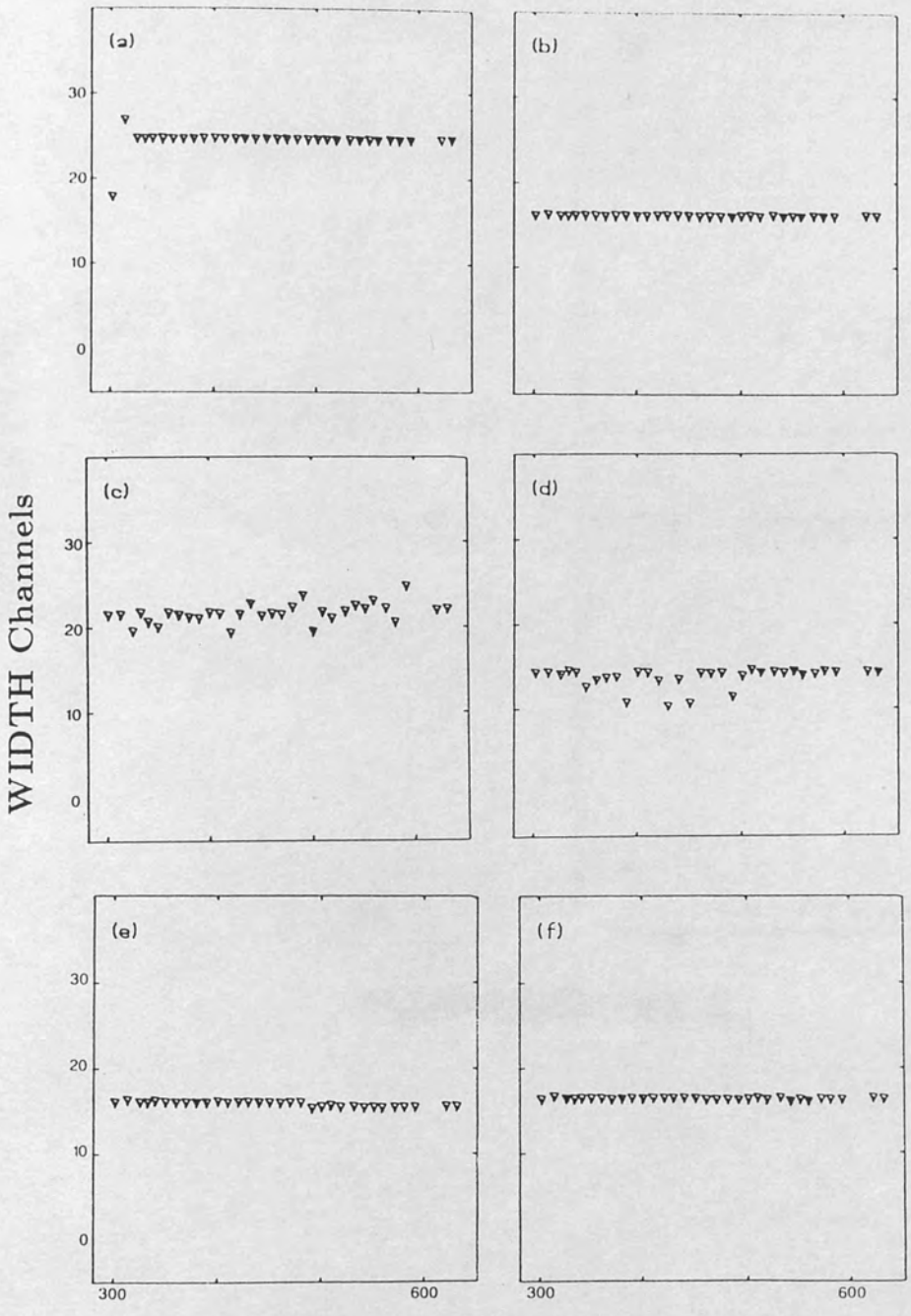

Figure 5.6

The width of the parabola in Cu(Kr) for different filters. Low-pass filters with cut-offs at 25 (a), 50 (b), 75 coefficients (c) and at first-minimum (d) and a dynamic filter with filtering factors of 1% (e) and 1.5% (f).

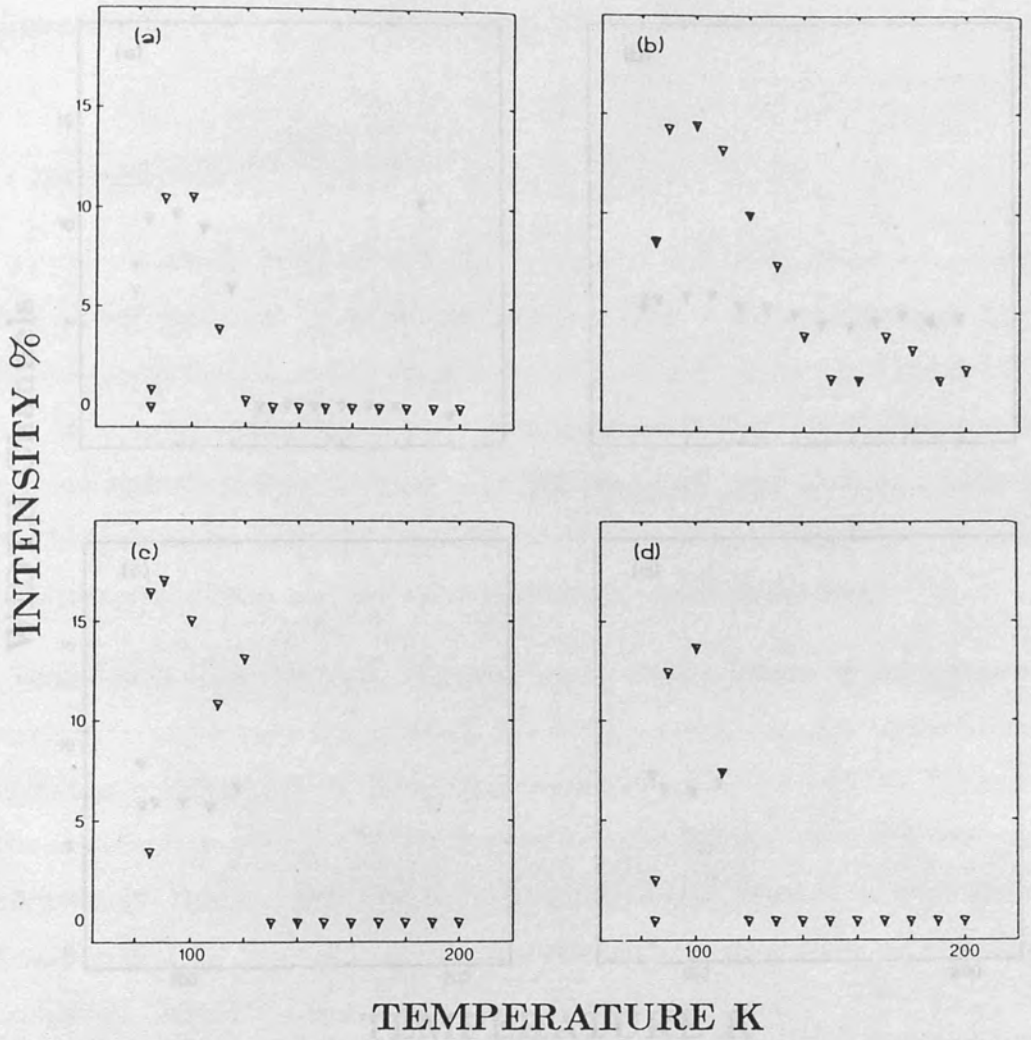

Figure 5.7

The intensity of the narrow Gaussian component in O_2 condensed on graphite for different filters. Low-pass filters with cut-offs at 50 (a) and 75 (b) coefficients and dynamic filters with filtering factors of 0.6% (c) and 0.8% (d).

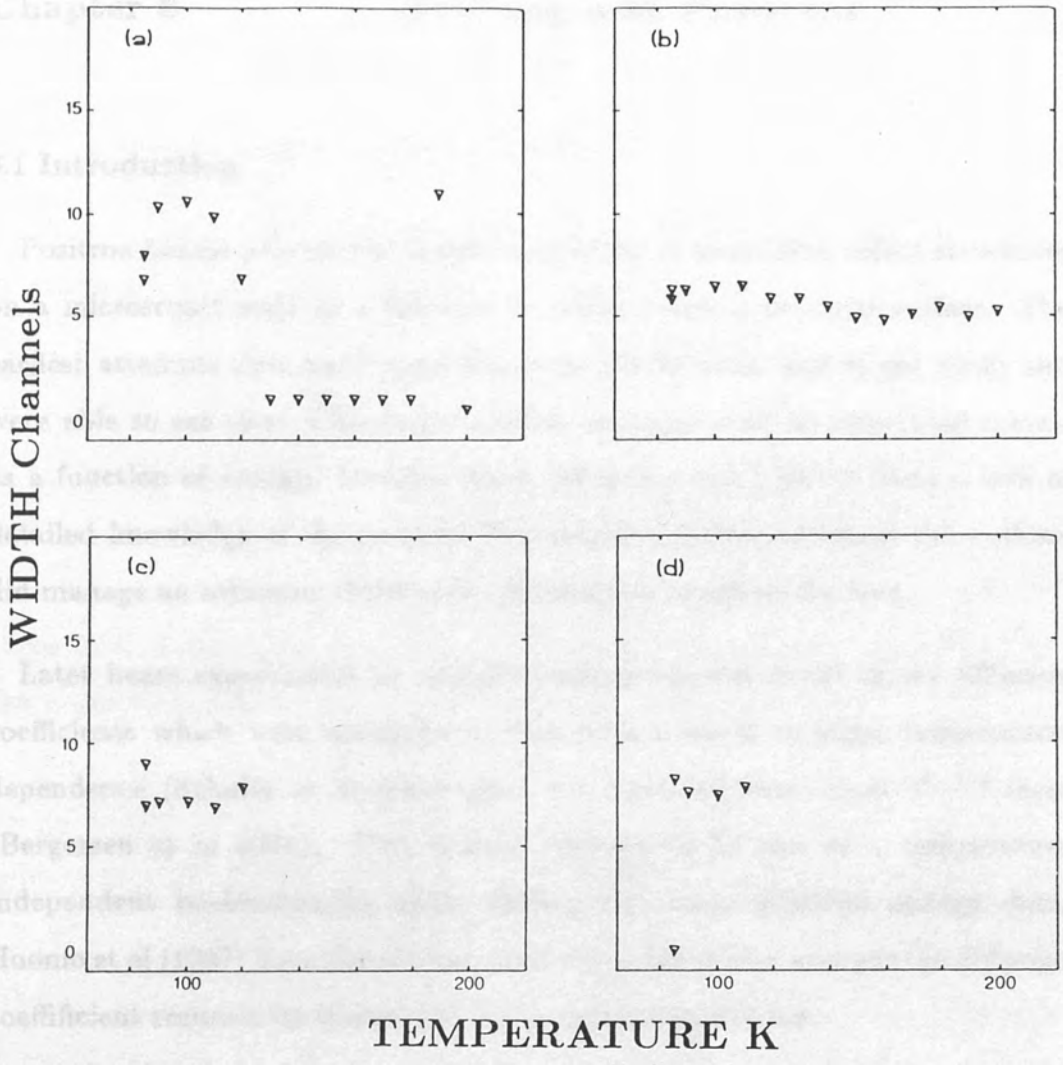

Figure 5.8

The width of the narrow Gaussian component in O_2 condensed on graphite for different filters. Low-pass filters with cut-offs at 50 (a) and 75 (b) coefficients and dynamic filters with filtering factors of 0.6% (c) and 0.8% (d).

Chapter 6 Profiling with Positrons

6.1 Introduction

Positron beams provide the unique possibility of examining defect structures on a microscopic scale as a function of depth below a material surface. The earliest attempts date back some five years (Trifthäuser and Kögel 1982) and were able to see clear differences between annealed and He implanted metals as a function of energy. However these measurements suffered from a lack of detailed knowledge of the positron implantation profile, although the authors did manage an estimate of the mean penetration depth of the ions.

Later beam experiments on annealed metals yielded values of the diffusion coefficients which were anomolously low with a much stronger temperature dependence (Schultz et al 1985) than the expected theoretical $T^{-1/2}$ form (Bergersen et al 1974). This is now believed to be due to a temperature independent backscattering effect fouling the lower positron energy data. Huomo et al (1987) have shown that when this is taken into account the diffusion coeffificient resumes its theoretical temperature dependence.

6.2 The Positron Implantation Profile

There are essentially two types of measurement which can give accurate information on the profile of a monoenergetic positron entering a material; transmission through a foil or the profiling of a known structure. In a transmission experiment the profile of electrons can be measured and is well known (Makhov 1960). The total transmission through a film of thickness x can be expressed as

$$T(x,E) = \exp(-x^m/z_0^m)$$

where

$$z_0 = \frac{\alpha}{\rho} E^n$$

with ρ being the material density and E measured in keV.

Differentiating the expression for $T(x, E)$ gives the probability of an electron or positron stopping at a distance z from the surface

$$P(z, E) = \frac{-\mathrm{d}}{\mathrm{d}z} e^{-z^m / z_0^m}$$

In Monte-Carlo calculations Valkealahti and Nieminen (1983,1984) showed that both positrons and electrons have the stopping profiles of this form with m=2 for positrons and 1.9 for electrons. These values are significantly greater than those from transmission experiments. The authors attributed this difference to the neglect of backscattering in the experimental measurements.

The end point of the Monte-Carlos for each particle history was taken as 20eV as at lower energies the particles have an isotropic direction distribution. The authors report a change of 1Å in the mean depth when the termination energy is changed from 100 to 20eV. Clearly this profile is not the final steady state positron profile and in any defect profiling measurement the definition of a "stopped" positron should be carefully considered. Similarly backscattering of the low energy positrons at lower depths will lead to an enhancement of the surface and epithermal states.

Vehanen et al (1987) have produced accurate values for the parameters in the Makhovian profile from a positron beam study of a known multilayer structure. The values reported for m,n and α are 2, 1.6 and 4.5μg/cm2 respectively. In this measurement positron diffusion was neglected due to the low mobility of positrons in the sample.

6.3 Positron Diffusion

In homogeneous media the diffusion of positrons back to the surface can be calculated from the stopping profile $P(z, E)$ If the Makhovian profile is assumed to represent the stopping of positrons down to thermal energies then the back diffusion probability J is given by the Laplace transform of the implantation profile.

$$J(z, E) = \int_0^\infty P(z, E) e^{-z/L_+} \, \mathrm{d}z$$

where the one-dimensional diffusion length is related to the diffusion coefficient D_+ by $L_+ = \sqrt{D_+/\lambda}$ where λ is the bulk annihilation rate. In uniformly defected materials λ is replaced by $\lambda + \kappa$ where κ is the trapping rate. J has been tabulated in appendix 2 as a function of z_0/L_+ for the Makhovian profile.

The back diffusion probability can be fitted directly to positronium fraction measurements as in metals Ps is only formed at the surface. This unfortunately requires clean well characterised surfaces. However Nielsen et al (1985) found, using this method, that in silicon the Makhovian profile ($m = 2$) gives better agreement than an exponential implantation profile ($m = 1$).

In 'dirty' systems thermal positronium production is suppressed by overlayers, principally of adsorbed oxygen and water, and Ps fraction data does not give a useful measure. Nevertheless if the surface contimanant is sufficiently thin so as not to contribute a bulk signal then it can be assumed that any positrons diffusing back will annihilate with a lineshape parameter corresponding to a generalised surface state. An intuitive upper limit on the thickness of the overlayer would be the mean free path of the positron in the sample.

Then any lineshape parameter measured as a function of incident positron energy $F(E)$ can be expressed by a simple two state model

$$F(E) = J f_s + (1 - J) f_b$$

where the subscripts s and b denote surface and bulk values.

6.4 Epithermal Effects

Positrons stopping near the surface of a material can backscatter through the surface before fully thermalising. A large fraction of these epithermal positrons can strip an electron from the surface and emerge as positronium. In positron back diffusion measurements this is usually regarded as an unwanted complication which fouls the low energy data. Huomo et al (1987) report that for Mo all data for incident positron energies below 4keV is significantly contiminated by epithermal Ps.

However the effect is important in its own right as a potential for moderator design and deserves further consideration. the most efficient moderator to date, solid Ne (Mills and Gullikson 1987), is believed to work by this method as are the original MgO smoked gold moderators.

At present the origin of epithermal positron emission is disputed with most researchers favouring a simple backscattering mechanism. Mills and Crane (1984) measured the emission energy of epithermal positrons from various ionic solids. They found a large spread of energies up to the band gap energy of the material. In their conclusion the authors postulate an Auger emission process whereby Ps diffusing to the surface loses its electron to an empty surface state.

Epithermal positronium emission has also been observed in Ps time-of- flight spectra (Howell et al 1986) from clean metal surfaces. Although the Auger process is feasible from a metal with a thin adsorbed overlayer it is extremely unlikley from the metal surface. This would necessitate freely diffusing Ps inside the metal which has never been observed.

The most probable mechanism of emission is backscattering of non-thermalised positrons from the near-surface. On implantation the positron rapidly loses energy by inelastic electron collisions down to a few eV. When the positron has a lower energy than the Fermi energy in a metal or the band gap

in an insulator it can no longer lose energy to electrons. Then thermalisation is dominated by lattice interactions which have a much lower energy transfer. At this stage the positron has the probability distribution calculated by Valkealahti and Nieminen (1983). Epithermal positrons can scatter isotropically from ion cores and may pass back through the surface.

If this description is correct it is a relatively simple matter to account for epithermal effects in profiling measurements. Starting from the Makhovian profile and assuming a characteristic scattering length l_+ the probability of scattering out of the surface from a depth z is given by $\exp(-z/l_+)$ and a backscattering probability J_{ep} can be defined

$$J_{ep} = \int_0^\infty P(z,E)e^{-z/l_+}\,\mathrm{d}z$$

and assuming a characteristic lineshape parameter for all epithermal states f_{ep} the expected lineshape parameter is simply

$$F(E) = J_{ep}f_{ep} + (1 - J_{ep})(Jf_s + (1 - J)f_b))$$

Fortran subroutines to calculate $F(E)$ for both the epithermal and simple back diffusion case are described in appendix 3. Also included are routines to calculate the back diffusion probability and and the Makhovian profile.

6.5 Defect Profiling

A defect profile $C(z)$ can be calculated from two different styles of measurement; from the back-diffusion fraction or from the variation of a lineshape parameter as a function of incident positron energy. The Helsinki group have had much success with the former method (Mäkinen et al 1986, Bentzon et al 1987). This method is capable of resolving defect structures very close to the surface, typically less than 20Å unlike lineshape parameter measurements which are sensitive to both the diffusion and scattering lengths.

Unfortunately back-diffusion measurements require UHV conditions and well characterised surfaces.

A trapping fraction $K(E)$ can be defined as

$$K(E) = 1 - \frac{J_{def}(E)}{J_{ref}(E)}$$

where the subscripts denote the defected and the reference sample. Using this definition the trapping fraction $K(E)$ represents the additional positrons trapped in the bulk by the defect distribution. As $K(E)$ represents a difference, if the epithermal effects can be assumed the same for each sample, they are automatically excluded from the data.

The curves of $K(E)$ can then be fitted to a solution of the quasi- stationary diffusion equation

$$D_+ \nabla^2 N(z,E) - (\lambda + \mu C(z))N(z,E) + P(z,E) = 0$$

where $N(z,E)$ is the steady-state positron distribution and μ is the defect specific trapping rate. The back diffusion probability is given by.

$$J(E) = |D_+ \nabla N(0,E)|$$

For deeper defects in systems with less well characterised surfaces where the positron back diffusion cannot be measured directly any positron annihilation lineshape parameter can be used.

For a defect distribution $C(z)$ the lineshape parameter at a depth z is given by a simple two-state model

$$f_z(z) = \frac{f_b + kC(z)f_d}{1 + kC(z)}$$

where the subscripts b and d denote bulk and defect values and $k = \mu/\lambda$ is a relative trapping rate.

The bulk lineshape parameter is the given as function of energy by

$$f(E) = \int_0^\infty f_z(z) N(z, E) \mathrm{d}z$$

Including back-diffusion and a surface state

$$F(E) = J f_s + (1 - J) f(E)$$

In the high defect regime where positron diffusion can be neglected the steady-state profile $N(z, E)$ can be replaced with the stopping profile $P(z, E)$ with a slight modification to $J(E)$. Differentiation of the Makhovian at $z = 0$ gives $J = 2D_+/z_0^2$ which becomes infinite as the implantation energy tends to zero. In the analysis reported in this thesis using this approximation J was replaced with a functional form with the correct assymptotic behaviour at high and low energies.

$$J = \frac{2D_+}{(z0 + \sqrt{2D_+})^2}$$

For a simple step function distribution

$$C(z \leq l) = 1 C(z > l) = 0$$

the integral for $f(E)$ becomes

$$f(E) = \frac{(f_b + k f_d) + k(f_b - f_d) e^{-l^2/z_0^2}}{1 + k}$$

More exact solutions to this problem are very expensive on computer time whereas the routine using this method (Appendix 3)typically gives a least squares fit within a few minutes.

Chapter 7 Profiling Pure Metals

7.1 Introduction

The models developed in Chapter 6 have been used to investigate positron diffusion and epithermal emission in different pure metals using both positron beam systems. In the case of Ga preliminary results are presented for both the liquid and the solid. It is arguable as to whether any significant differences were observed between the liquid and solid phases, or between the high and low temperature solids.

In every analysis the the positron stopping profile was fixed with a Makhovian form with the values determined by Vehanen et al (1987)

$$P(z,E) = \frac{-\mathrm{d}}{\mathrm{dz}} e^{-z^2/z_0^2}$$

where

$$Z_0 = \frac{4.5\mu\mathrm{g/cm}^2}{\rho} E^{1.6}$$

with E measured in keV.

7.2 Slow Positron Study of Gallium

Gallium is known to be a very peculiar metal. Like water the solid phase has a lower density than the liquid. It also has a tendency to supercool. With regards to fast positron studies the bulk shows no change in positron lifetime or electron momenta with temperature in the solid. However there is a large change in lifetime on melting (Brandt & Waung 1968). There is also a significant narrowing of the annihilation line (Gustafson & Mackintosh 1963) with a greater probability of annihilation with conduction electrons. These observations suggest that the denser liquid has more open volume defects, which act as traps for the positron. This is supported by more recent ACAR

measurements compared with Compton scattering in liquid metals (Itoh & Suzuki 1979). These measurements suggest that while positrons are delocalised in liquid Na, in Ga they are highly localised.

7.2.1 Experimental and Analytical Method

While still under development the cryostat positron beam system was set up for preliminary measurements on liquid metal surfaces. The spectrometer control system from horizontal beam line was used in conjunction with a co-axial high purity germanium detector alongside the cryostat tail. The temperature of the sample was recorded using a gold/iron-chromel thermocouple referenced at 77K and maintained by resistive heating of a non-inductively wound furnace.

The gallium sample was supported in a small cup in thermal contact with the heater (fig. 7.1), being put in when molten. Before melting the sample was cleaned in nitric acid to remove bulk contaminants and the surface was skimmed off while molten.

Annihilation spectra were recorded over a range of target biases from 0 to 2500V. The lineshape parameter F, being the normalised contents of the centre 7 channels of the peak, was calculated for each bias. This was then fitted using a least squares minimisation routine to a modelled two state function $F(E) = Jf_s + (1 - J)f_b$. J was calculated as the Laplace transform of the positron profile

$$J = \int_0^\infty P(z, E)e^{-z/L_+}\,\mathrm{d}z$$

The Laplace transform was calculated numerically over a range $10z_0/3$ to an accuracy of 1000 array elements. Both the maximum depth and the number of elements could be reduced without an appreciable loss in accuracy of the fit. Figure 7.2 shows a scaled Makhovian profile with element 1000 marked as limit of integration. Clearly the intensity of the function ceases to be significant

beyond a depth $\sim 7.5z_0/3$. In the simple two- state model reducing the number of elements to 750 would increase the computing speed by 33%. With 1000 elements a typical fit to the data takes 2 hours on a VAX 8200 minicomputer.

7.2.2 Results and Discussion

The lineshape parameter profile measurements and the fitted curves to them are shown in figures 7.3, 7.4 and 7.5 for liquid Ga at 420K, solid at 95K and at 295K respectively. All have the same characteristic shape rising from a low value at low incident positron energies to a plateau beyond 800V with a possible downward trend at higher energies. Within the experimental errors there is no difference between the experimental measurements. The difference in bulk value may be due to the difference in phase but this cannot be stated definitely as there was a change in geometry between two of the three experiments.

The fitted parameters (table 7.6) indicate an extremely short diffusion length compared to the estimated theoretical value of 2100Å (Nieminen and Manninen 1979, Begersen et al 1974). Furthermore within the limits of measurement this has a constant value of 13 ± 5Å over a temperature range of 325^o and a change of phase. This is remarkably close to the calculated positron mean free path of 12Å given in the same reference. A mean depth of 2100Å would correspond to an incident positron energy of 3.4keV. As this experiment utilised positrons with a lower energy only a small fraction are likely to annihilate in the bulk.

Therefore the simplest interpretation of these results is that the two-state model applies to a surface and an epithermal state with the exponential length being a mean scattering length. As such the data yields very little information about the Ga itself but does lend weight to the simple scattering model of epithermal emission.

Fit to Diffusion Model for Gallium

Temp K	f_s	f_b	L_+	Reduced χ^2
95	0.3266	0.3405	7.28	0.3796
295	0.3226	0.3391	18.34	0.3937
420	0.3247	0.3447	14.95	0.2704

Table 7.6

Fit to the two-state model for the lineshape parameter profiles in Ga.

7.3 Slow Positron Study of Molybdenum

7.3.1 Experimental and Analytical Method

An annealed polycrystalline molybdenum foil was studied using the original positron beam spectrometer system described in chapter 4. The surface was cleaned with propanol but not etched, which was impractical as the Mo surface was the reverse of an ion implanted sample (Chapter 10).

Annihilation spectra were recorded over the range 0-12kV and the lineshape parameter S_r was calculated from RID analysis referenced to the lineshape for 12keV incident positrons. The RID width parameter B_r was constant at 20 channels indicating that the S_r parameter was valid as the maximum change in the conventional lineshape parameter F.

The same set of data was then analysed in terms of a simple diffusion model and with an additional epithermal state and scattering length. The positron profile was fixed as a Makhovian function with $\alpha = 4.5\mu\text{gcm}^{-2}$, m=2 and n=1.6. The Laplace transforms were both calculated numerically over 1000 elements up to a depth $10z_0/3$. Including the second transform for epithermal scattering increased the required computing time by a factor of 4. The fitting routine used an unweighted least-squares minimisation.

7.3.2 Results and Discussion

The fits to the experimental points are shown in figure 7.7. The solid line represents the simple diffusion model with two components and one diffusion length; the broken line includes epithermal backscattering.

These results are qualitatively different from those for Ga which indicate a very wide line at low incident energies. This difference is probably an effect of the target-detector geometry. In the cryostat sytem the detector samples in the plane of the surface whereas in this system it is alligned along the beam direction. This system also has the target in a field free region so that reemitted positrons can escape from the target region. So essentially only *positronium* emitted at large angles with a low longtitudinal velocity contributes to the epithermal state. This results in a narrow annihilation line as the Doppler-broadening due to the motion of Ps along the line of sight is small. This is supported by a large decrease in count rate at low target biases.

In the cryostat system the detector samples photons emitted transversely from the sample and a region 3cm above it. Therefore the epithermal state includes Ps emitted at all angles from $-\pi/2$ to $+\pi/2$ resulting in a much wider lineshape. There will also be a contribution from positrons being forced back into the sample by the potential barrier when the target is attractive with respect to the beam line.

Fitting to S_r for Mo yields a diffusion length of 1300Å without considering the epithermal fraction. Including this extra term gives a longer diffusion length of 1600Å and a scattering length of 20Å. These values are significantly longer than that reported by Huomo et al (1987) for single crystal Mo(111), although these authors used a slightly lower value of n in the Makhovian profile. Close examination of the fitted curves shows that the curves coincide in the range 4-10kV with the epithermal model giving closer agreement with the data below 4kV (fig. 7.8). This agrees with the findings of Huomo et al where a simple

diffusion model could only be fitted succesfully above an incident positron energy of 4keV.

7.4 Concluding Remarks

These analyses indicate that epithermal emission of positrons and positronium is dominated by simple elastic scattering of positrons. The Makhovian profile is a valid model for the positron stopping profile if a "stopped" positron is taken to mean an epithermal positron with insufficient energy to excite an electron state.

The scattering length is equivalent to the mean free path of a hot positron in the material. As such any structure narrower than this is unlikely to be resolved in a profiling experiment. This also gives an indication of the thickness of the overlayer which can be tolerated in a profiling measurement. A layer thinner than the scattering length would only contribute to a 'surface state' and would not be seen independently. Doppler-broadening experiments are therefore useful for profiling samples with dirty surfaces with coverages up to about 10 monolayers, compared with the clean surfaces necessary for positronium fraction measurements.

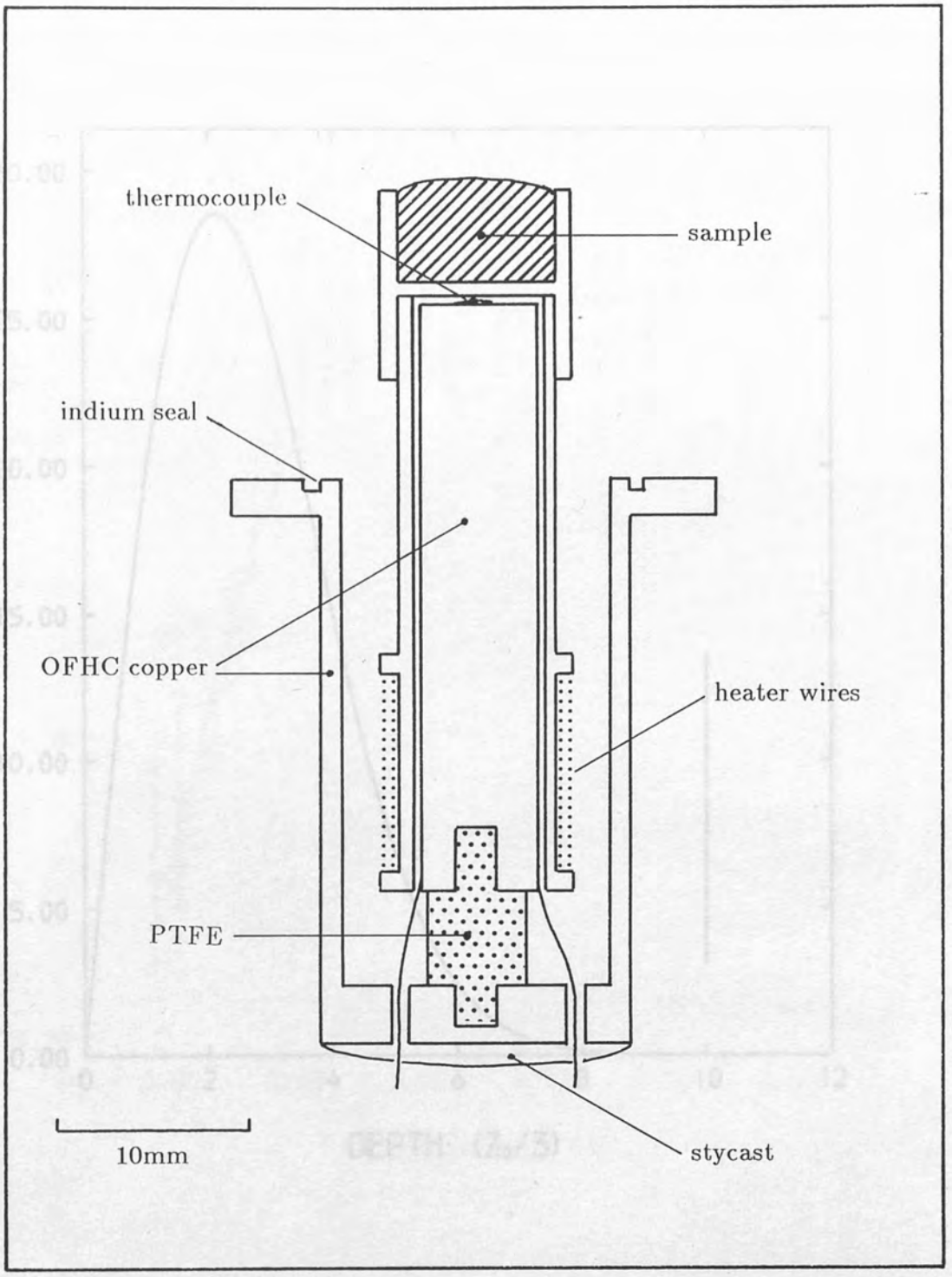

Figure 7.1

Sample holder for use with liquid targets in the cryostat positron beam.

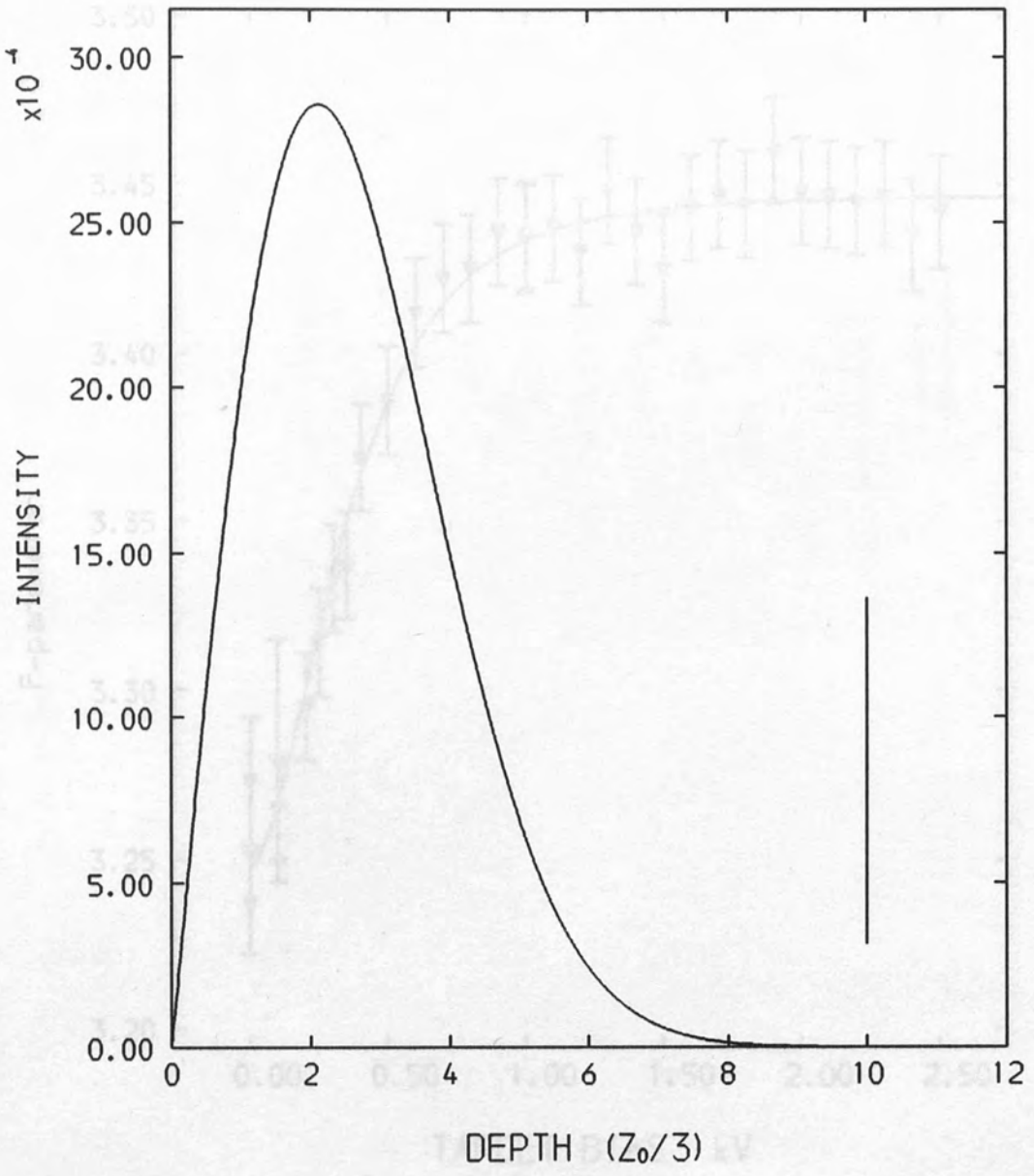

Figure 7.2

Scaled Makhovian profile with shaping $m = 2$. The Laplace transform is calculated over 1000 elements up to the line at $10z_0/3$.

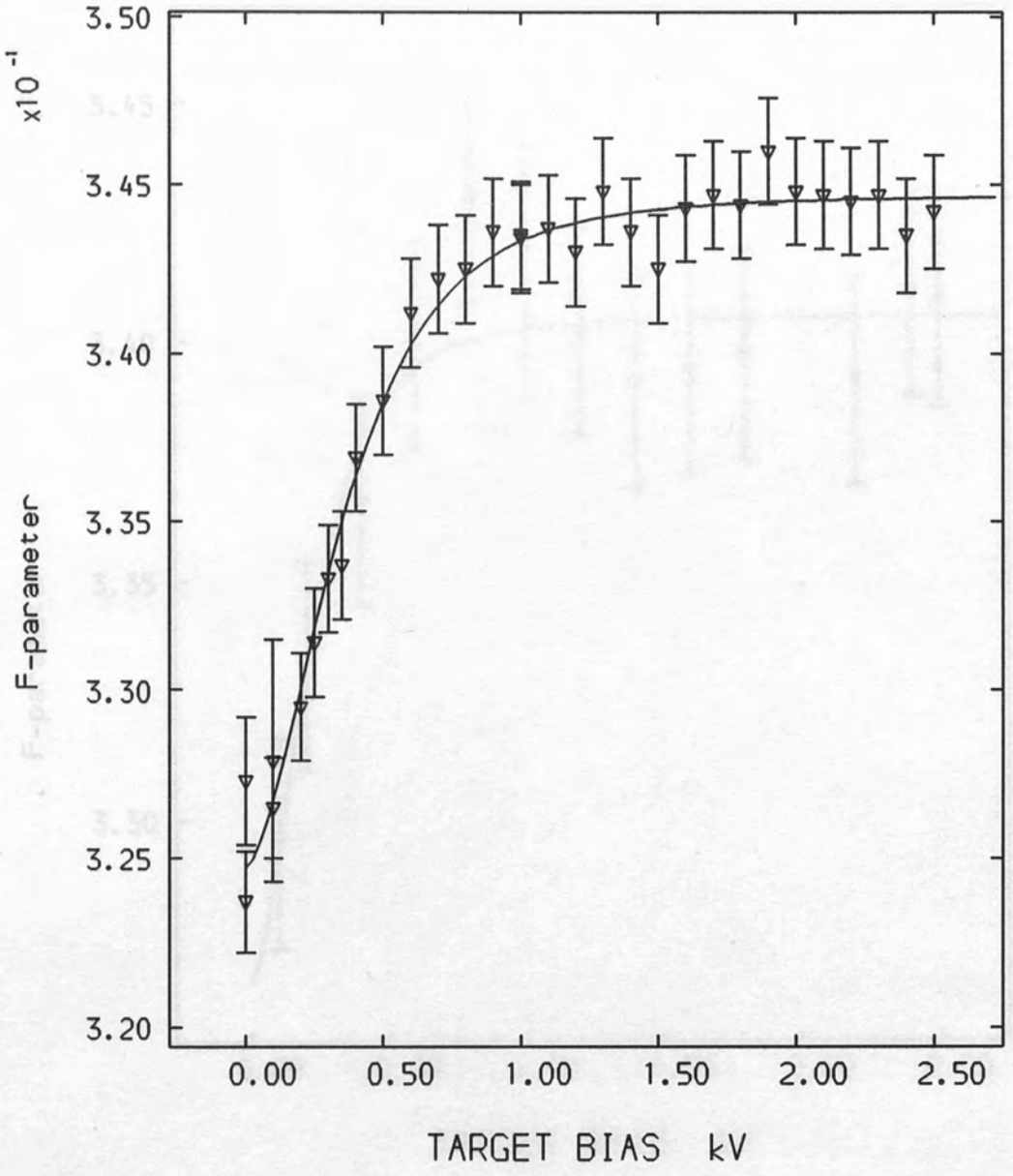

Figure 7.3

Fit of the back diffusion model to lineshape parameters for low energy positrons incident on liquid Ga at 420K.

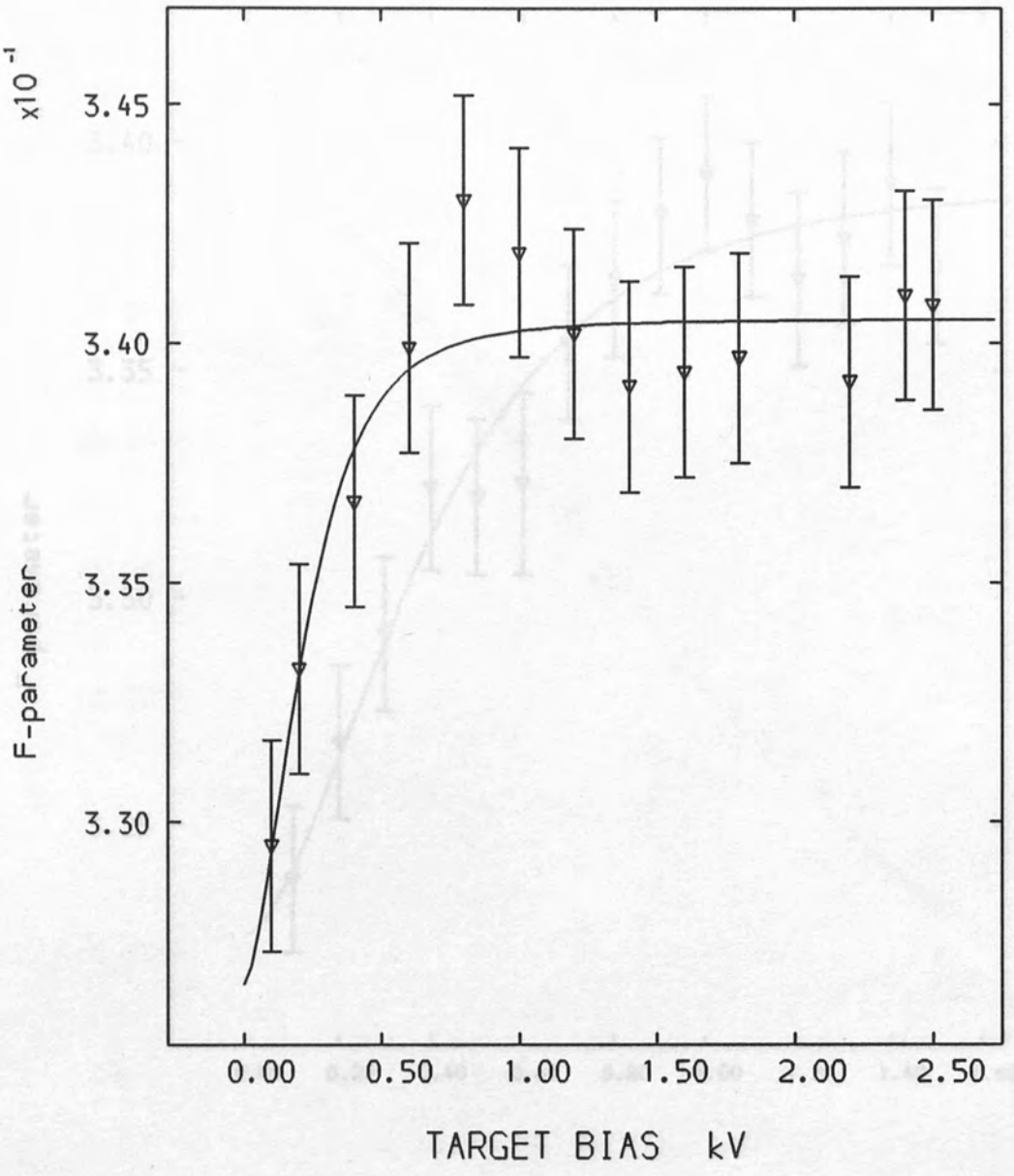

Figure 7.4

Fit of the back diffusion model to lineshape parameters for low energy positrons incident on solid Ga at 95K.

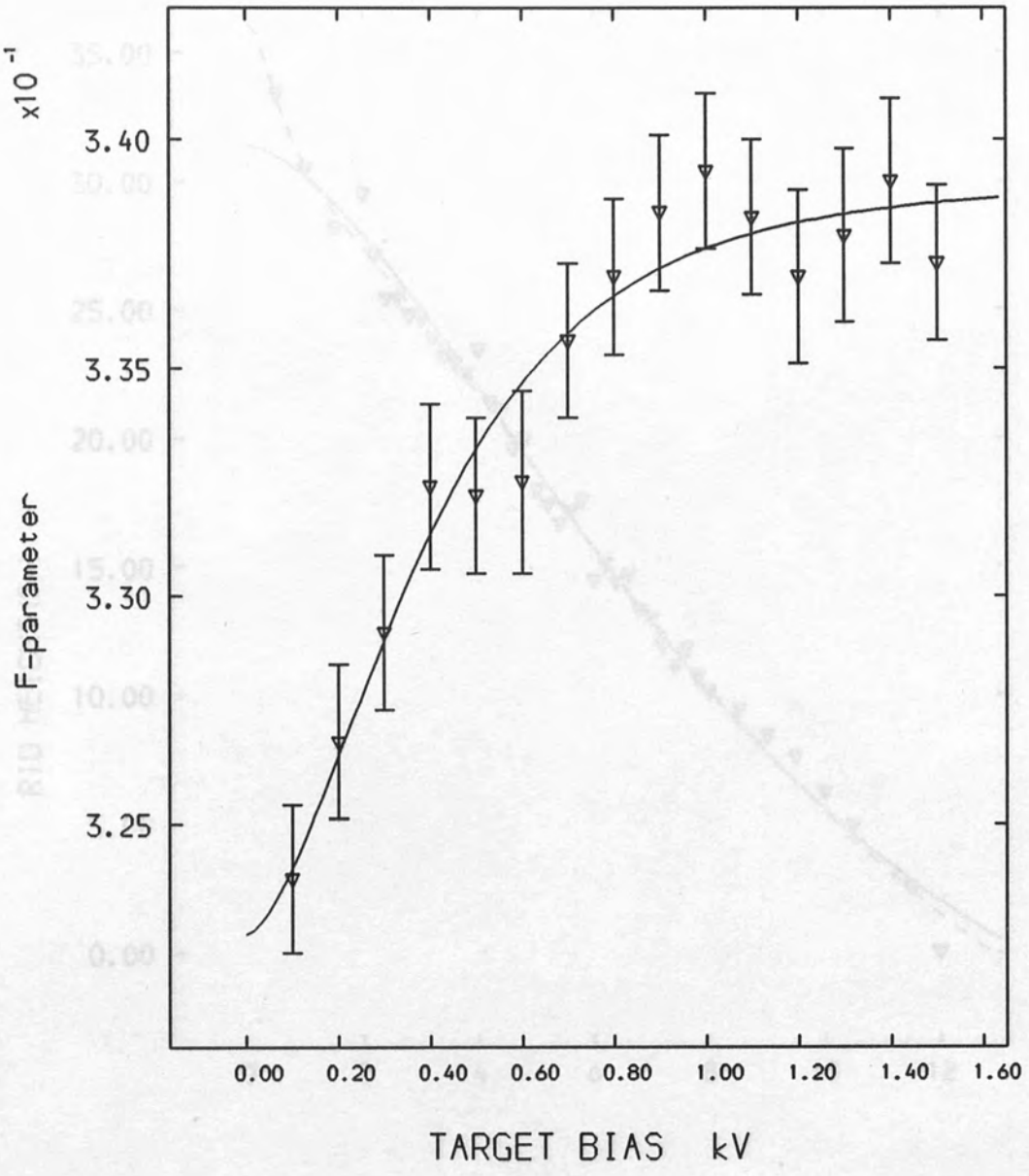

Figure 7.5

Fit of the back diffusion model to lineshape parameters for low energy positrons incident on solid Ga at 295K.

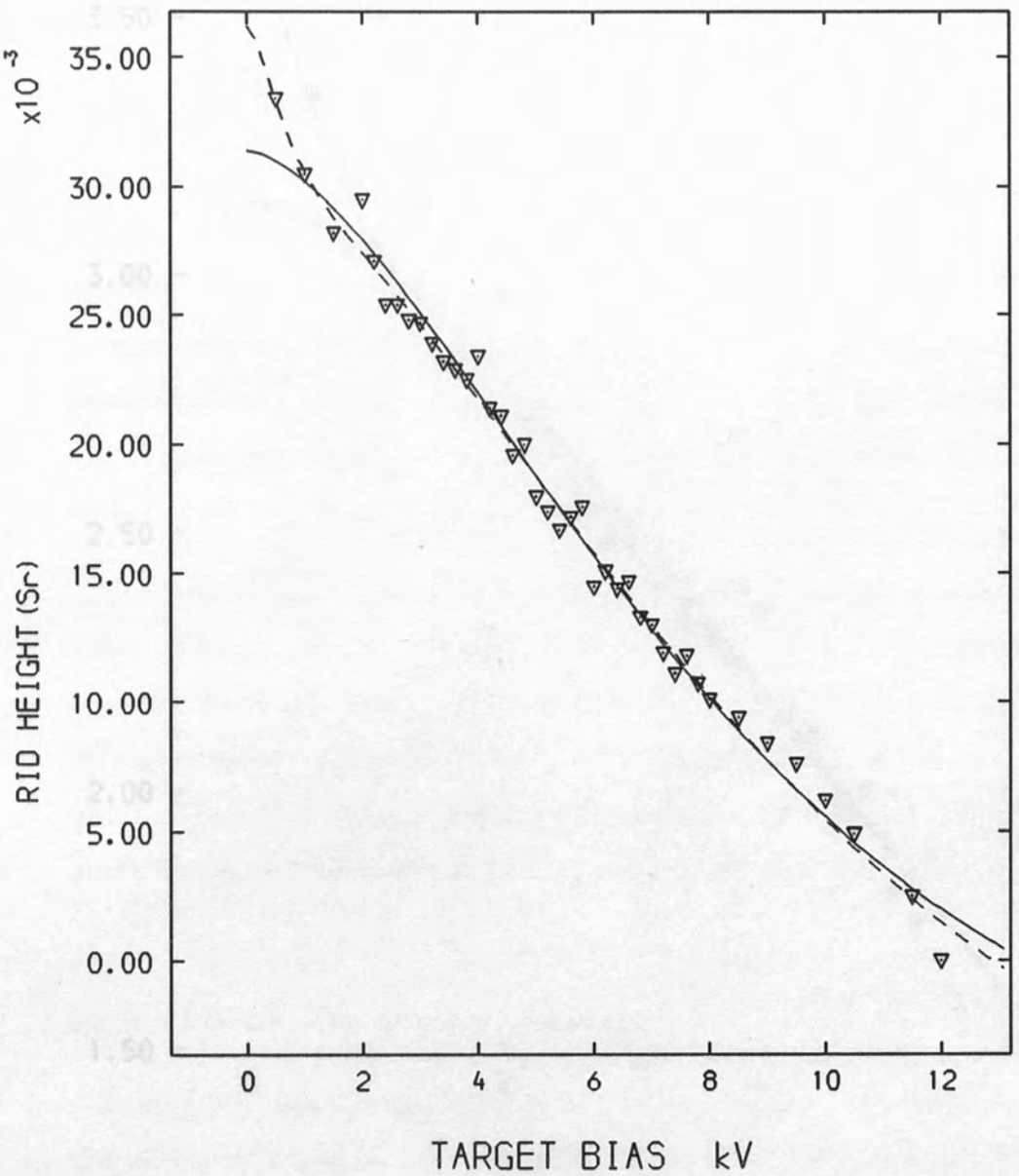

Figure 7.7

RID height S_r for slow positrons on annealed Mo. The solid line is a fit to the back diffusion equation, the broken line includes epithermal backscattering.

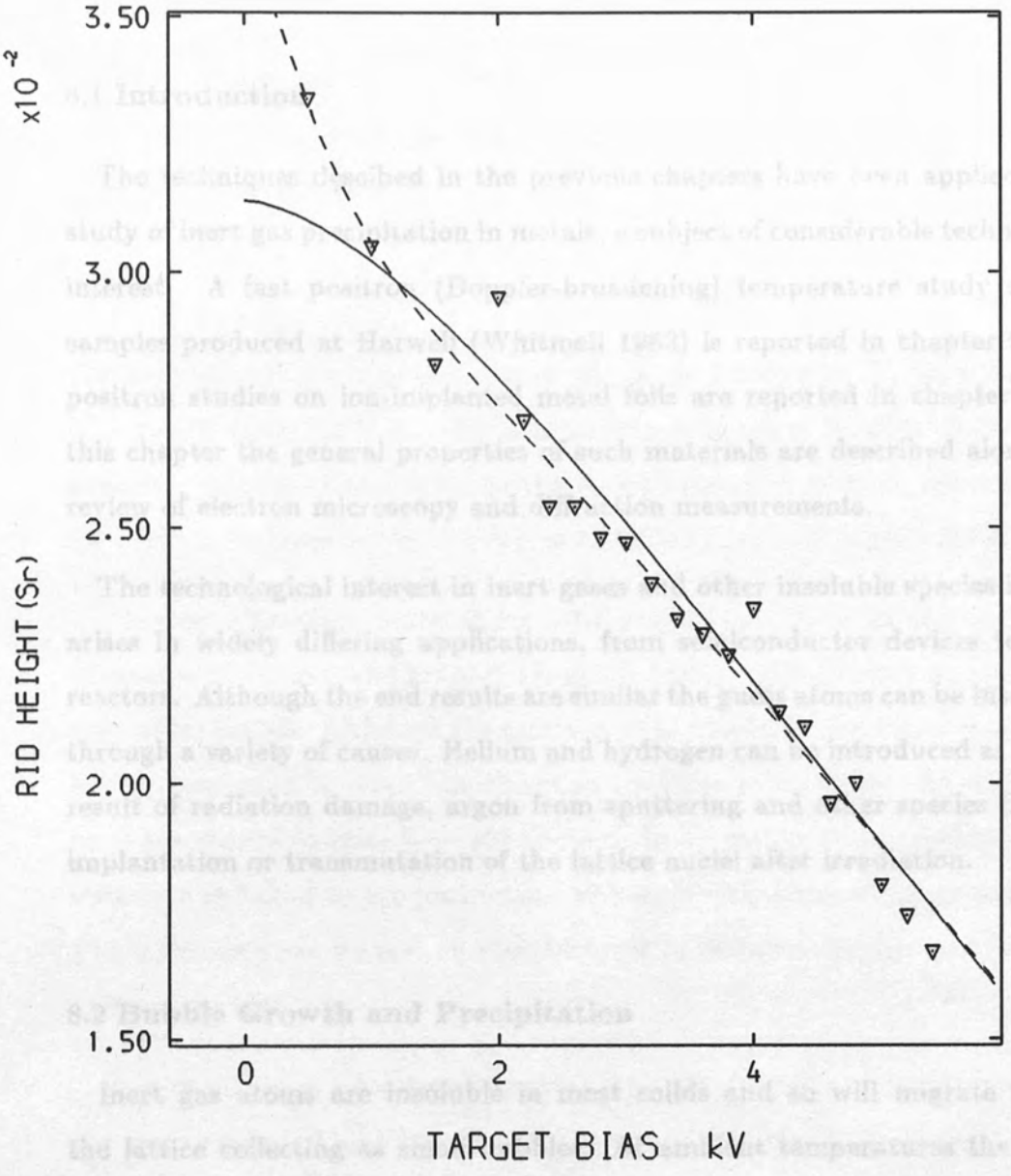

Figure 7.8

Expanded plot of the modelled lineshape parameters for positrons in Mo showing convergence of the two curves above 4keV incident energy.

Chapter 8 Inert Gas Precipitates in Metals

8.1 Introduction

The techniques descibed in the previous chapters have been applied to the study of inert gas precipitation in metals, a subject of considerable technological interest. A fast positron (Doppler-broadening) temperature study on bulk samples produced at Harwell (Whitmell 1982) is reported in chapter 9. Slow positron studies on ion-implanted metal foils are reported in chapter 10. In this chapter the general properties of such materials are described alongside a review of electron microscopy and diffraction measurements.

The technological interest in inert gases and other insoluble species in solids arises in widely differing applications, from semiconductor devices to fusion reactors. Although the end results are similar the guest atoms can be introduced through a variety of causes. Helium and hydrogen can be introduced as a direct result of radiation damage, argon from sputtering and other species from ion implantation or transmutation of the lattice nuclei after irradiation.

8.2 Bubble Growth and Precipitation

Inert gas atoms are insoluble in most solids and so will migrate through the lattice collecting as small bubbles. At ambient temperatures the growth of the cavities is driven by the excess pressure caused by the incorporation of additional gas atoms (Evans 1986), probably through some mechanism such as dislocation loop punching. The pressure P in the bubble is therefore determined by the shear modulus of the material (Evans & Mazey 1986)

$$\mathrm{P} = \frac{\mu b}{r} + \frac{2\gamma}{r}$$

where b is the Burgers vector of the dislocation, μ is the shear modulus of the material, r the radius of the bubble and gamma is a surface tension term.

Empirically all the available measurements for krypton and xenon in different metals can be fitted by $P = \mu/(16 \pm 4)$.

The pressures in the bubbles for krypton and xenon in most metals easily exceeds that required to solidify the gas given by empirical Simon equation (Simon & Glatzel 1929)

$$P = A\left(\left(\frac{T}{T_0}\right)^C - 1\right)$$

For krypton the appropriate values are $A = 2.376$kBar, $T_0 = 115.7$K and $C = 1.6169$ (Bab 1963) leading to a melting pressure of 8.7kBar at 300K. The pressure, calculated according to the Ronchi equation of state (Ronchi 1980), for krypton bubbles in Cu at 293K is 32.5kBar (Evans & Mazey 1985).

Electron diffraction patterns for solid argon (vom Felde et al 1984), xenon (Templier et al 1984) and krypton (Evans & Mazey 1985a) have been reported in several *fcc* metals. Although the terms 'gas' and 'bubble' are almost nonsensical in this context it is more convenient to continue using them, the state of the inert gas should be clear from the context. In *fcc* metals these gases have an *fcc* structure epitaxial to the host lattice although with a larger lattice parameter. This mismatch can be seen in Moiré fringes in electron micrographs (Donnelly & Rossouw 1985).

In molybdenum, a *bcc* metal, krypton precipitates with an *fcc* structure with the close packed (111) plane parallel to one of the Mo (011) planes (Evans & Mazey 1985b). The calculated pressure from the packing density was 62kBar. Using this pressure in the Simon equation yielded a melting temperature of 873K in reasonable agreement with the observed temperature of 923K. However for xenon in iron, also a *bcc* metal, Templier et al (1986) report no allignment of the precipitate with the host matrix.

In *hcp* metals xenon (Templier et al 1986) and krypton (Evans & Mazey 1986) precipitate with a hcp structure epitaxial to the host lattice. The collected

properties of inert gas precipitates are summarised in table 8.1.

8.3 Bulk Metal(Gas) Composites

The raison d'être of the bulk samples produced at Harwell (Whitmell 1982) is the long term storage of ^{85}Kr which is released during the reprocessing of nuclear fuel, although the initial samples contained non- active krypton. ^{85}Kr has a half-life of 10.8 years, decaying through β^- decay to ^{85}Ru which may cause corrosion problems during storage. Ideally the gas should be stored for at least a century; at present it is released into the atmosphere during reprocessing.

Should the reprocessing of spent fuel be stepped up then it may become necessary to restrict its release into the environment. Storage of the gas at high pressures in cylinders is possible but has several clear disadvantages. A leak would discharge a large quantity of the gas, inspection of the cylinders would be difficult and the cost of engineered stores to overcome these limitations would be very high. Disposal at sea of gaseous krypton is not permitted. Imobilisation in a solid matrix is therefore the most promising solution.

The process developed at Harwell produces samples with an extended homogeneous bubble distribution similar to the defected layer in ion- implanted samples. This extends the range of techniques which can be used to study the behaviour of any implanted species. 5 atomic % of krypton, equivalent to 170 litres of gas at STP per litre of metal, can be incorporated into a range of metals including copper and nickel. In the event of the metal matrix being damaged only the gas in the bubbles at the point of fracture (a negligible amount) will be released.

8.3.1 Combined Implantation and Sputtering Process

Figure 8.2 shows the Harwell implantation and sputtering plant with the principles of operation shown in figure 8.3. A glow discharge is generated in the krypton at 0.1 mBar between the two co-axial cylindrical electrodes by applying a potential difference of between 3 and 5kV. This discharge is used a source of negative ions for both implantation of krypton and sputtering of the negative electrode. When the outer electrode is negative the krypton is implanted into the surface. The implanted layer is then covered with a layer of fresh metal sputtered from the central electrode by switching the negative potential to this electrode. By repeating the process several times a second a layer several centimetres thick can be slowly built up. The process is controlled by adjusting the voltages and relative electrical charges used for each stage.

The half-scale pilot plant operated, with copper, at 30kW incorporating more than $0.3l$/h of gas. A 30kg deposit 22mm thick contained over $300l$ of gas (at STP), corresponding to an average concentration of 3.3 at. %. A full size system operating at 100kW is expected to deposit a layer 20mm thick containing $2100l$ of gas in 90 days.

8.3.2 Properties of Bulk Cu(Kr)

The material produced at Harwell has similar physical properties to many copper alloys (Whitmell 1982) having a thermal conductivity of 8 $Wm^{-1}K^{-1}$ and a similar specific heat and melting point to pure copper. It is extremely hard, with a Vickers hardness number of 340, and brittle and is 5 times more resistant to corrosion than Cu. The bulk density is slightly lower than pure copper (Evans et al 1985) at 8.46g/cm^3 compared with 8.92. The lattice parameter for the as-deposited material, as measured with X-ray diffraction was 3.629Å compared with 3.615Å for pure copper, although it returned to the lower value after annealing at 773K.

The structure and annealing behaviour of the material has been studied by Evans et al (1985) using transmission electron microscopy (TEM). The material is polycrystalline with a very small (0.2-0.3 μm) randomly orientated grains . The bubbles have diameters in the range 15-20Å and are randomly packed with a packing density of $\sim 4 \times 10^{24}$ m^{-3}. Later electron diffraction work (Evans & Mazey 1985) has shown krypton to be solid with a lattice parameter of 5.2Å corresponding to a packing density of 2.85×10^{28} m^{-3}. This corresponds to a pressure determined from the Ronchi equation of state (Ronchi 1981) of 32.5 kBar. In nickel the krypton has a higher packing density (3.2×10^{28} m^{-3}) and a correspondingly higher pressure of 62 kBar.

Host	Guest	Matrix	Precip.	P kBar	Reference
Al	Xe	*fcc*	*fcc* ep.	13	Templier et al 1986
Ag	Xe	*fcc*	*fcc* ep.	11	Templier et al 1986
Au	Xe	*fcc*	*fcc* ep.	8	Templier et al 1986
Ni	Xe	*fcc*	*fcc* ep.	29	Templier et al 1986
Cu	Xe	*fcc*	*fcc* ep.	14	Templier et al 1986
Cu	Kr	*fcc*	*fcc* ep.	32.5	Evans & Mazey 1985*a*
Ni	Kr	*fcc*	*fcc* ep.	62	Evans & Mazey 1985*a*
Au	Kr	*fcc*	*fcc* ep.	12.5	Evans & Mazey 1985*a*
Mo	Kr	*bcc*	*fcc*	62	Evans & Mazey 1985*b*
Fe	Xe	*bcc*	*fcc*	29	Templier et al 1986
Ti	Kr	*hcp*	*hcp* ep.	20	Evans & Mazey 1986
Zn	Xe	*hcp*	*hcp* ep.	42	Templier et al 1986

Table 8.1

The structure and pressures of inert gas precipitates in different metals. The pressures P are those reported by the authors in the references given calculated from lattice parameter measurements using the Ronchi (1980) equation of state. In column 4 "ep." indicates that the precipitate is epitaxial to the host lattice.

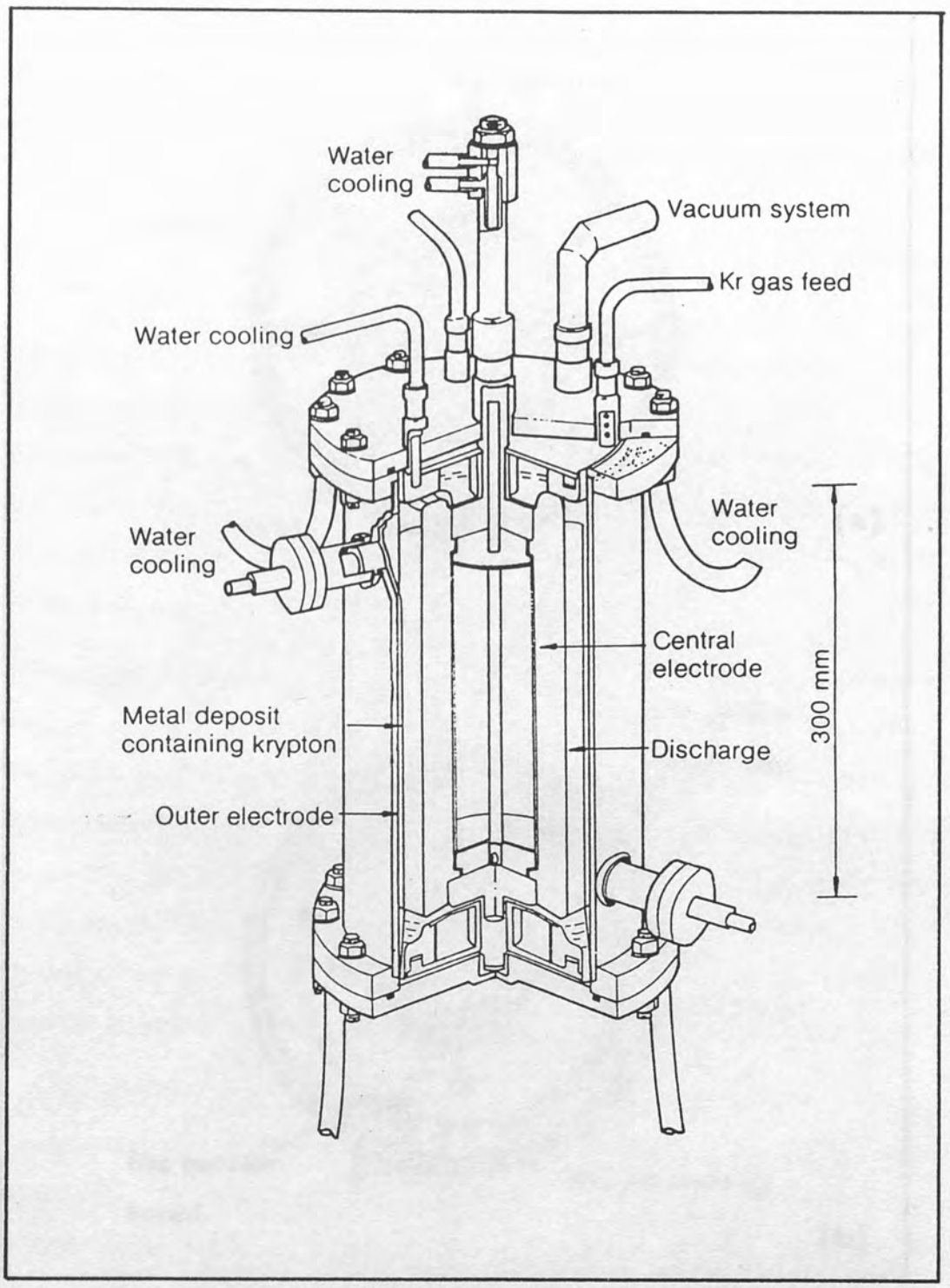

Figure 8.2

The Harwell combined implantation and sputtering plant (Whitmell 1982).

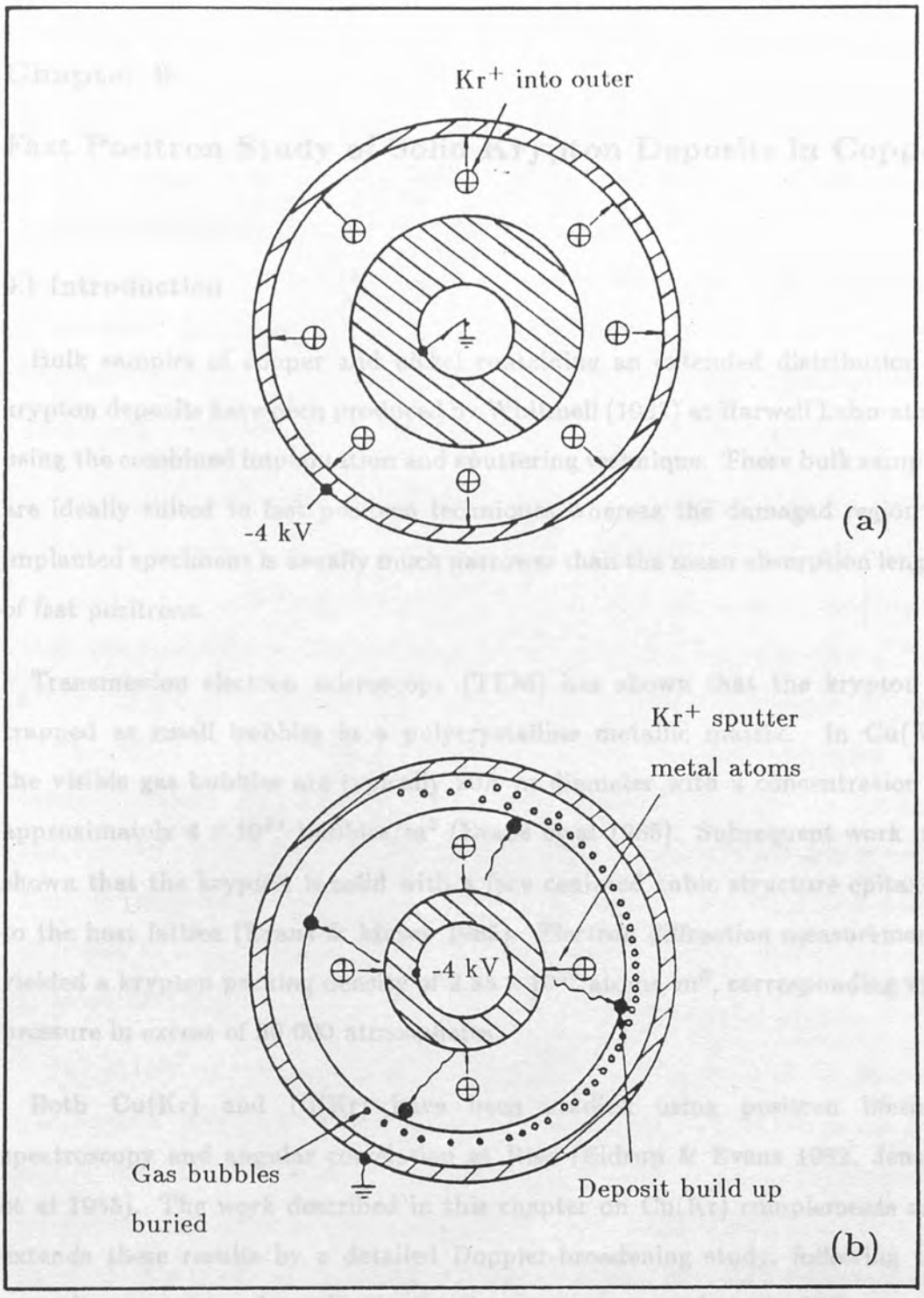

Figure 8.3

The Harwell process: (a) Kr is implanted into the outer cylinder; (b) Metal is sputtered from the inner cylinder to the outer.

Chapter 9

Fast Positron Study of Solid Krypton Deposits in Copper

9.1 Introduction

Bulk samples of copper and nickel containing an extended distribution of krypton deposits have been produced by Whitmell (1982) at Harwell Laboratory using the combined implantation and sputtering technique. These bulk samples are ideally suited to fast positron techniques whereas the damaged region in implanted specimens is usually much narrower than the mean absorption length of fast positrons.

Transmission electron microscopy (TEM) has shown that the krypton is trapped as small bubbles in a polycrystalline metallic matrix. In Cu(Kr) the visible gas bubbles are typically 20Å in diameter with a concentration of approximately 4×10^{24} bubbles/m^3 (Evans et al 1985). Subsequent work has shown that the krypton is solid with a face centered cubic structure epitaxial to the host lattice (Evans & Mazey 1985). Electron diffraction measurements yielded a krypton packing density of 2.85×10^{28} atoms/m^3, corresponding to a pressure in excess of 30 000 atmospheres.

Both Cu(Kr) and Ni(Kr) have been studied using positron lifetime spectroscopy and angular correlation at Risø (Eldrup & Evans 1982, Jensen et al 1985). The work described in this chapter on Cu(Kr) complements and extends these results by a detailed Doppler-broadening study, following the annealing process and continuing the temperature range down to 80K.

9.2 Experimental and Analytical Method

Squares of side 1cm and thickness 1.5mm were cut by spark erosion from an

as-deposited sample of copper containing approximately 3 atomic % krypton. After etching with nitric acid, conventional source sandwiches were made. Two different types of source were used with two different sets of samples; for measurements taken in the temperature range up to 600K, carrier free ^{22}NaCl solution was deposited directly onto the centres of the inner faces of one pair of samples. Evaporation problems inhibited the use of this source at higher temperatures and so, in the high temperature regime neutron irradiated copper (producing ^{64}Cu) foils were used between the other pair of specimens.

The annihilation spectra were recorded with a high-resolution Ge detector and the automated spectrometer system developed by K.U.Rao (1987) while the sample was held at the required temperature. For measurements in the range 80-450K the temperature was maintained by mounting the first sample set (^{22}NaCl source) in a double-jacket liquid-nitrogen cryostat fitted with a sample heater; above 450K the appropriate sample pair was held in an electric furnace. Some overlap between the respective temperature ranges for the different apparatus and sources was allowed for normalisation of the lineshape parameter values. This 'at-temperature' procedure differs from the isochronal annealing method of Jensen et al (1985) where the post-anneal measurements were always made at room temperature.

The 511kV annihilation lines were analysed both in terms of the lineshape parameter F, being the normalised count in the centre 15 channels of the peak, and by fast Fourier transform deconvolution. In both cases a complementary error-function background was subtracted beforehand (Chaglar et al 1981), although this is not necessary for F parameter analysis. The assymmetry of the lineshape, caused by incomplete charge collection in the detector, does have a significant effect, however, on the Fourier spectrum. Both sides of the deconvoluted peak were fitted with an unweighted least squares fit to a modelled function of two Gaussian curves and an inverted parabola. In a simple metal there are two distinct components to the lineshape; a parabola

due to annihilation with the (almost) free conduction electrons and a Gaussian which approximately represents annihilation with core electrons. Copper is a marginal case but Doppler-broadened lineshapes have been succesfully fitted with this model using repeated numerical convolution (Rice-Evans et al 1976). A second Gaussian was included to represent annihilation with the krypton atomic electrons.

9.3 Results and Discussion

9.3.1 Lineshape Parameter

The clearest indication of changes in the positron response with temperature are seen in a plot of normalised F parameters (fig 9.1). These changes have the same form as the mean-lifetime data reported by Jensen et al (1985) and can be correlated rather well with the electron diffraction and microscope observations during heating (Evans et al 1985, Evans & Mazey 1985) and with the associated physical processes taking place at the positron traps. There are at least three distinct stages of the F parameter behaviour beginning with an initial slow rise from 100K upwards, followed by a rapid rise starting between 500 and 600K and finally a sharp fall above 800K. Between about 450 and 550K a possible transient region can be detected.

Remembering that the material was manufactured, and had been stored for some time, at ambient temperature the initial rise from 100K up to at least 300K can be attributed to the normal thermal expansion effects customarily seen in metals in the pre-vacancy region (see for example West 1979). However the remaining stages of the F parameter response are clearly associated with changes in positron trapping as the physical state of the Cu(Kr) changes with temperature. The starting material with a very high density of small krypton-filled cavities would certainly be expected to give 100% trapping as indicated by the single lifetime component in the results of Eldrup and Evans (1982). It

is then clear that any subsequent narrowing of the line (increase in F) must be associated with changes in, or at, the positron trap.As the bubble pressure starts high and is expected to drop on annealing the obvious correletion is to associate the rise in F with a drop in the krypton packing density and pressure as the bubbles gain matrix vacancies. On this basis an initial transient rise of F from 400 to 550K, above that due to thermal expansion, might be due to a continuation of the pressure-driven cavity growth that occurs during the original incorporation of the krypton in the bubbles. Only now, instead of the pressure increase being due to the addition of new gas atoms in the bubbles, the pressure increase is now simply a result of the temperature increase. In both cases the gain of vacancies is due to the well-known dislocation loop punching mechanism (Greenwood et al 1959).

The rather dramatic rise in F starting between 500 and 600K is of particular interest since it is in this region that the melting of the krypton has been demonstrated in similar Cu(Kr) material. As suggested by Evans & Mazey (1985) melting will remove any barrier to thermal migration of the small bubbles expected by surface diffusion processes at high temperatures (see for example Gruber 1967). The overall physical effect is a general coarsening of the bubble structure as the bubbles migrate and coallesce with a drop in bubble pressure, particularly at the higher temperatures when thermal vacancies become available. The TEM work already mentioned many times showed an increase in the average bubble diameter from 22 to 60Å over the range 625-675K, a factor of 20 in the average volume. Above 800K the krypton begins to be expelled from the metal via grain boundary channels (Evans et al 1985) and as clearly reflected in the F parameter the fraction of positrons trapped at the bubbles must fall during this process.

9.3.2 Component Analysis

Deconvolution analysis leads to a more detailed understanding of the nature of the positron trap at the krypton bubble. In the as-prepared material with 100% trapping at the bubbles the most surprising result is perhaps that the krypton Gaussian component is only 35% (fig 2.2); a large fraction of trapped positrons appear to annihilate with both copper core and conduction electrons. Also, in pure copper the ratio of the Gaussian and parabola intensities is 3:1 (Rice-Evans et al 1976) whereas for this material this ratio starts at just over 2:1. Thus in the initial material annihilation with the copper conduction electrons appears to be enhanced. This result, together with the relatively low fraction of annihilations with the krypton electrons, leads to the suggestion that the positron could be trapped at the surface of the bubbles. This possibility was also mentioned in explaining the high momentum tails of angular correlation curves measured on similar samples (Eldrup & Evans 1982). Of particular relevance on this point are the results of molecular dynamics simulations for noble gases in metals (Finnis et al 1983, Jensen & Nieminen 1987). These simulations, as well as unpublished work on Cu(Kr) (K.O.Jensen priv. comm. 1986), show that for helium with a high packing density between a sandwich of metal atoms (i.e. a bubble with a platelet configuration) there is a larger spacing between the first helium layer and the metal than the He-He nearest neighbour distance. This significant stand-off distance between the gas atom and the metal is due to the repulsive gas-metal potential and is expected for other inert-gas metal systems. Clearly this gap at the interface is a plausible site for positron trapping.

The intensity behaviour of the deconvoluted components during annealing (figs. 9.2 and 9.3) is consistent with this trapping picture. As expected from the previous description of the F parameter, the changes below 550K are small but above this temperature, large effects can be seen. It was perhaps a little unfortunate that the change in sample pairs at 600K coincided with the start

of the rapid bubble annealing since there were significant differences between the two sets of samples in both intensities and widths of the components.

Above 800K when the krypton starts to be expelled from the metal, there are large relative changes in all three components. Significantly there is a sharp drop in the intensity of the narrow Gaussian component, supporting its identification with annihilation with the krypton electrons. Also of interest is the relative behaviour of the two other components corresponding to annihilation with the copper electrons. As the positron trapped fraction drops below 100% (in the lifetime results of Jensen et al (1985) this occurs at 775K) there should be a clear tendency for the relative intensities of these components to revert to the pure metal case. This is exactly what is seen with the final ratio of the copper Gaussian to parabola moving towards the ratio of 3:1 for this temperature (Rice-Evans et al 1976).

Concentrating on the component behaviour between 600 and 800K (fig. 9.3), it is interesting that there is a rise in the parabola intensity at the same time as a fall in the intensity of the Gaussian due to annihilation with krypton electrons. In this temperature region there must be a significant drop in the krypton packing density in the bubbles as the pressure drops. Thus an increase in open volume at the bubble surface would not be surprising and would lead to the component changes observed.

To complete the description of the results, figures 9.4 and 9.5 show the behaviour of the component widths with annealing temperature. The width of the krypton Gaussian is significantly narrower than that found with angular correlation measurements on solid krypton (Varlashkin 1971). The full width at half maximum calculated from a width of 11 channels is 1.72keV compared with 2.26keV (8.84 mrad) for solid krypton. This difference may be explained by the nature of the Cu-Kr interface because, in the event of trapping within the inter-space gap, the positrons would sample fewer higher momentum krypton

electrons. The same effect is seen in the same effect is seen in the copper Gaussian with the value here 12% lower than that previously found in pure copper (Rice-Evans et al 1976) whereas the parabola is some 8% wider.

9.4 Conclusions

These measurements are the first to investigate high concentrations of inert-gas atoms in metals using a detailed Doppler-broadening study of the positron annihilation radiation. There is a general agreement with the results of two previous studies using positron lifetime and angular correlation techniques, and good agreement with the physical picture of inert gas bubble annealing obtained from TEM studies.

Deconvolution analysis indicates that the positron is localised at the gas-metal interface which is in good agreement with current theoretical models which propose a stand-off distance between the metal lattice and the gas atoms. There is an indication of the existence of this gap in the narrowing of the component due to annihilation with electrons bound to the krypton atoms.

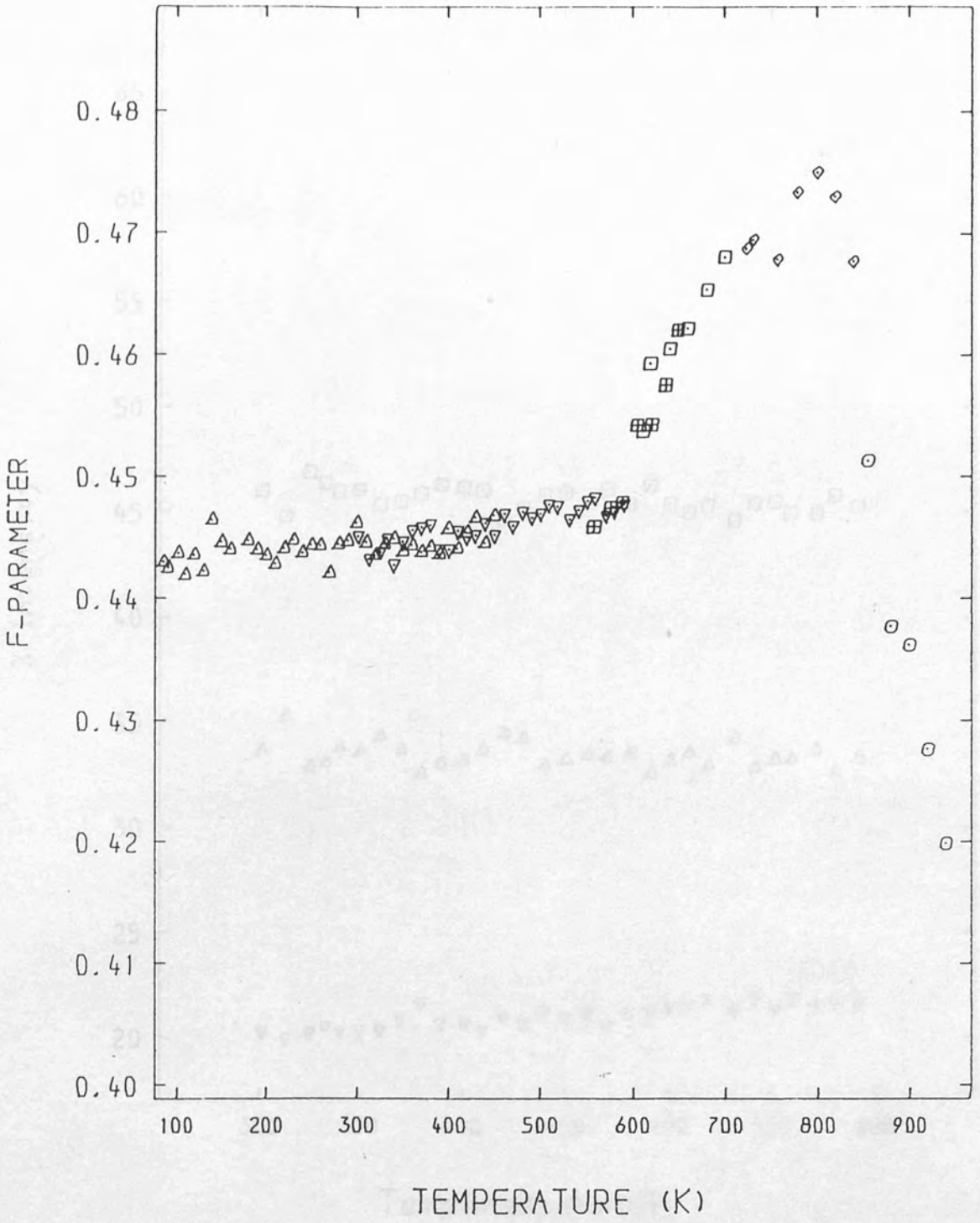

Figure 9.1

Variation in lineshape parameter F with temperature for bulk Cu(Kr). The different symbols indicate differences in equipment and sources.

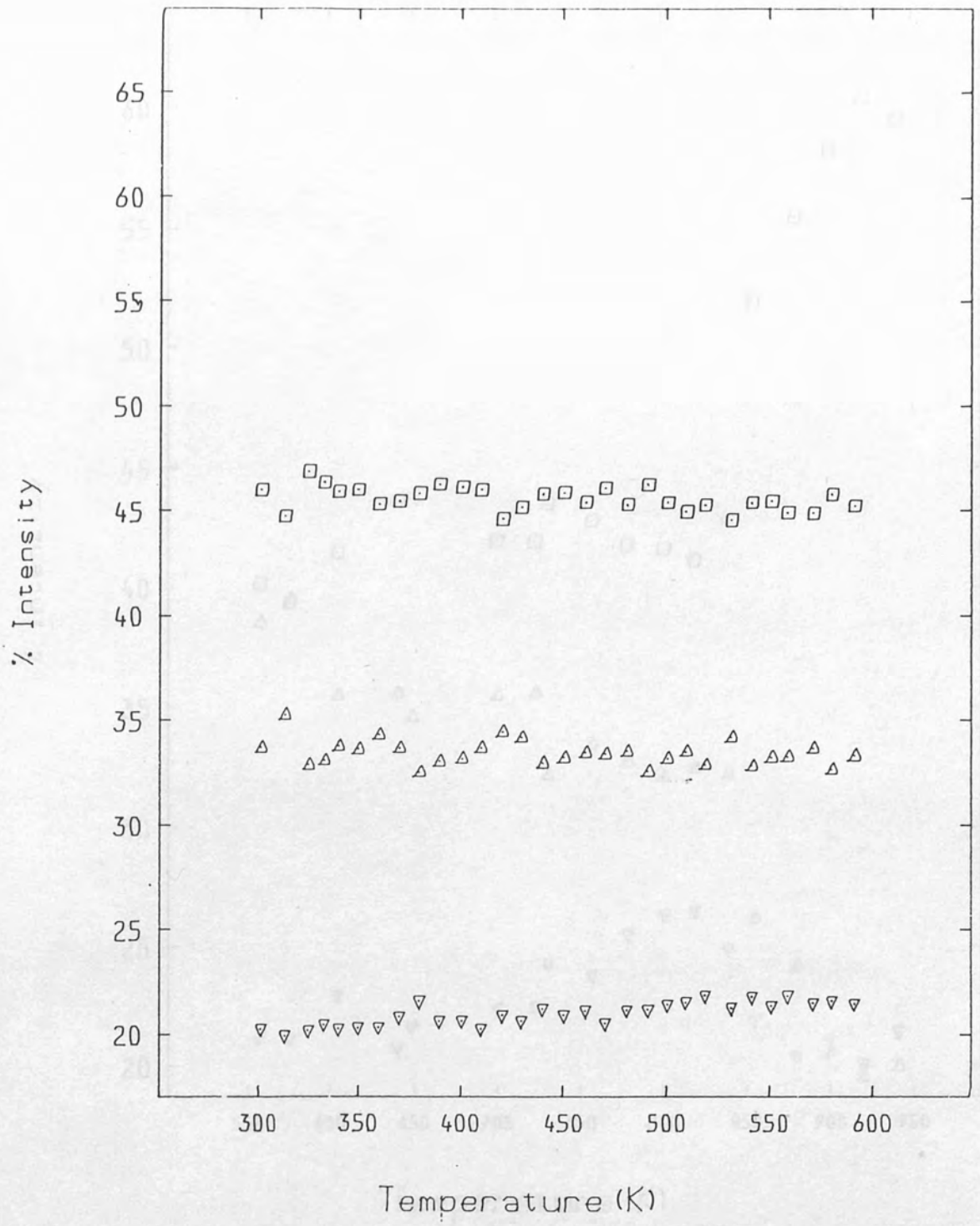

Figure 9.2

The components intensities in the range 300-600K. The narrow Gaussian is represented by the upwards triangle, the wide Gaussian by the square & the parabola by the downwards triangle.

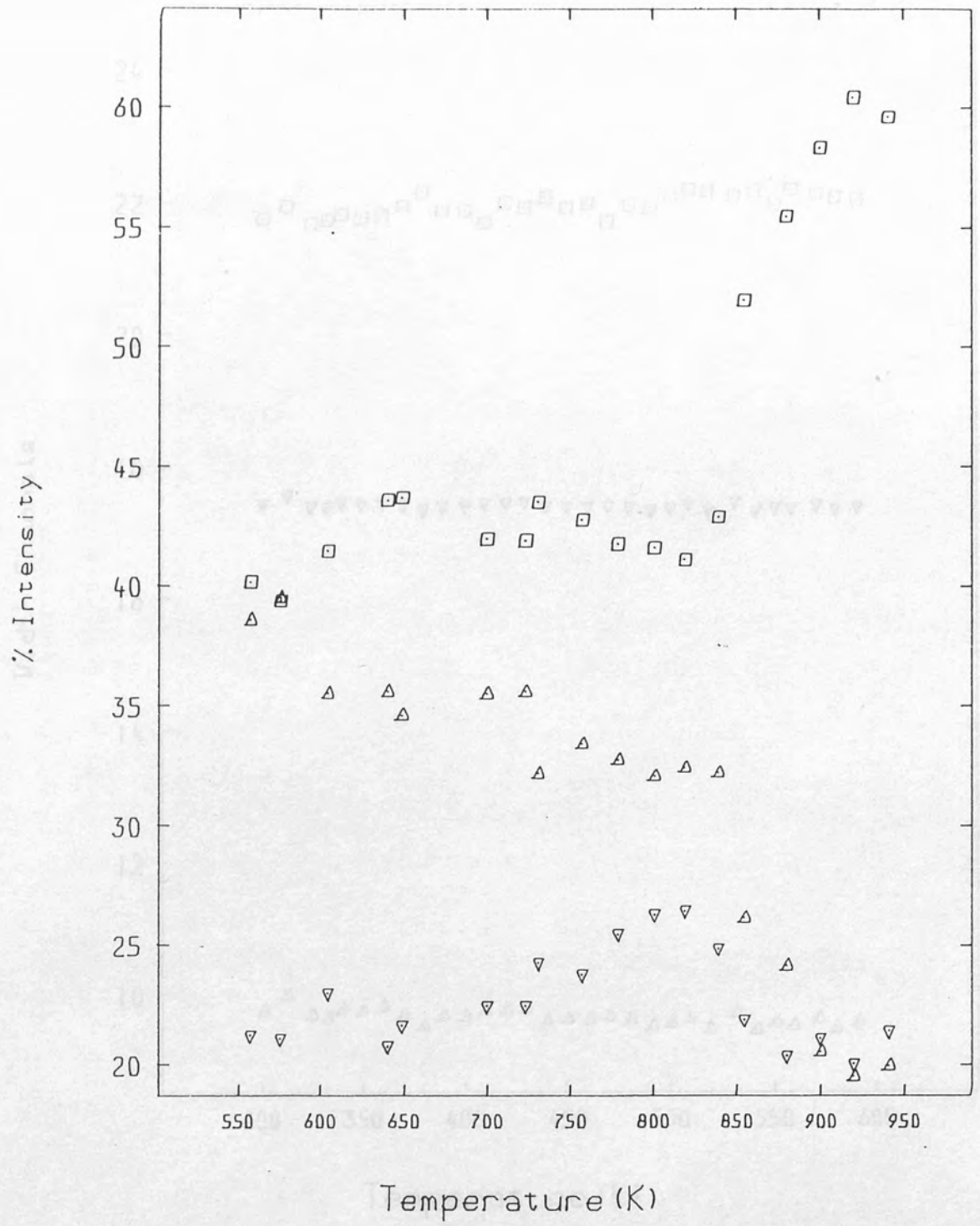

Figure 9.3

The components intensities in the range 550-940K. The narrow Gaussian is represented by the upwards triangle, the wide Gaussian by the square & the parabola by the downwards triangle.

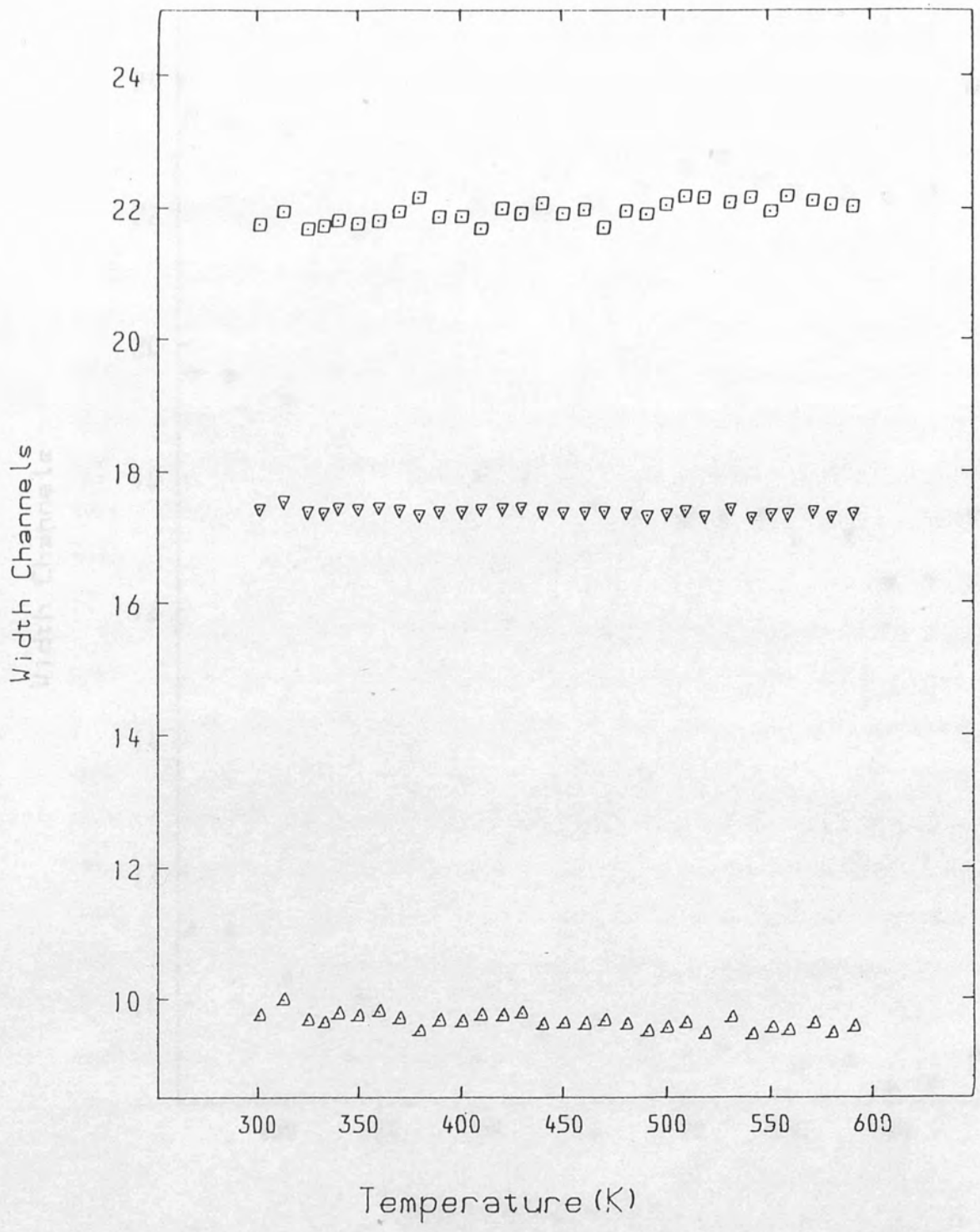

Figure 9.4

The components widths in the range 300-600K. The narrow Gaussian is represented by the upwards triangle, the wide Gaussian by the square & the parabola by the downwards triangle.

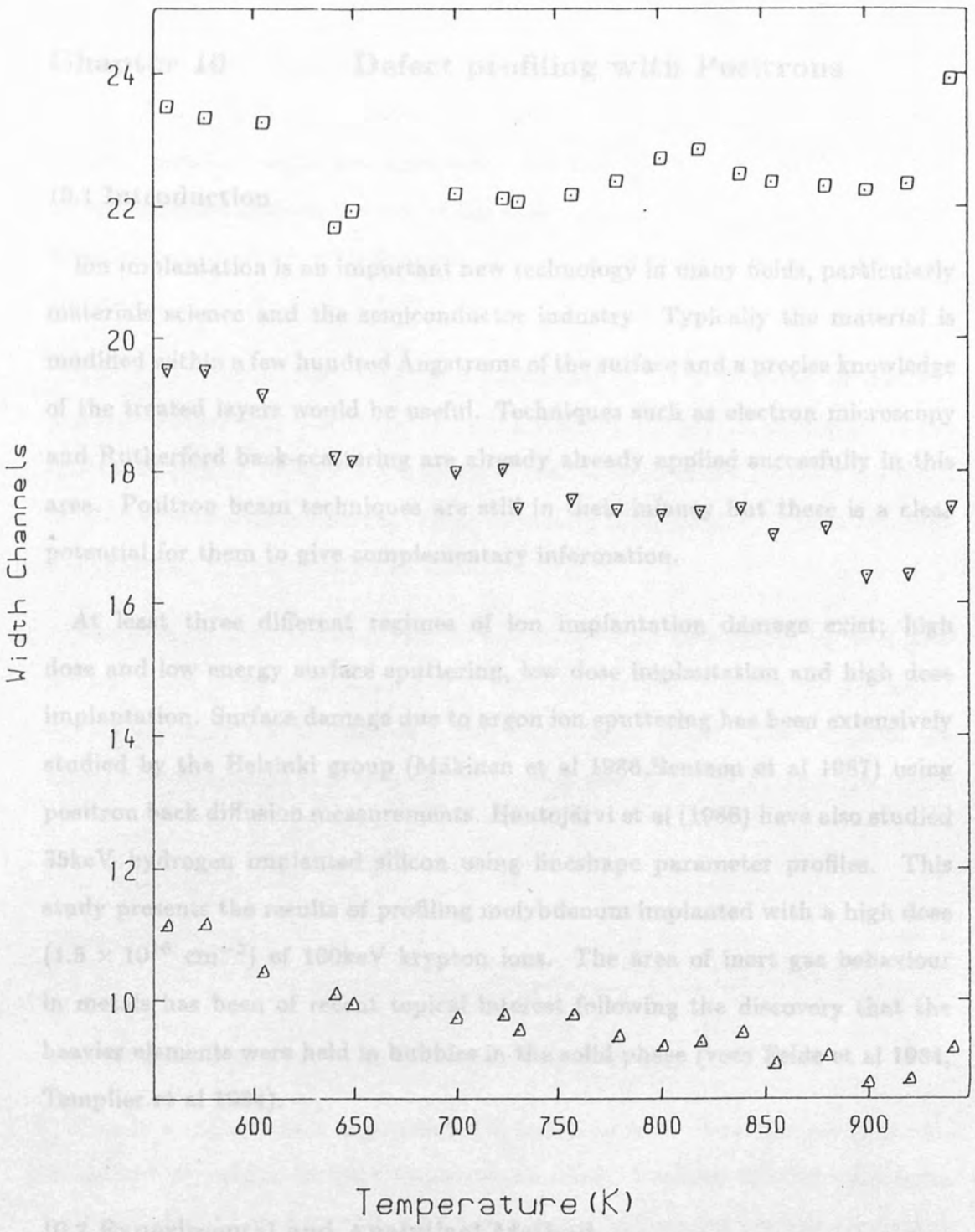

Figure 9.5

The components widths in the range 550-940K. The narrow Gaussian is represented by the upwards triangle, the wide Gaussian by the square & the parabola by the downwards triangle.

Chapter 10 Defect profiling with Positrons

10.1 Introduction

Ion implantation is an important new technology in many fields, particularly materials science and the semiconductor industry. Typically the material is modified within a few hundred Ångstroms of the surface and a precise knowledge of the treated layers would be useful. Techniques such as electron microscopy and Rutherford back-scattering are already already applied succesfully in this area. Positron beam techniques are still in their infancy but there is a clear potential for them to give complementary information.

At least three different regimes of ion implantation damage exist; high dose and low energy surface sputtering, low dose implantation and high dose implantation. Surface damage due to argon ion sputtering has been extensively studied by the Helsinki group (Mäkinen et al 1986,Bentzon et al 1987) using positron back diffusion measurements. Hautojärvi et al (1986) have also studied 35keV hydrogen implanted silicon using lineshape parameter profiles. This study presents the results of profiling molybdenum implanted with a high dose (1.5×10^{16} cm^{-2}) of 100keV krypton ions. The area of inert gas behaviour in metals has been of recent topical interest following the discovery that the heavier elements were held in bubbles in the solid phase (vom Felde et al 1984, Templier et al 1984).

10.2 Experimental and Analytical Method

The experiment was performed on annealed polycrystalline molybdenum foil irradiated at Harwell with 100keV krypton ions to a total dose of 1.5×10^{16}cm^{-2}. The sample was mounted in the beam line described previously (Chap.3) in a Faraday cup held at the required bias voltage. The surface was degreased and

washed but not subjected to any chemical or mechanical polishing. To have done so would have removed the implanted layer and in the relatively low vacuum of this beam line would also have been pointless. Because of this the profiling measurements relied on the use of lineshape parameters, a technique which is actually improved by a 'dirty' surface which suppresses thermal positronium emission.

The change in 511keV lineshape parameter S_r as a function of incident positron energy was calculated from the running integrated difference (RID) spectra (Coleman 1976) relative to the lineshape from 12keV incident positrons on pure annealed molybdenum. These are shown in figure 10.1 for both annealed molybdenum and the irradiated specimen.

The data for the irradiated sample was fitted by an unweighted least-squares minimisation using a derivative of a Gaussian as the positron profile and a simple model of a step function defect distribution (§6.5). The values of the material independent scaling α and the power term n in the Makhovian profile

$$P(z,E) = \frac{-\mathrm{d}}{\mathrm{d}z} e^{-z^2/z_0^2}$$

where

$$z_0 = \frac{\alpha}{\rho} E^n$$

were taken as $4.5\mu\mathrm{g/cm}^2$ and 1.6 respectively (Vehanen et al 1986).

This is a rather crude approximation but does allow very fast analysis and is not too unrealistic for high implantation doses. Positron lifetime studies on bulk samples of copper containing a high density of krypton bubbles (Jensen et al 1986) indicates only one type of trap for the positron. Further work using high resolution Doppler-broadening spectroscopy (Chap. 9) suggests that this trap is at the precipitate. From this it follows that the trapping rate profile should map the krypton concentration profile. At high defect concentrations positron diffusion can be neglected.

To a first approximation the ion profile can be described as a simple step. Although the ion implantation profile is described by a Gaussian curve with a mean range and standard deviation, sputtering of the surface atoms enhances the concentration up to the peak (J.H.Evans priv comm). At very high doses (not achieved here) the profile has a steady state form approximating to an error function which is independent of ion dose. The calculated profile for this case is shown in figure 10.2 which includes a sputtering term of 6 atomic volumes per incident ion (Matsunami et al 1983). The range and standard deviation were both calculated as 149Å (Townsend et al 1976).

10.3 Results and Discussion

The fit of a simple step profile to the experimental data is shown in figure 10.3. Bulk, surface and defect values for S_r were fitted as free parameters as well as the diffusion coefficient at the surface, the relative trapping rate and the width of the defected layer. Depending on the initial guesses of the parameters the width of the defect step falls within the range 171 ± 2Å. The surface and bulk lineshape parameters are constant at 0.034 and -0.003. The diffusion coefficient returned was always very nearly zero ($\sim 10^{-6}\text{cm}^2/\text{s}$). This should not be interpreted as the true diffusion coefficient in Mo as in the fitting this parameter only plays a minor rôle affecting only the inclusion of the surface state at very low incident energies. Its very low value indicates saturation trapping in the defected region near the surface. The relative trapping rate and the defect value vary widely and are interconnected. In the fit shown in figure 10.3 the relative trapping rate was 0.7 of the bulk decay rate and the defect lineshape parameter was 0.062(6).

In order to improve the model to take into account the sizable tail in the ion distribution (fig. 10.2) a second box was added with its own depth and relative trapping rate. In fitting the trapping rate for this additional tail was

invariably returned as zero. A true chi-squared cannot be quoted as no weights were used in the least-squares minimisation but the scaled sum of squares was significantly higher (3.1 compared to 2.8) than for the single step. The width of the non-zero step was returned as 210Å with a relative trapping rate of 0.5 and a much lower value for the lineshape parameter associated with the defects (0.0001).

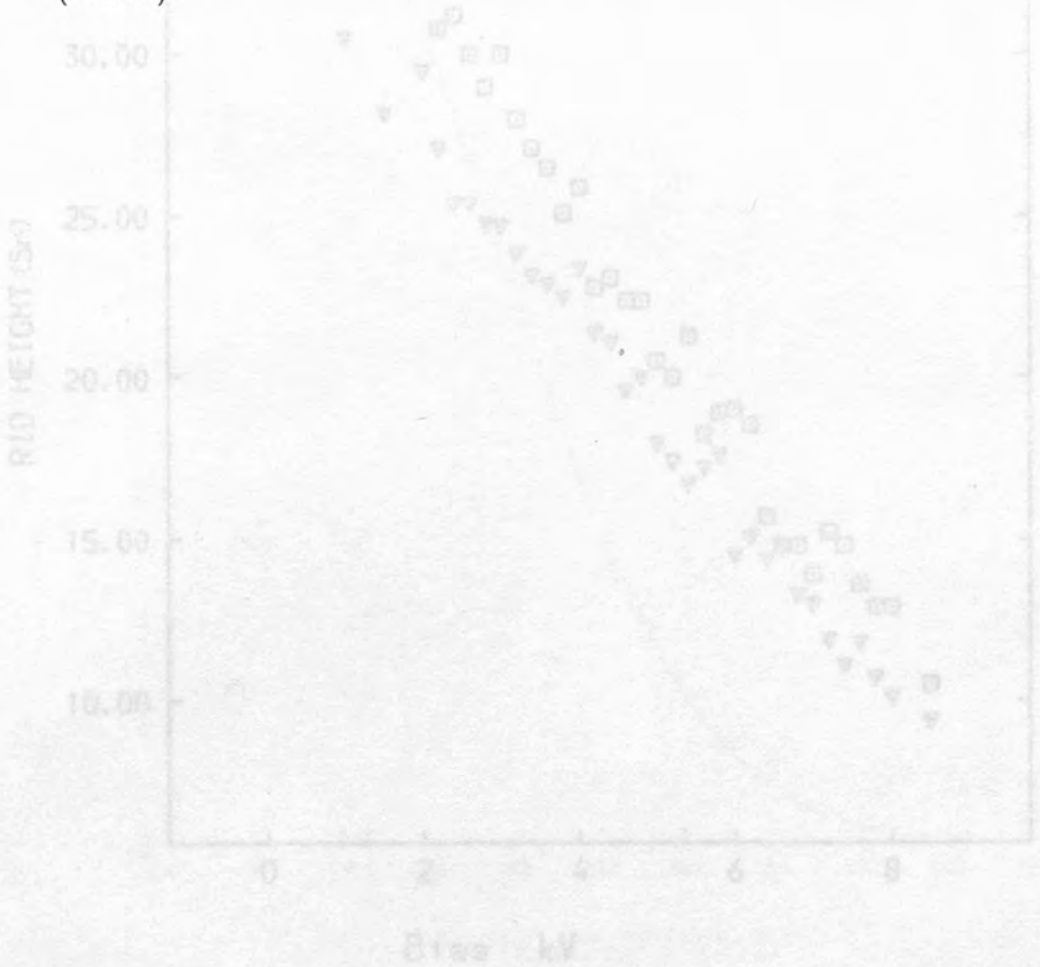

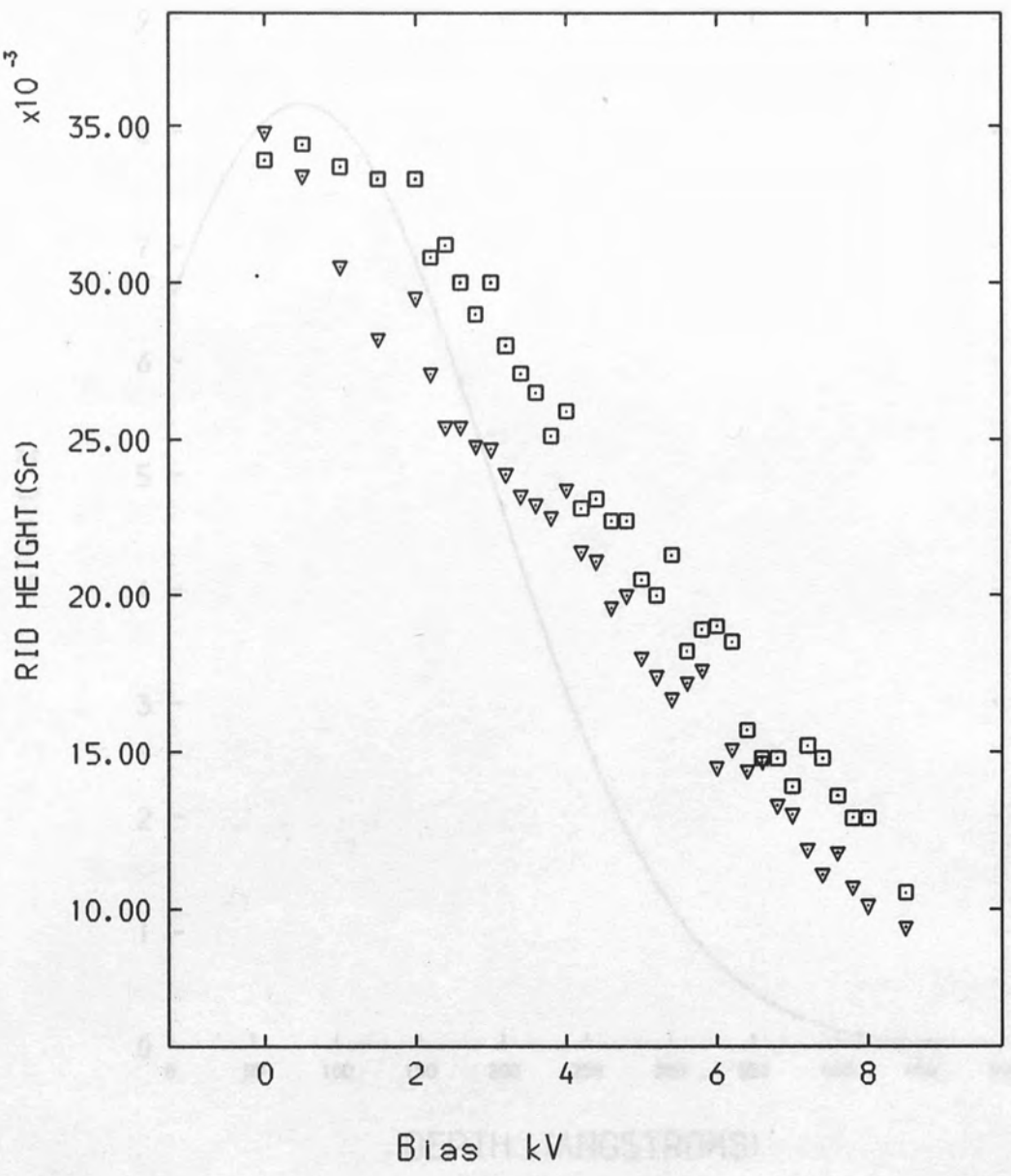

Figure 10.1

RID height S_r for annealed Mo (triangles) and Kr implanted Mo (squares) with positron energy. Referenced to the line for 12keV positrons on Mo.

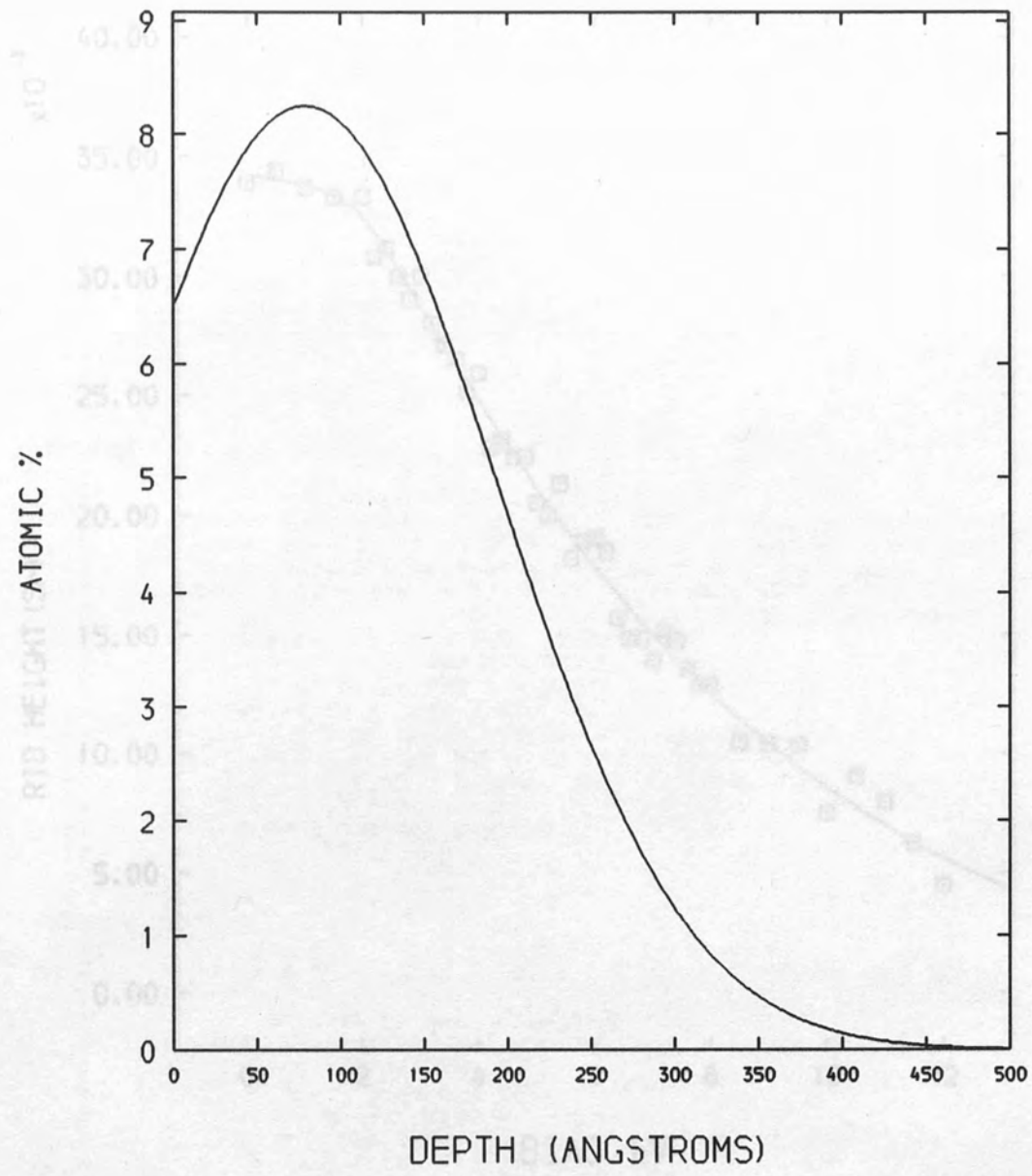

Figure 10.2

Calculated ion profile for 100keV krypton ions implanted into molybdenum to a total dose of $1.5 \times 10^{16}\text{cm}^{-2}$.

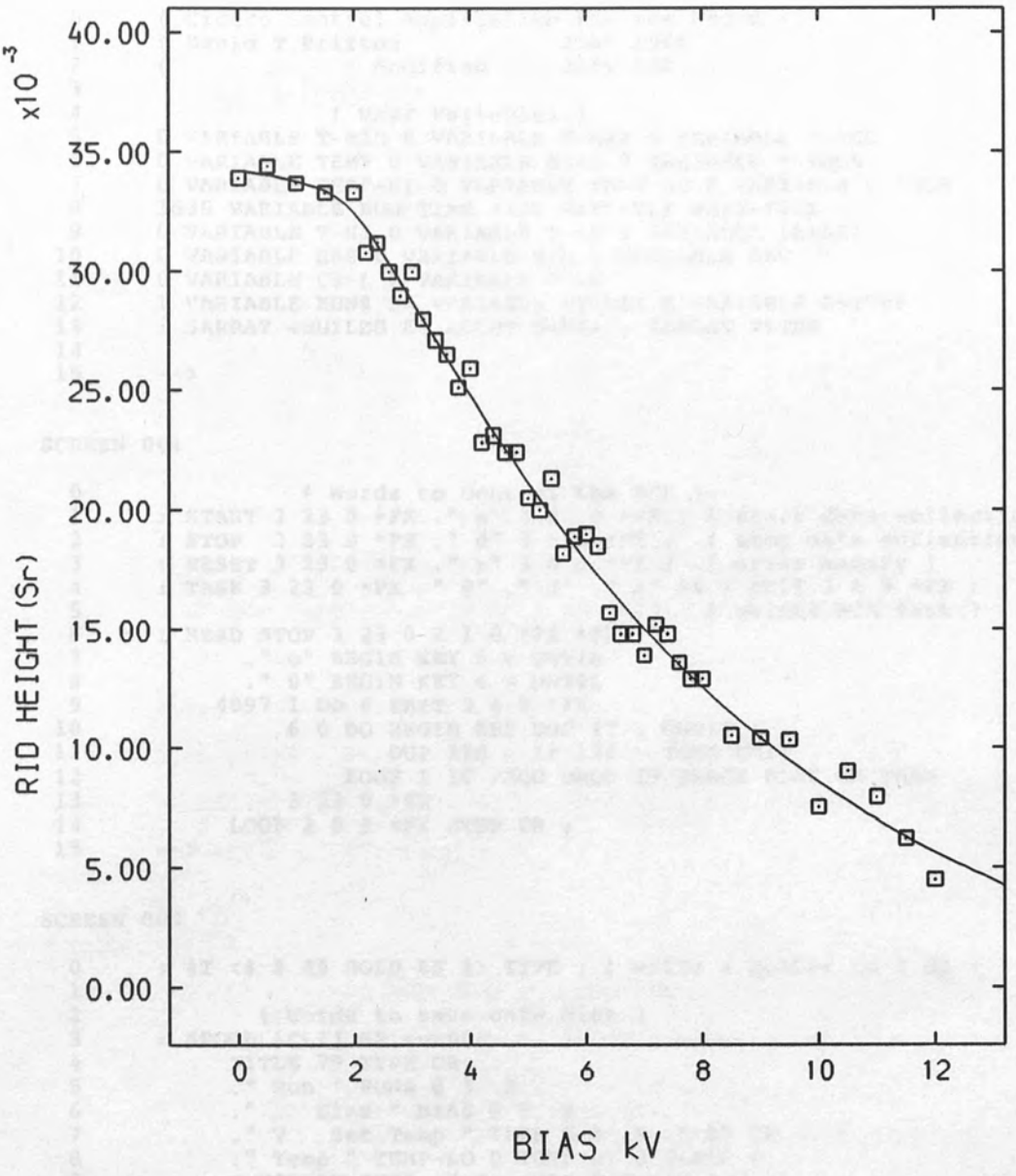

Figure 10.3

Unweighted least squares fit to the RID height S_r for a modelled step function defect distribution of depth 171Å.

Appendix 1

```
SCREEN 000

  0     ( Cicero Control Application for the BBC-B )
  1     ( David T Britton            June 1986 )
  2     (          Modified          July 1987 )
  3
  4                ( User Variables )
  5     0 VARIABLE T-MIN 0 VARIABLE T-MAX 0 VARIABLE T-ACC
  6     0 VARIABLE TEMP 0 VARIABLE BIAS 0 VARIABLE T-INCR
  7     0 VARIABLE TEMP-HI 0 VARIABLE TEMP-LO 0 VARIABLE V-INCR
  8     3630 VARIABLE RUN-TIME 3530 VARIABLE WAIT-TIME
  9     0 VARIABLE T-HI 0 VARIABLE T-LO 0 VARIABLE (BIAS)
 10     0 VARIABLE HRS 0 VARIABLE MIN 0 VARIABLE SEC
 11     0 VARIABLE CT-L 0 VARIABLE CT-H
 12     1 VARIABLE RUN# 24 VARIABLE CYCLE# 0 VARIABLE DRIVE#
 13     : $ARRAY <BUILDS 80 ALLOT DOES> ; $ARRAY TITLE
 14
 15     -->

SCREEN 001

  0              ( Words to Control the MCA )
  1     : START 3 23 0 *FX ." a" 3 6  0 *FX ; ( start data collection )
  2     : STOP  3 23 0 *FX ." d" 3 6 0 *FX ;  ( stop data collection )
  3     : RESET 3 23 0 *FX ." e" 3 6 0 *FX ;  ( erase memory )
  4     : TASK 3 23 0 *FX ." @" ." 3" ." A" 64 + EMIT 3 6 0 *FX ;
  5                                          ( select MCA Task )
  6     : READ STOP 3 23 0 2 1 0 *FX *FX
  7            ." o" BEGIN KEY 6 = UNTIL
  8            ." 0" BEGIN KEY 6 = UNTIL
  9          4097 1 DO 6 EMIT 3 4 0 *FX
 10               6 0 DO BEGIN KEY DUP 47 > UNTIL
 11                      DUP 128 > IF 128 - THEN EMIT
 12                   LOOP I 10 /MOD DROP IF SPACE ELSE CR THEN
 13               3 23 0 *FX
 14           LOOP 2 0 0 *FX STOP CR ;
 15     -->

SCREEN 002

  0     : #T <# # 46 HOLD #S #> TYPE ; ( write a number to 1 dp )
  1
  2           ( Words to save onto disk )
  3     : SPOOL [CLI] SP.run000
  4          TITLE 79 TYPE CR
  5          ." Run " RUN# @ 3 .R
  6          ."    Bias " BIAS @ 5 .R
  7          ." V   Set Temp " TEMP @ 4 .R ." K" CR
  8          ." Temp " TEMP-LO @ TEMP-HI @ T-ACC @
  9          M/MOD #T DROP ." K   Min " T-MIN @ 0 #T
 10         ." K   Max " T-MAX @ 0 #T ." K"
 11        CR READ CR [CLI] SP. ;
 12
 13     LATEST PFA 9 + VARIABLE RUN#_ADD
 14     ( store address of 000 in spool)
 15     -->
```

```
SCREEN 003

 0      : SAVE 0 24 MTC
 1              RUN# @ 0 <# # # # #> RUN#_ADD
 2              @ SWAP CMOVE SPOOL ;
 3
 4      : (DRIVE) [CLI] DR.0 ;
 5
 6      LATEST PFA 6 + VARIABLE DRIVE_ADD
 7      ( store address of 0 in drive)
 8
 9      : DRIVE 0 <# # #> DRIVE_ADD @ SWAP CMOVE (DRIVE) ;
10
11      : +DRIVE DRIVE# DUP @ 2 +
12           DUP 3 > IF 1 + 2 /MOD DROP THEN
13           DUP ROT ! DRIVE ;
14
15      -->

SCREEN 004

 0      : BAUD DUP 7 SWAP 0 *FX 8 SWAP 0 *FX ; ( Select RS432 Baud Rate)
 1
 2               ( Words to read and monitor the BBC Clock )
 3
 4      : D< ROT SWAP < DUP IF SWAP DROP SWAP DROP ELSE DROP < THEN ;
 5
 6      : SET-CLOCK HRS ! MIN ! SEC ! 0 0 0 TIME ;
 7
 8      : GET-TIME TIME@ DROP 256 U* ROT 0 D+ ;
 9
10      : SET-TIME 0 GET-TIME 100 M/MOD ROT DROP D+ T-HI ! T-LO ! ;
11
12      : CHECK-TIME T-LO @ T-HI @ GET-TIME 100 M/MOD ROT DROP D< ;
13
14      : (CLOCK)    GET-TIME
15      -->

SCREEN 005

 0            100 M/MOD ROT DROP 60 M/MOD 60 U/
 1             ROT SEC @ + DUP 59 >
 2                   IF 60 - ROT 1+ ROT ROT THEN
 3             ROT MIN @ + DUP 59 >
 4                   IF 60 - ROT 1+ ROT ROT THEN
 5             ROT HRS @ + DUP 23 > DUP IF
 6                   SWAP BEGIN 24 - DUP 24 < UNTIL SWAP THEN ;
 7      : CLOCK (CLOCK)  DROP
 8            70 0 MTC 2 .R ." :" 2 .R ." :" 2 .R ;
 9            ( Words to set and monitor the temperature )
10      HEX
11
12      : ?ADC 8 + FEC0 C!
13           BEGIN FEC0 C@ 80 < UNTIL
14           FEC2 C@ FEC1 C@ 100  * + ;
15      -->
```

```
SCREEN 006

 0      : IN DUP FE62 + 0 SWAP C! FE60 + C@ ;
 1      : OUT DUP FE62 + FF SWAP C! FE60 + C! ;
 2
 3      DECIMAL
 4
 5      : 0-CLOCK  (CLOCK)  IF
 6                     SET-CLOCK
 7                 ELSE DROP DROP DROP
 8                 THEN ;
 9
10      : ?TIMER GET-TIME 30000 U/ DROP 10 < ;
11      : ?TEMP 3 ?ADC 1310 - 10000 U* SWAP DROP 0 2732 0 D+ ;
12
13      : MON-T   ?TEMP OVER DUP T-MIN @ <
14                IF T-MIN !
15      -->


SCREEN 007

 0              ELSE DUP T-MAX @ >
 1                   IF T-MAX !
 2                   ELSE DROP
 3                   THEN
 4               THEN  ?TIMER
 5               IF OVER OVER TEMP-LO @ TEMP-HI @ D+ T-ACC
 6                  DUP @ 1 + SWAP ! TEMP-HI ! TEMP-LO !
 7               THEN 30  0 MTC #T ." K   " ;
 8
 9               ( Words to define the screen displays )
10
11      : "TIME" 30 0 D+ 60 M/MOD ROT DROP 60 M/
12               SWAP MIN @ + DUP 59 >
13                  IF 60 - SWAP 1 + SWAP THEN
14               SWAP HRS @ + DUP 23 >
15      -->


SCREEN 008

 0                IF BEGIN 24 - DUP 24 < UNTIL THEN
 1              2 .R ." :" 2 .R ;
 2
 3      : START/STOP 3 4 0 *FX 1 6 0 DLC
 4             CLT 0 0 MTC ." Run No. " RUN# @ .
 5             0 10 MTC TITLE 80 TYPE
 6             CT-L @ CT-H @ 100 M/MOD ROT DROP
 7             WAIT-TIME @ 0 D+ OVER OVER
 8              15 15 MTC ." START      " "TIME"
 9             RUN-TIME @ 0 D+
10              45 15 MTC ." STOP   " "TIME"
11             BIAS @ TEMP @
12               15 16 MTC ." SET TEMP  " 5 .R ." K"
13               45 16 MTC ." BIAS  " 5 .R ." V" ;
14
15      -->
```

```
SCREEN 009

  0     : CURSOR-ON 154 156 0 *FX ;
  1
  2     : CURSOR-OFF 154 28 0 *FX ;
  3
  4     : FRONT-PAGE 3 4 0 *FX CLT 1 3 0 DLC
  5           TITLE 79 TYPE
  6            15 4 MTC ." 0       Enter Title"
  7            15 5 MTC ." 1         Set Clock"
  8            15 6 MTC ." 2       Set Run No."
  9            15 7 MTC ." 3       No. of runs"
 10            15 8 MTC ." 4        Disk Drive"
 11            15 9 MTC ." 5         Wait Time"
 12           15 10 MTC ." 6          Run Time"
 13            15 11 MTC ." 7       Temperature"
 14            15 12 MTC ." 8       Target Bias"
 15     -->

SCREEN 010

  0          15 13 MTC ." 9       EXIT SET UP"
  1          40 6 MTC RUN# @ .            40 7 MTC CYCLE# @ .
  2          40 8 MTC DRIVE# @ .          40 9 MTC WAIT-TIME @ .
  3          40 10 MTC RUN-TIME @ .       40 11 MTC TEMP @ .
  4          45 11 MTC ." K  " T-INCR @ . 40 12 MTC BIAS @ .
  5          45 12 MTC ." V " V-INCR @ . 0 23 MTC ;
  6
  7     : BACK-PAGE 1 2 0 3 MODE DLC
  8           ." Run No. " RUN# @ . 0 10 MTC TITLE 80 TYPE
  9           25 12 MTC ." CICERO Control Application" 0 21 MTC
 10     ."   F0   |   F1  |   F2  |   F3  |   F4  |   F5  |   F6  |"
 11     ."    F7  |   F8  |   F9  |"   0 22 MTC
 12     ." SET UP | START | STOP  | SAVE  | RESET | CYCLE | BASIC |"
 13     ."  COMM  | FORTH |  MCA  |"
 14          3 6 0 *FX ;
 15     -->

SCREEN 011

  0
  1                    ( Words to enter data into Application )
  2
  3     : SET-TEMP 273 - 255 1000 */ 0 OUT ;
  4
  5     : (NUMIN) WORD HERE NUMBER DROP ;
  6
  7     : TIME-IN QUERY 58 (NUMIN) 58 (NUMIN) 32 (NUMIN)
  8              SWAP ROT SET-CLOCK ;
  9
 10     : T-IN QUERY 32 (NUMIN) DUP TEMP !
 11                  45 11 MTC ." K  ?     "
 12                  48 11 MTC QUERY 32 (NUMIN)
 13                  T-INCR ! SET-TEMP ;
 14
 15     -->
```

```
SCREEN 012

 0      HEX
 1      : (SET-V) 40 /MOD SWAP 1 OUT
 2                4  /MOD SWAP 40 + 1 OUT
 3                C1 1 OUT
 4                1 OUT
 5                C2 1 OUT C3 1 OUT ;
 6      : SET-V A FE6C C! 2710 SWAP - 64 7A */ (SET-V) ;
 7      : MON-V (BIAS) @ BIAS @ 0 ?ADC 0 10 U/ SWAP DROP 229 80 */ DUP
 8              28 0 MTC 0 <# #S #> TYPE ." V  " - 800 / DUP
 9              0 > IF DROP 0 > IF 1 -  DUP (BIAS) ! (SET-V) THEN
10               ELSE 0 < IF 3FFF < IF 1+ DUP (BIAS) ! (SET-V) THEN
11              THEN THEN ;
12      DECIMAL
13      : V-IN QUERY 32 (NUMIN) DUP BIAS ! 45 12 MTC ." V  ?      "
14         48 12 MTC QUERY 32 (NUMIN) V-INCR ! SET-V ;
15      -->


SCREEN 013

 0      : CLR-TITLE TITLE 80 BLANKS ;
 1
 2      : SET-TITLE TITLE 80 BLANKS CR
 3              13 WORD HERE COUNT TITLE SWAP CMOVE ;
 4
 5      : SET-UP FRONT-PAGE
 6               BEGIN KEY 44 - DUP 40 SWAP OVER OVER MTC
 7                     ." ?          " MTC DUP 4 =
 8                     IF DUP 40 SWAP MTC ."   " 0 0 MTC
 9                        80 0 DO 32 EMIT LOOP
10                        0 0 MTC QUERY SET-TITLE
11                     THEN DUP 5 = IF
12                        TIME-IN THEN
13                     DUP 6 = IF
14                        QUERY 32 (NUMIN) RUN# ! THEN
15      -->


SCREEN 014

 0                   DUP 7 = IF
 1                      QUERY 32 (NUMIN) CYCLE# ! THEN
 2                    DUP 8 = IF
 3                      QUERY 32 (NUMIN)
 4                      DUP DRIVE# ! DRIVE THEN
 5                    DUP 9 = IF
 6                      QUERY 32 (NUMIN) WAIT-TIME ! THEN
 7                    DUP 10 = IF
 8                      QUERY 32 (NUMIN) RUN-TIME ! THEN
 9                   DUP 11 = IF T-IN THEN
10                   DUP 12 = IF V-IN THEN
11                   0 23 MTC 13 = UNTIL BACK-PAGE ;
12
13                    ( Words to control autocycling )
14      -->
15
```

```
SCREEN 015

 0
 1     : WAIT BEGIN CLOCK MON-T ( MON-V ) ?ESC
 2                IF SET-UP START/STOP
 3                  25 12 MTC ." I've Been Interfered With!"
 4                  CURSOR-OFF
 5                THEN CHECK-TIME UNTIL ;
 6
 7     : RESET-TEMP 0 0 0 T-ACC ! TEMP-HI ! TEMP-LO !
 8                  ?TEMP DROP DUP T-MIN ! T-MAX ! ;
 9
10     : CYCLE 16 0 0 *FX CURSOR-OFF
11             0 DO GET-TIME CT-H ! CT-L !
12               WAIT-TIME @ SET-TIME START/STOP
13               25 12 MTC ." WAITING FOR GODOT              "
14                    WAIT
15     -->

SCREEN 016

 0               STOP RESET START
 1               RUN-TIME @ SET-TIME 3  4 0 *FX
 2               25 12 MTC ." RUNNING FOR PRESIDENT          "
 3               RESET-TEMP WAIT ( 0 0 OUT ) SAVE RESET-TEMP
 4             ( CURSOR-ON SET-UP CURSOR-OFF Manual Interrupt ONLY )
 5               RESET
 6               RUN# DUP @ DUP 6 /MOD DROP 0 =
 7                 IF +DRIVE THEN    1+ SWAP !
 8               TEMP DUP @ T-INCR @ + DUP SET-TEMP SWAP !
 9               BIAS DUP @ V-INCR @ + DUP SET-V SWAP !
10               0-CLOCK LOOP CURSOR-ON ;
11
12     : CYCLES CYCLE# @ CYCLE 3 4 0 *FX BACK-PAGE ;
13     : *BASIC 3 4 0 *FX [CLI] BASIC ;
14     : *COM. 3 4 0 *FX [CLI] COMMUNICATOR ;
15     -->

SCREEN 017

 0     : KEYS [CLI] KEY0SET-UP|M  [CLI] KEY1START|M
 1            [CLI] KEY2STOP|M    [CLI] KEY3SAVE|M
 2            [CLI] KEY4RESET|M   [CLI] KEY5CYCLES|M
 3            [CLI] KEY6*BASIC|M  [CLI] KEY7*COM.|M
 4            [CLI] KEY8*FORTH|M  [CLI] KEY9BACK-PAGE|M ;
 5
 6                  (  Initialise the Application )
 7     0 DUP DRIVE# ! DRIVE 4 BAUD
 8     CLR-TITLE 3 MODE KEYS BACK-PAGE 2 TASK
 9
10
11
12
13
14
15     ;S
```

Appendix 2

Back Diffusion Probabilities for Makhovian Profile with m= 2.0

As a function of Zo/L

	0.00	0.01	0.02	0.03	0.04	0.05	0.06	0.07	0.08	0.09
0.0	1.0000	0.9912	0.9825	0.9739	0.9654	0.9570	0.9487	0.9405	0.9324	0.9244
0.1	0.9164	0.9086	0.9008	0.8931	0.8855	0.8780	0.8706	0.8632	0.8560	0.8488
0.2	0.8416	0.8346	0.8276	0.8207	0.8139	0.8072	0.8005	0.7939	0.7874	0.7809
0.3	0.7745	0.7682	0.7619	0.7557	0.7496	0.7435	0.7375	0.7316	0.7257	0.7199
0.4	0.7141	0.7084	0.7028	0.6972	0.6917	0.6862	0.6808	0.6755	0.6702	0.6649
0.5	0.6597	0.6546	0.6495	0.6445	0.6395	0.6345	0.6296	0.6248	0.6200	0.6153
0.6	0.6106	0.6059	0.6013	0.5968	0.5923	0.5878	0.5834	0.5790	0.5747	0.5704
0.7	0.5661	0.5619	0.5577	0.5536	0.5495	0.5455	0.5415	0.5375	0.5336	0.5297
0.8	0.5258	0.5220	0.5182	0.5144	0.5107	0.5071	0.5034	0.4998	0.4962	0.4927
0.9	0.4892	0.4857	0.4823	0.4789	0.4755	0.4721	0.4688	0.4655	0.4623	0.4590
1.0	0.4559	0.4527	0.4495	0.4464	0.4434	0.4403	0.4373	0.4343	0.4313	0.4284
1.1	0.4255	0.4226	0.4197	0.4169	0.4141	0.4113	0.4085	0.4058	0.4031	0.4004
1.2	0.3977	0.3951	0.3925	0.3899	0.3873	0.3847	0.3822	0.3797	0.3772	0.3748
1.3	0.3723	0.3699	0.3675	0.3651	0.3628	0.3605	0.3581	0.3558	0.3536	0.3513
1.4	0.3491	0.3469	0.3447	0.3425	0.3403	0.3382	0.3360	0.3339	0.3318	0.3298
1.5	0.3277	0.3257	0.3237	0.3217	0.3197	0.3177	0.3157	0.3138	0.3119	0.3100
1.6	0.3081	0.3062	0.3044	0.3025	0.3007	0.2989	0.2971	0.2953	0.2935	0.2918
1.7	0.2900	0.2883	0.2866	0.2849	0.2832	0.2815	0.2799	0.2782	0.2766	0.2750
1.8	0.2733	0.2718	0.2702	0.2686	0.2670	0.2655	0.2640	0.2624	0.2609	0.2594
1.9	0.2580	0.2565	0.2550	0.2536	0.2521	0.2507	0.2493	0.2479	0.2465	0.2451
2.0	0.2437	0.2424	0.2410	0.2397	0.2383	0.2370	0.2357	0.2344	0.2331	0.2318
2.1	0.2305	0.2293	0.2280	0.2268	0.2255	0.2243	0.2231	0.2219	0.2207	0.2195
2.2	0.2183	0.2171	0.2160	0.2148	0.2137	0.2125	0.2114	0.2103	0.2092	0.2081
2.3	0.2070	0.2059	0.2048	0.2037	0.2027	0.2016	0.2005	0.1995	0.1985	0.1974
2.4	0.1964	0.1954	0.1944	0.1934	0.1924	0.1914	0.1904	0.1895	0.1885	0.1875
2.5	0.1866	0.1856	0.1847	0.1838	0.1828	0.1819	0.1810	0.1801	0.1792	0.1783
2.6	0.1774	0.1765	0.1757	0.1748	0.1739	0.1731	0.1722	0.1714	0.1705	0.1697
2.7	0.1689	0.1681	0.1672	0.1664	0.1656	0.1648	0.1640	0.1632	0.1625	0.1617
2.8	0.1609	0.1601	0.1594	0.1586	0.1579	0.1571	0.1564	0.1556	0.1549	0.1542
2.9	0.1534	0.1527	0.1520	0.1513	0.1506	0.1499	0.1492	0.1485	0.1478	0.1471
3.0	0.1464	0.1458	0.1451	0.1444	0.1438	0.1431	0.1425	0.1418	0.1412	0.1405
3.1	0.1399	0.1393	0.1386	0.1380	0.1374	0.1368	0.1361	0.1355	0.1349	0.1343
3.2	0.1337	0.1331	0.1326	0.1320	0.1314	0.1308	0.1302	0.1297	0.1291	0.1285
3.3	0.1280	0.1274	0.1268	0.1263	0.1257	0.1252	0.1247	0.1241	0.1236	0.1231
3.4	0.1225	0.1220	0.1215	0.1210	0.1204	0.1199	0.1194	0.1189	0.1184	0.1179
3.5	0.1174	0.1169	0.1164	0.1159	0.1155	0.1150	0.1145	0.1140	0.1135	0.1131
3.6	0.1126	0.1121	0.1117	0.1112	0.1107	0.1103	0.1098	0.1094	0.1089	0.1085
3.7	0.1081	0.1076	0.1072	0.1067	0.1063	0.1059	0.1055	0.1050	0.1046	0.1042
3.8	0.1038	0.1034	0.1029	0.1025	0.1021	0.1017	0.1013	0.1009	0.1005	0.1001
3.9	0.0997	0.0993	0.0989	0.0985	0.0982	0.0978	0.0974	0.0970	0.0966	0.0963
4.0	0.0959	0.0955	0.0952	0.0948	0.0944	0.0941	0.0937	0.0933	0.0930	0.0926
4.1	0.0923	0.0919	0.0916	0.0912	0.0909	0.0905	0.0902	0.0899	0.0895	0.0892
4.2	0.0888	0.0885	0.0882	0.0878	0.0875	0.0872	0.0869	0.0865	0.0862	0.0859
4.3	0.0856	0.0853	0.0850	0.0846	0.0843	0.0840	0.0837	0.0834	0.0831	0.0828
4.4	0.0825	0.0822	0.0819	0.0816	0.0813	0.0810	0.0807	0.0804	0.0802	0.0799
4.5	0.0796	0.0793	0.0790	0.0787	0.0785	0.0782	0.0779	0.0776	0.0773	0.0771
4.6	0.0768	0.0765	0.0763	0.0760	0.0757	0.0755	0.0752	0.0749	0.0747	0.0744
4.7	0.0742	0.0739	0.0736	0.0734	0.0731	0.0729	0.0726	0.0724	0.0721	0.0719
4.8	0.0716	0.0714	0.0712	0.0709	0.0707	0.0704	0.0702	0.0700	0.0697	0.0695
4.9	0.0693	0.0690	0.0688	0.0686	0.0683	0.0681	0.0679	0.0676	0.0674	0.0672

Appendix 2

Back Diffusion Probabilities for Makhovian Profile with m= 2.0

As a function of Zo/L

	0.00	0.01	0.02	0.03	0.04	0.05	0.06	0.07	0.08	0.09
5.0	0.0670	0.0667	0.0665	0.0663	0.0661	0.0659	0.0657	0.0654	0.0652	0.0650
5.1	0.0648	0.0646	0.0644	0.0642	0.0640	0.0638	0.0635	0.0633	0.0631	0.0629
5.2	0.0627	0.0625	0.0623	0.0621	0.0619	0.0617	0.0615	0.0613	0.0611	0.0609
5.3	0.0607	0.0606	0.0604	0.0602	0.0600	0.0598	0.0596	0.0594	0.0592	0.0590
5.4	0.0589	0.0587	0.0585	0.0583	0.0581	0.0579	0.0578	0.0576	0.0574	0.0572
5.5	0.0571	0.0569	0.0567	0.0565	0.0564	0.0562	0.0560	0.0558	0.0557	0.0555
5.6	0.0553	0.0552	0.0550	0.0548	0.0547	0.0545	0.0543	0.0542	0.0540	0.0538
5.7	0.0537	0.0535	0.0534	0.0532	0.0530	0.0529	0.0527	0.0526	0.0524	0.0523
5.8	0.0521	0.0519	0.0518	0.0516	0.0515	0.0513	0.0512	0.0510	0.0509	0.0507
5.9	0.0506	0.0504	0.0503	0.0501	0.0500	0.0499	0.0497	0.0496	0.0494	0.0493
6.0	0.0491	0.0490	0.0489	0.0487	0.0486	0.0484	0.0483	0.0482	0.0480	0.0479
6.1	0.0477	0.0476	0.0475	0.0473	0.0472	0.0471	0.0469	0.0468	0.0467	0.0465
6.2	0.0464	0.0463	0.0462	0.0460	0.0459	0.0458	0.0456	0.0455	0.0454	0.0453
6.3	0.0451	0.0450	0.0449	0.0448	0.0446	0.0445	0.0444	0.0443	0.0441	0.0440
6.4	0.0439	0.0438	0.0437	0.0435	0.0434	0.0433	0.0432	0.0431	0.0430	0.0428
6.5	0.0427	0.0426	0.0425	0.0424	0.0423	0.0421	0.0420	0.0419	0.0418	0.0417
6.6	0.0416	0.0415	0.0414	0.0413	0.0411	0.0410	0.0409	0.0408	0.0407	0.0406
6.7	0.0405	0.0404	0.0403	0.0402	0.0401	0.0400	0.0399	0.0398	0.0397	0.0395
6.8	0.0394	0.0393	0.0392	0.0391	0.0390	0.0389	0.0388	0.0387	0.0386	0.0385
6.9	0.0384	0.0383	0.0382	0.0381	0.0380	0.0379	0.0378	0.0378	0.0377	0.0376
7.0	0.0375	0.0374	0.0373	0.0372	0.0371	0.0370	0.0369	0.0368	0.0367	0.0366
7.1	0.0365	0.0364	0.0363	0.0363	0.0362	0.0361	0.0360	0.0359	0.0358	0.0357
7.2	0.0356	0.0355	0.0354	0.0354	0.0353	0.0352	0.0351	0.0350	0.0349	0.0348
7.3	0.0348	0.0347	0.0346	0.0345	0.0344	0.0343	0.0342	0.0342	0.0341	0.0340
7.4	0.0339	0.0338	0.0337	0.0337	0.0336	0.0335	0.0334	0.0333	0.0333	0.0332
7.5	0.0331	0.0330	0.0329	0.0329	0.0328	0.0327	0.0326	0.0326	0.0325	0.0324
7.6	0.0323	0.0322	0.0322	0.0321	0.0320	0.0319	0.0319	0.0318	0.0317	0.0316
7.7	0.0316	0.0315	0.0314	0.0313	0.0313	0.0312	0.0311	0.0311	0.0310	0.0309
7.8	0.0308	0.0308	0.0307	0.0306	0.0306	0.0305	0.0304	0.0303	0.0303	0.0302
7.9	0.0301	0.0301	0.0300	0.0299	0.0299	0.0298	0.0297	0.0297	0.0296	0.0295
8.0	0.0295	0.0294	0.0293	0.0293	0.0292	0.0291	0.0291	0.0290	0.0289	0.0289
8.1	0.0288	0.0287	0.0287	0.0286	0.0285	0.0285	0.0284	0.0283	0.0283	0.0282
8.2	0.0282	0.0281	0.0280	0.0280	0.0279	0.0278	0.0278	0.0277	0.0277	0.0276
8.3	0.0275	0.0275	0.0274	0.0274	0.0273	0.0272	0.0272	0.0271	0.0271	0.0270
8.4	0.0269	0.0269	0.0268	0.0268	0.0267	0.0267	0.0266	0.0265	0.0265	0.0264
8.5	0.0264	0.0263	0.0263	0.0262	0.0261	0.0261	0.0260	0.0260	0.0259	0.0259
8.6	0.0258	0.0257	0.0257	0.0256	0.0256	0.0255	0.0255	0.0254	0.0254	0.0253
8.7	0.0253	0.0252	0.0252	0.0251	0.0251	0.0250	0.0249	0.0249	0.0248	0.0248
8.8	0.0247	0.0247	0.0246	0.0246	0.0245	0.0245	0.0244	0.0244	0.0243	0.0243
8.9	0.0242	0.0242	0.0241	0.0241	0.0240	0.0240	0.0239	0.0239	0.0238	0.0238
9.0	0.0237	0.0237	0.0236	0.0236	0.0235	0.0235	0.0234	0.0234	0.0233	0.0233
9.1	0.0233	0.0232	0.0232	0.0231	0.0231	0.0230	0.0230	0.0229	0.0229	0.0228
9.2	0.0228	0.0227	0.0227	0.0227	0.0226	0.0226	0.0225	0.0225	0.0224	0.0224
9.3	0.0223	0.0223	0.0223	0.0222	0.0222	0.0221	0.0221	0.0220	0.0220	0.0219
9.4	0.0219	0.0219	0.0218	0.0218	0.0217	0.0217	0.0216	0.0216	0.0216	0.0215
9.5	0.0215	0.0214	0.0214	0.0214	0.0213	0.0213	0.0212	0.0212	0.0211	0.0211
9.6	0.0211	0.0210	0.0210	0.0209	0.0209	0.0209	0.0208	0.0208	0.0207	0.0207
9.7	0.0207	0.0206	0.0206	0.0205	0.0205	0.0205	0.0204	0.0204	0.0203	0.0203
9.8	0.0203	0.0202	0.0202	0.0202	0.0201	0.0201	0.0200	0.0200	0.0200	0.0199
9.9	0.0199	0.0199	0.0198	0.0198	0.0197	0.0197	0.0197	0.0196	0.0196	0.0196

Appendix 3

Fortran Subroutine Library

Decon

SUBROUTINE DECON(S, R, N, filter, factor)

DOUBLE PRECISION S(N), R(N), factor

INTEGER filter, N

Uses a fast Fourier transform to deconvolute the normalised resolution function R from the normalised peak S. The Fourier transform is evaluated over 1024 elements.

Parameters

S: Normalised experimental lineshape in an array with less than 1024 elements.

R: The normalised resolution function in an array of the same length as S.

N: The number of array elements in S and R.

filter: Used to select the type of filtering (§5.4.1) used in the deconvolution process

filter=0 Dynamic filter is used with a filtering factor passed to the subroutine as the parameter factor.

$0 <$ filter ≤ 512 Fixed low-pass filter with cut-off at the value of filter.

filter > 512 Dynamic low-pass filter with cut-off at the first minimum in the Fourier spectrum.

factor: The value of the filtering factor used in the dynamic filter.

Return Values

The deconvoluted curve is passed back in S. R is unchanged on exit.

Routines & Libraries Referenced: NAg version 11

Appendix 3

Fortran Subroutine Library

Easyprof

SUBROUTINE EASYPROF(F, E, N, Fs, Fb, Fd, x, D, k, alpha, rho)
DOUBLE PRECISION F(N), E(N), Fs, Fb, Fd, x, D, k, alpha, rho
INTEGER N

Calculates the expected lineshape parameter values for the set of incident positron energies E for a step function defect distribution in the limit of zerp positron diffusion in the bulk

This routine evaluates assumes that the steady-state positron profile is a derivative of a Gaussian (Makhovian), only the material independent scaling can be changed.

Parameters

F: The set of calculated lineshape parameter values corresponding to the energies held in E.
E: The set of positron incident energies (keV) for which the lineshape parameters are to be calculated.
N: The number of array elements in F and E.
Fs: The surface lineshape parameter value.
Fb: The bulk lineshape parameter value.
Fd: The defect lineshape parameter value
x: The depth of the defect layer.
D: Positron diffusion coefficient (cm^2/s) near the surface.
k: Relative trapping rate = trapping rate×free lifetime.
alpha: Material scaling α ($\mu g/cm^3$) for $z_0 = \frac{\alpha}{\rho}$ in the Makhovian profile.
rho: Material density ρ (g/cm^3)

Return Values

The calculated lineshape values for the set of incident energies E(i,i=1,N) are returned in the corresponding elements of F. All other are parameters unchanged on exit.

Routines & Libraries Referenced: None

Appendix 3

Fortran Subroutine Library

Posprof

FUNCTION POSPROf(z, E, m, n, alpha, rho)

DOUBLE PRECISION z, E, m, n, alpha, rho

A function to evaluate the positron implantation profile at a given depth for a specific incident positron energy.

Parameters

z: The depth in Å at which the implantation profile is required.

E: The positron energy in keV for which the profile is required.

m: The shape factor in the profile

$$P(z, E) = \frac{-d}{dz} e^{-z^m / z_0^m}.$$

n: The shape factor in the scaling length

$$z_0 = \frac{\alpha}{\rho} E^n.$$

alpha: The material independent scaling factor α in $\mu g/cm^2$.

rho: The material density in g/cm^3.

Return Values

The function value is the value of the positron implantation profile. All parameters are unchanged on exit.

Routines & Libraries Referenced: None

Appendix 3

Fortran Subroutine Library

Laplace

FUNCTION LAPLACE(A, N, d, p)

DOUBLE PRECISION A(N), d, p

INTEGER N

Calculates the Laplace transform of an array to a single point in the transformed space.

$$L(p) = \sum_{i=1}^{N} A_i e^{x_i p}$$

where

$$x_i = (i - 1)d$$

Parameters

A: An array containing the values of the function A(x), evaluated at constant intervals in x, to be transformed.

N: The number of elements in A.

d: The interval in x between successive elements in A.

p: The point in transformed space for which the value of the transformed function is required.

Return Values

The function value returns the value of the Laplace transform. All other parameters are unchanged on exit.

Routines & Libraries Referenced: None

Appendix 3

Fortran Subroutine Library

Homoprof

FUNCTION HOMOPROF(E, m, n, alpha, rho, Fs, Fb, L)

DOUBLE PRECISION E, m, n, alpha, rho, Fs, Fb, L

A function to calculate the expected value of a lineshape parameter for monoenergetic positrons incident on a homogeneous sample. Uses a two state model with the probabilities taken from the calculated back diffusion probability. A Makhovian profile with variable parameters is included.

Parameters

E: The incident positron energy in keV

m: The shape factor in the Makhovian profile $\frac{-d}{dz}\exp(-z^m/z_0^m)$.

n: The shape factor in the Makhovian length $z_0 = \frac{\alpha}{\rho}E^n$.

alpha: The material independent scaling α in$\mu g/cm^2$.

rho: The material density ρ in g/cm^3.

Fs: The lineshape parameter value associated with the surface.

Fb: The lineshape parameter value associated with the bulk.

L: The positron diffusion length in Å.

Return Values

The function value returns the calculated lineshape parameter. All parameters are unchanged on exit.

Routines & Libraries Referenced: POSPROF, LAPLACE

Appendix 3

Fortran Subroutine Library

Epiprof

FUNCTION EPIPROF(E, em, en, alpha, rho, Fs, Fb, Ld, Fep, l)

DOUBLE PRECISION E, em, en, alpha, rho, Fs, Fb, Ld, Fep, l

Calculates the expected value of a lineshape parameter for monoenergetic positrons incident on a homogeneous sample. Uses a nested pair of two state models with the probabilities taken from the calculated back diffusion and epithermal backscattering probabilities.

Parameters

E: The incident positron energy in keV

m: The shape factor in the Makhovian profile $\frac{-d}{dz}\exp(-z^m/z_0^m)$.

n: The shape factor in the Makhovian length $z_0 = \frac{\alpha}{\rho}E^n$.

alpha: The material independent scaling α inμg/cm^2.

rho: The material density ρ in g/cm^3.

Fs: The lineshape parameter value associated with the surface.

Fb: The lineshape parameter value associated with the bulk.

Ld: The positron diffusion length in Å.

Fep: The lineshape parameter value associated with epithermal emission

l: The mean positron epithermal scattering length in Å.

Return Values

The function value returns the calculated lineshape parameter. All parameters are unchanged on exit.

Routines & Libraries Referenced: POSPROF, LAPLACE

Appendix 4

Personal Bibliography

Design of a Low Energy Positron Beam, D.T.Britton, P.C.Rice-Evans and J.H.Evans: Nucl. Inst. Meth. **B12**,426 (1985)

Evidence for Detrapping of Positrons in Cadmium at Low Temperatures, P.C.Rice-Evans, A.A.Berry and D.Britton: in "Positron Annihilation" (Eds. P.C.Jain, R.M.Singru & K.P.Gopinathan), World Scientific, Singapore (1985)

Positronium Formation at Physisorbed Monolayer Surfaces of Argon, Nitrogen and Oxygen on Graphite, P.Rice-Evans, M.Moussavi-Madani, K.U.Rao, D.T.Britton and B.P.Cowan: Phys. Rev. **B34**,6117 (1986)

Positron Annihilation Study of the Temperature Behaviour of Solid Krypton Deposits in Copper, D.T.Britton, P.C.Rice-Evans and J.H.Evans: Phil. Mag. **A55**,347 (1987)

A Vertical Positron Beam for Low Temperature Surface Studies, P.C.Rice-Evans, D.T.Britton and B.P.Cowan: Appl. Phys. **A**,43,283 (1987)

Fast Fourier Transform Deconvolution of Positron Annihilation Lineshapes, D.T.Britton and P.C.Rice-Evans: *submitted to* J. Phys. D

Depth Profiling with Positrons of Krypton Implanted in Molybdenum, D.T.Britton, P.C.Rice-Evans and J.H.Evans: *to be submitted to* J. Phys. F.

Slow Positron Study of Krypton Implanted in Molybdenum, D.T.Britton, P.C.Rice-Evans and J.H.Evans: Proc. European Meeting on Positron Studies of Defects, G.D.R (1987)

Positronium at Monolayers and Design of a Positron Beam for Low Temperature Surface Measurements, P.Rice-Evans, D.T.Britton, M.M.Madani, K.U.Rao and B.P.Cowan: Slow Positron Workshop, Univ. East Anglia, Norwich, U.K. (1986)

Edward I in the Firing Line, D.T.Britton and P.C.Rice-Evans: Slow Positron Workshop, Univ. East Anglia, Norwich, U.K. (1986)

Study of Implanted Krypton in Copper with a Positron Beam, D.T.Britton, P.C.Rice-Evans and J.H.Evans: Slow Positron Workshop, Univ. East Anglia, Norwich, U.K. (1986)

Positron Annihilation at Liquid Metal Surfaces, P.C.Rice-Evans and D.T.Britton: Proc.International Symposium on Positron Annihilation Studies of Fluids, Univ. Texas at Arlington, U.S.A (1987)

Epithermal Positron Effects in Surface Measurements, D.T.Britton, P.C.Rice-Evans and J.H.Evans: Proc NATO ARW "Atomic Physics with Positrons", University College London (1987)

Acknowledgements

No thesis is ever the work of one person. For this work I have had to rely heavily on many of the physics staff, both at the new college and at Bedford College. I would particularly like to thank those who built the two beam lines; Messrs F Grimes & A King at Bedford College and Messrs R Elton, E Herrmann, B Porter and S Foreman at RHBNC. Mr J Henley played the most significant rôle in assembling and installing the cryostat system as well as providing general technical support. For additional advice and help on this system I would like to thank Messrs M Thyer, D C Smith and F Greenough.

In addition to plumbing, the two beam lines also need electrics. For excellent design and support in the field of electronics I am most grateful to Messrs L Ellison, A K Betts and F R Jordan.

Even with the necessary equipment this thesis would not have been possible without the help and supervision of Dr P C Rice-Evans and the advice of Dr J H Evans. For help and discussions I am also grateful to the past and present members of the positron group at RHBNC; Messrs S C Creamer, K U Rao, D L Smith, Dr M Moussavi-Madani and Mr C A Erin. Others whose advice has guided the course of my work are Drs M Charlton, C D Beling, M Eldrup, K O Jensen, A Vehanen, H Huomo, K F Canter, M Fluss, B P Cowan and Prof D W O Heddle.

Analysis and presentation of data would not have been possible without the support and advice of the computer unit; especially Miss S Marshall and Messrs L Nodes,G J Rock and P Taylor, and Dr M G Green for the Physics VAX.

Finally I would like to thank all other members of the technical and secretarial staff for their support during the period of my work; particularly Messrs J D Sales,G Wells and C Winterton, Mrs S Pearson and Mrs V Leach.

This work was carried out under a SERC-Harwell CASE studentship

References

Bab,S.E. Rev. Mod. Phys. **35**,400 (1963)

Beling,C.D., Simpson,R.I., Charlton,M., Jacobsen,F.M., Griffiths,T.C., Moriarty,P. & Fung,S. Appl. Phys. **A42**,111 (1987)

Bentzon,M.D.,Huomo,H., Vehanen,A., Hautojärvi,P., Lahtinen,J. & Hautala,M. J. Phys **F** in press (1987)

Bergersen,B., Pajanne,E., Kubica,P., Stott,M.J. & Hodges,C.H. Sol. Stat. Comm. **15**,1377 (1974)

Brandt,W. in *Positron Solid State Physics* (W.Brandt & A.Dupasquier Eds.), North Holland, Amsterdam (1983)

Brandt.W & Paulin,R. Phys. Rev. **B15**,2511 (1977)

Brandt,W. & Waung,H.F., Phys. Lett. **A27**,700 (1968)

Canter,K.F., Coleman,P.G., Griffith,T.C. & Heyland J. Phys.**B5**,L167 (1972)

Canter,K.F., in *Positrons in Solids, Surfaces and Atoms* (A.P.Mills Jr., K.F.Canter, W.S.Crane Eds.), World Scientific, Singapore (1986)

Canter,K.F., Proc EPOS 86, Gießen, FRG Appl. Phys. A in press (1987)

Canter,K.F., Brandes,G.R., Horsky,T.N., Lippel,P.H. & Mills,A.P. Jr. Proc NATO Adv. Res. Workshop on Atomic Physics with Positrons, University College London (1987)

Carbotte,J.P. in *Positron Solid State Physics* (W.Brandt & A.Dupasquier Eds.), North Holland, Amsterdam (1983)

Chaglar,I., Rice-Evans,P., El Khangi,F.A.R. & Berry,A.A. Nucl. Inst. Meth. **187**,581 (1981)

Coleman,C.F. Appl. Phys. **19**,87 (1976)

Dahm,J., Ley.R., Niebling,K-D., Picard.,A. & Werth,G. Proc EPOS 86, Gießen, FRG Appl. Phys. A in press (1987)

Dale,J.M., Hulett,L.D. & Pendyala,S. Surf. & Interf. Anal. **2**,199 (1980)

Dirac,P.A.M. Proc. Camb, Phil. Soc. **26**,361 (1930)

Donnelly,S.E & Rossouw,C.J. Science **230**,1272 (1985)

Dupasquier,A. in *Positron Solid State Physics* (W.Brandt & A.Dupasquier Eds.), North Holland, Amsterdam (1983)

Dupasquier,A. & Zecca,A. Rev. Nuov. Cim. **8**,No.12 (1985)

Eldrup,M. & Evans,J.H. J. Phys. **F12**,1265 (1982)

Evans,J.H. Nucl. Inst. Meth. **B18**,16 (1986)

Evans,J.H. & Mazey,D.J. J.Phys **F15**,L1 (1985) (a)

Evans,J.H. & Mazey,D.J. Scripta Met. **19**,621 (1985) (b)

Evans,J.H. & Mazey,D.J. J. Nucl. Materials **138**,176 (1986)

Evans,J.H., Williamson,R. & Whitmell,D.S. Proc 12th Sympos. on the Effects of Radiation on Materials (F.A.Garner & J.S.Perrin Eds.), ASTM, Philadelphia (1985)

vom Felde,A., Fink,J., Müller-Heinzerling,Th., Pflüger,J.,Scheerer,B., Linker,G. & Kaletta,D. Phys. Rev. Lett. **53**,922 (1984)

Finnis,M.W, van Veen,A. & Caspers,L.M. Radiat. Effects. **78**,121 (1983)

Greenwood, G.W., Foreman,A.J.E. & Rimmer,D.E. J. Nucl. Mater. **4**,305 (1959)

Gruber,E.E. J. Appl. Phys. **38**,243 (1967)

Gullikson,E.M & Mills,A.P. Jr. Phys. Rev. Lett. **57**,376 (1986)

Gustafson,D.R. & Mackintosh,A.R. Phys.Lett. **5**,234 (1963)

Hautojärvi,P. and Vehanen,A. in *Positrons in Solids* (P.Hautojärvi Ed.), Springer, Berlin (1979)

Häutojarvi,P. Huomo,H., Lahtinen,J., Mäkinen,J. & Vehanen,A. in *Defects in Semiconductors* (H.J. von Bardeleben Ed.) Mat. Sci. Forum **10-12**,527 (1986)

Hodges,C.H. & Stott,M.J. Phys. Rev. **B7**,73 (1973)

Howell,R.H., Rosenberg,I.J. & Fluss,M.J. Phys. Rev. **B34**,3069 (1986)

Huomo,H., Vehanen,A., Bentzon.M.D. & Hautojärvi,P. Phys. Rev. **B35**,8252 (1987)

Hutchins,S.M., Coleman P.G., Stone,R.J. & West,R.N. J. Phys. **E19**,282 (1986)

Itoh,F. & Suzuki,K. in *Positron Annihilation* (R.R.Hasiguti & K.Fujiwara Eds.), Japan Inst. Metals, Sendai 980, Japan (1979)

Jean,Y.C., Yu,C. & Zhou,D.M. Phys. Rev. **B32**,4313 (1985)

Jensen,K.O., Eldrup,M. & Evans,J.H. in *Positron Annihilation* (P.C.Jain, R.M.Singru & P.C.Jain Eds.), World Scientific, Singapore (1985)

Jensen.,K.O. & Nieminen,R.M. Phys. Rev. **B35**,2087 (1987)

Kaupilla,W.E., Stein,T.S., Jesion,G., Dababneh,M.S. & Pol,V. Rev. Sci. Inst. **48**,822 (1977)

Lahtinen,J., Vehanen,A., Huomo,H., Mäkinen,J., Huttunen,P., Rytsöla,K., Bentzon,M. & Hautojärvi,P. Nucl. Inst. Meth **B17**,73 (1986)

Mäkinen,J., Vehanen,A., Hautojärvi,P., Huomo,H., Lahtinen,J., Nieminen,R.M.

& Valkealahti,S. Surf. Sci. **175**,385 (1986)

Makhov,A.F. Sov. Phys. Solid State **2**,1934 (1960)

Mackenzie,I.K., Eady,J.A. & Gingerich,R.R. Phys. Lett. **A33**,279 (1970)

MacKenzie,I.K. *Positron Solid State Physics* (W.Brandt & A.Dupasquier Eds.), North Holland, Amsterdam (1983)

Matsunami,M., Yamamura,Y. & Itikawa,Y. Report IPPJ-AM-32, Inst. Plasma Phys., Nagoya Univ. (1983)

Mills,A.P. Jr., Appl. Phys. Lett. **35**,427 (1979)

Mills,A.P. Jr. Appl. Phys. **23**,189 (1980)

Mills,A.P. Jr. & Crane,W.S. Phys. Rev. Lett. **53**,2165 (1984)

Nielsen,B., Lynn,K.G. & Vehanen,A. Phys. Rev. **B32**,2296 (1985)

Nieminen,R.M. in *Positron Solid State Physics* (W.Brandt & A.Dupasquier Eds.), North Holland, Amsterdam (1983)

Nieminen,R.M. & Hodges,C.H. Sol. Stat. Com. **18**,1115 (1976)

Nieminen,R.M & Manninen,M.J. in *Positrons in Solids* (P.Hautojarvi Ed.), Springer, Berlin (1979)

Rao,K.U. Ph.D. Thesis, Univ. London (1987)

Rice-Evans,P., Hlaing,T. & Rees,D.B. J. Phys. **F6**,1079 (1976)

Rice-Evans,P., Chaglar,I. & El Khangi,F.A.R Phys. Lett. **A81**,480 (1980)

Rice-Evans,P., Moussavi-Madani,M., Rao,K.U., Britton,D.T. & Cowan,B.P. Phys. Rev. **B34**,6117 (1986)

Rice-Evans,P.C. & Moussavi-Madani,M. Phys. Lett. **122**,187 (1987)

Ronchi,C. J. Nucl. Materials **96**,314 (1981)

Schaffer,J.P., Shaughnessy,E.J. & Jones,P.L. Nucl. Inst. Meth. **B5**,75 (1984)

Schaffer,J.P. & Jones,P.L. J. Phys. **F16**,1885 (1986)

Schödlbauer,D., Sperr,P., Kögel,G. & Trifthäuser,W. Proc Int. Symp. "Production of Low-Energy Positrons with Accelerators & Applications", Gießen, FRG (1986).

Schultz,P.J., Proc Slow Positron Workshop, Helsinki Univ. Tech. (1984)

Schultz.,P.J., Lynn,K.G. & Nielsen,B. Phys Rev **B32**,1369 (1985)

Simon,F.E. & Glatzel.,G. Z. Anorg. Allg. Chem. **178**,309 (1929)

Templier,C., Jaouen,C., Rivière,J.P., Delafond,J. & Grilhé,J. Compt. Rend. Hebd. Séanc. Acad. Sci., Paris **299**,613 (1984)

Templier,C., Garem,H. & Rivière,J.P. Phil. Mag. **A53**,667 (1986)

Townsend,P.D., Kelly,J.C. & Hartley.N.E.W. *Ion Implantation, Sputtering and their Applications*, Academic Press, London (1976)

Trifthäuser,W. & Kögel,G. in *Positron Annihilation* (P.G.Coleman, S.C.Sharma & L.M.Diana Eds.), North Holland, Amsterdam (1982)

Valkealahti,S. & Nieminen,R.M. Appl. Phys. **A32**,95 (1983)

Valkealahti,S. & Nieminen,R.M. Appl. Phys. **A**35,51 (1984)

Varlashkin,P.G. Phys. Rev. **A3**,1230 (1971)

Vehanen,A., Saarinen ,K., Hautojärvi,P. & Huomo,H. Phys. Rev. B in press Helsinki Univ. Tech. Report 160 (1986)

Weber,M., Lynn,K.G., Roellig,L.O., Mills,A.P. Jr., Frieze,W.E. & Moodenbaugh,A.R. Proc Slow Positron Workshop, Univ. East Anglia, Norwich (1986)

West,R.N. *Positron Studies of Condensed Matter*,Taylor & Francis, London (1974)

West,R.N. in *Positrons in Solids* (P.Hautojärvi Ed.), Springer, Berlin (1979)

Whitmell,D.S. Nucl. Energy **21**,181 (1982)